AN ABSTRACT OF THE THESIS OF

Songshi S. Peng for the degree of Doctor of Philosophy in Physics presented on May 23, 1991.

Title: Electronic Structures and Magnetic Properties of Iron in Various Magnetic States and Structural Phases

Abstract approved: _____ Henri J. F. Jansen

Total energy calculations based on density functional theory are generally a good approach to obtain the properties of solids. The local density approximation (LDA) is widely used for calculating the ground state properties of electronic systems; for excited states the errors are in general unknown. The important aspects of LDA pertain to the modeling of the exchange-correlation interaction. If the exchange-correlation potential is approximately the same for the ground and excited states, one expects good results from the LDA calculations for excited states. In this thesis, we utilize the total energy technique for numerical computations of the electronic structure of iron in several magnetic phases and crystalline structures.

1. Body-centered-cubic iron in the ferromagnetic and several antiferromagnetic configurations. We use the total energy results to obtain the parameters in a model Heisenberg Hamiltonian. These include the interaction parameters up to 6-th nearest neighbors. Based on this model Hamiltonian we calculate properties such as the critical (Curie) temperature and spin stiffness constant. We assume that the total exchange-correlation energy functional is the same in the ferromagnetic ground state and the antiferromagnetic excited states. Our model parameters are based directly on *ab initio* calculations of the electronic structure. Our calculation yields good results compared with experimental values and earlier work. Some other physical quantities, related to the phase transition, and spin waves are also discussed.

2. Face-centered-tetragonal iron. If iron is grown on a proper substrate (e.g., Cu(100)), the crystal structure of the thin film displays a face-centered-tetragonal distortion

due to the lattice constant misfit between the film and substrate. Therefore, we performed calculations for fct iron in its ferromagnetic, antiferromagnetic, and nonmagnetic phases for a wide range of values of the lattice parameters. In the ferromagnetic calculations, we found two minima in the total energy: one is close to the bcc structure and the other (with a lower energy) is close to fcc. In the antiferromagnetic and nonmagnetic calculations, we found in each case that there is only one minimum near the fcc structure, providing us clear evidence that the antiferromagnetic and nonmagnetic states are (meta)stable near the fcc region and unstable in bcc region. The antiferromagnetic and nonmagnetic states are almost degenerate near the fcc minimum, but the antiferromagnetic phase has the lowest total energy in the whole fct region. Magnetic moments are also calculated for a variety of fct structures. Near the fcc minimum we found that two ferromagnetic phases co-exist, one with a low spin and one with a high spin. These results are consistent with experimental facts and other earlier calculations. Some structural properties, such as the elastic constants and the bulk modulus, are also studied and compared with experimental data and some earlier calculations.

Electronic Structures and Magnetic Properties of Iron in Various Magnetic States and Structural Phases

by

Songshi S. Peng

A THESIS

submitted to

Oregon State University

in partial fulfillment of
the requirements for the
degree of

Doctor of Philosophy

Completed May 23, 1991

Commencement June 1992

APPROVED:

Redacted for Privacy

Associate Professor of Physics in charge of major

Redacted for Privacy

Chairman of the Department of Physics

Redacted for Privacy

Dean of Graduate School

Date thesis is presented May 23, 1991

Typed by Songshi S. Peng for Songshi S. Peng

Acknowledgement

I would like to take this opportunity to thank a few special people who helped me through the work of this thesis.

First of all, I would like to express my deepest gratitude to Dr. Henri J. F. Jansen, my major professor, for his constant support, encouragement, and assistance during the course of this work and the years of my graduate study which made this work possible. Special thanks go to Dr. Kristl B. Hathaway who stimulated me to work on the project and provided helpful suggestions. I would also like to thank the College of Science at Oregon State University for granting computing time on the OSU Floating Point System, on which we finished a large portion of the calculations. Many thanks to Dr. George H. Keller and his wife Sue, for their hospitality and care through the years I spent at Oregon State University in Corvallis.

Many of my colleagues and friends gave me assistance in different ways. In particular, I wish to thank Michael J. Love, Martin Rosenbauer, and Yiqing Zhou. Special thanks go to Mark A. Gummin for reading the manuscript carefully and making grammar corrections.

Finally, I wish especially to thank my wife Lan, for her love, understanding, and patience through all these years.

Table of Contents

List of Figures

List of Tables

List of Appendix Tables

Electronic Structures and Magnetic Properties of Iron in Various Magnetic States and Structural Phases

Chapter 1. Introduction

The theory of quantum mechanics as well as the theory of relativity are both essential for the interpretation of the magnetic behavior of solids.[1-2] For iron, one of the most important transition metals, much work has been done to obtain the electronic properties through *ab initio* calculations. Most relevant for our work are references 3 and 4. There are still questions concerning the treatment of the exchange-correlation potential and the short-range order of the magnetic moments. In addition, few of the *ab initio* calculations are directly related to magnetic properties, such as the transition temperature and spin wave excitations, without resorting to some approximation. Also, all the calculations for iron are performed for cubic structures. Calculations for a different structure are useful to discuss the magnetic behavior of thin films. In this thesis, we perform these calculations and we believe that they help us to understand the nature of magnetism in solids.

Density-functional theory, with effective single-particle equations in which the exchange-correlation potential is approximated by the local-spin density form, is the computationally efficient method we use to obtain the total energy of iron. The single-particle equations are solved self-consistently by the full-potential linearized augmented-plane-wave method. In Chapter 2, we describe the above techniques in detail in the following order: density functional theory (§2.1.1), local density approximation (§2.1.2), total energy behavior in charge- and spin-density space (§2.1.3), the self-consistent process (§2.1.4), FLAPW method (§2.1.5), and finally band fitting procedures (§2.1.6). In Chapter 3 and 4, we give an initial and a complete discussion of critical temperature, spin wave behavior, and related properties from the electronic structure calculations of bcc iron. Ferromagnetic and antiferromagnetic electronic properties of face-centered-tetragonal

are discussed in Chapter 5 and 6, respectively. Chapter 3 through 6 are in the form of published papers: Chapter 3 -- J. Appl. Phys.**64**, 5607(1988), Chapter 4 -- Phys. Rev. B**43**, 3518(1991), Chapter 5 -- J. Appl. Phys.**67**, 4567(1990), and Chapter 6 -- accepted for publication in J. Appl. Phys. Some details of the results can be found in the appendix.

Chapter 2. Theoretical Background

2.1 General Theoretical Formalisms

2.1.1 Density Functional Theory

The energy of the electrons in a crystal consists of the kinetic energy, classical Coulomb energy, external energy (due to the interactions between the electrons and the atomic nuclei, and the interactions between the electrons and external fields), and the exchange-correlation energy. Once the decision on a suitable approximation for the exchange-correlation potential has been made -- our choice is the Local Spin Density Approximation, or LSDA, which will be discussed in detail in the next section -- the *ab initio* calculation of the electronic structure for a crystal is in principle relatively straightforward; the task can be achieved simply by solving the Schrödinger equation directly, although the process may be extremely complicated and not analytically soluable in most cases. Density functional theory provides an effective approach, both numerically and theoretically, to obtain the total energy of a solid in a given crystal structure.

Density Functional Theory,[5-7] or DFT, describes the total energy E of the electronic system as a general functional of its charge density (and spin density as well in a magnetic system), i.e., $E=E[\rho]$. Given this functional one's main task is to minimize E in the space of physically allowed charge densities to obtain the ground state energy. The global minimum of E always corresponds to the total energy of the ground state. Sometimes this process ends up with a local minimum; if it corresponds to a physical state (in most cases, it does not !), this will be an excited state of the system.

The total energy is defined as the sum of three contributions: many body kinetic energy, many body Coulomb energy, and external energy (due to the atomic nuclei and other external fields). In density functional theory these terms in the total energy are described as a general functional of the electronic charge density, which may be further

divided into spin-up and spin-down charge densities in a magnetic case. They are approximated by the kinetic energy of a non-interacting system with the same charge and spin densities, the classical Coulomb energy, and the same external energy as in the real system. One adds a correction term to arrive at:

$$E_{total}[\rho_c,\rho_s] = E_k[\rho_c,\rho_s] + E_{Coul}[\rho_c,\rho_s] + E_{ext}[\rho_c,\rho_s] + E_{xc}[\rho_c,\rho_s] \ .$$

The correction term, named exchange-correlation energy, is by definition the difference between the real total energy and the contribution of the first three in density functional theory. Obviously, all the many body effects are included in the exchange-correlation energy. The LSDA is applied to the exchange-correlation energy in the calculations to obtain an expression for the exchange-correlation energy in terms of the charge densities. The basic aim of density functional theory is to find the global/local minima in the energy as a function of the charge density (and spin density in magnetic case), and verify that they correspond to ground/excited states of the system in the real world.

2.1.2 Local Density Approximation

Although the application of density-functional theory can provide an effective approach to an electronic-structure calculation, the relation between the potential and electronic densities has to be found. The simplest form of such a relation is constructed in the Thomas-Fermi model of the inhomogeneous electron gas,[8] where at most two electrons can occupy a cell with volume h^3 in phase space. The total number of electrons can be expressed as :

$$N = 2 \cdot \frac{4\pi P_f^3 V}{3h^3} \longrightarrow \rho = \frac{8\pi P_f^3}{3h^3}$$

where P_f is the Fermi momentum and ρ is the electronic charge density.

In solids, of course, this form will be invalid and has to be generalized to include the periodic potential in a crystal. In this case, $E_f = P_f^2(\mathbf{r})/(2m) + V(\mathbf{r})$, and the relation between $\rho(\mathbf{r})$ and $V(\mathbf{r})$ is:

$$\rho(\mathbf{r}) = \frac{8\pi}{3h^3} P_f^3(\mathbf{r}) = \frac{8\pi(2m)^{3/2}}{3h^3} [E_f - V(\mathbf{r})]^{3/2} .$$

More importantly, we also have to find the dependence between the density and the exchange-correlation contributions; thus, the above formula is too simple for a real crystal.

The standard Local Density Approximation (LDA)[5-7,9] is based on the results for an inhomogeneous interacting electron gas. For the ground state of an electronic system, Hohenberg and Kohn[5] showed in 1964 that all aspects of the electronic structure are determined by its electronic density $\rho(\mathbf{r})$. On this fundamental basis, Kohn and Sham[6] derived a set of self-consistent one-particle equations, known as the Kohn-Sham equations, to describe the electronic ground state. The one-particle effective potential $v_{eff}(\mathbf{r})$ depends on the charge density $\rho(\mathbf{r})$ in a complicated way and takes into account all the many body effects. In practice, one often applies the so-called Local Density Approximation, or LDA, in which the effective potential depends only in a simple manner on the electronic charge density $\rho(\mathbf{r})$ at the point $\mathbf{r}$. This ignores all the terms in a gradient expansion normally used to improve the calculations for an electronic system with a charge density which varies rapidly in space. Typically, the results of calculations using the Kohn-Sham equations with LDA are better than those of Hartree-Fock calculations, since the former includes a good estimate of the exchange-correlation energy while in Hartree-Fock the exchange contribution is included exactly but the correlation effects are totally ignored.

We follow the Kohn-Sham approach to show the derivation of self-consistent one-particle equations. As discussed in the section on density functional theory, the total energy can be written as:

$$E_{total}[\rho(\mathbf{r})] = T^{NI}[\rho(\mathbf{r})] + \frac{1}{2}\int\frac{\rho(\mathbf{r})\rho(\mathbf{r}')}{|\mathbf{r}-\mathbf{r}'|}d\mathbf{r}d\mathbf{r}' + \int\rho(\mathbf{r})v(\mathbf{r})d\mathbf{r} + E_{xc}[\rho(\mathbf{r})]$$

where $T^{NI}[\rho(\mathbf{r})]$ is the kinetic energy of a non-interacting system with the same charge density as in the real system; $E_{xc}[\rho(\mathbf{r})]$ is, by definition, the exchange-correlation energy; $v(\mathbf{r})$ is the external potential. To minimize the total energy with the condition $\int \rho(\mathbf{r})\, d\mathbf{r} = N$, we have to satisfy the following condition:

$$\frac{\delta T^{NI}[\rho]}{\delta\rho(\mathbf{r})} + \phi(\mathbf{r}) + v_{xc}(\mathbf{r}) - \mu = 0$$

where: $\phi(\mathbf{r}) = v(\mathbf{r}) + \int \frac{\rho(\mathbf{r})}{|\mathbf{r}-\mathbf{r}'|}d\mathbf{r}$, $v_{xc}(\mathbf{r}) \equiv \frac{\delta E_{xc}[\rho]}{\delta\rho(\mathbf{r})}$, and μ is the Lagrange parameter determined by the normalization condition, which is equal to the chemical potential.

Further detailed proofs show that the above process is equivalent to solving the following one-particle equations, known as Kohn-Sham self-consistent equations:

$$\{ -\Delta + v_{eff}(\mathbf{r}) \}\, \psi_i(\mathbf{r}) = \varepsilon_i\, \psi_i(\mathbf{r})$$

where: $v_{eff}(\mathbf{r}) = \phi(\mathbf{r}) + v_{xc}(\mathbf{r})$, $\rho(\mathbf{r}) = \sum|\psi_i(\mathbf{r})|^2$. Therefore, the total energy is given by:

$$E_{total} = \sum_i \varepsilon_i - \frac{1}{2}\int\frac{\rho(\mathbf{r})\rho(\mathbf{r}')}{|\mathbf{r}-\mathbf{r}'|}d\mathbf{r}d\mathbf{r}' + E_{xc}[\rho(\mathbf{r})] - \int\rho(\mathbf{r})v_{xc}(\mathbf{r})d\mathbf{r}$$

The terms with a minus sign in the formula above are needed to avoid double counting of the Coulomb and exchange-correlation contribution of the total energy. The whole idea behind this is to solve the kinetic energy $T^{NI}[\rho]$ in a "reference system" for the non-interacting electronic system with charge density $\rho(\mathbf{r})$. For the system with a slowly varying charge density (without considerable change in a distance ~ k_F^{-1}), we can apply the LDA in the form of:

$$E_{xc}[\rho] = \int \varepsilon_{xc}(\rho(\mathbf{r}))\, \rho(\mathbf{r})\, d\mathbf{r},$$

where $\varepsilon_{xc}(\rho)$ is the exchange-correlation energy per particle in a homogeneous electron gas with charge density $\rho(\mathbf{r})$. The exchange-correlation potential can then be written as:

$$v_{xc}(\mathbf{r}) = \frac{d}{d\rho}\{\varepsilon_{xc}(\rho(\mathbf{r}))\rho(\mathbf{r})\}$$

It only depends in a simple manner on the charge density. Various forms have been proposed for $\varepsilon_{xc}(\rho)$ and $v_{xc}(\mathbf{r})$, e.g., Gunnarsson and Lundqvist give,[7] in atomic units:

$$\varepsilon_{xc}(\rho) = -\frac{0.458}{r_s} - 0.0666\, G(\frac{r_s}{11.4}),$$

where r_s is the radius of atomic Wigner-Seitz spheres and G(x) is defined as following:

$$G(x) \equiv \frac{1}{2}[(1+x^3)\log(1+x^{-1}) - x^2 + \frac{x}{2} - \frac{1}{3}].$$

2.1.3 $E[\rho_c,\rho_s]$ Behavior in E-$\{\rho_c,\rho_s\}$ Space

In a magnetic system the term "charge density" in the discussion above now consists of two parts: the real electronic charge density and the spin density, which is the difference between the charge density of spin-up and spin-down electrons. The potential has to be modified to include the spin-spin interaction between electrons, since every electron moves in an effective magnetic field due to other electrons in the system. Again, the associated single particle problem has to be solved self-consistently and the corresponding LDA applied to this spin-polarized system is now called the local spin density approximation (LSDA). In our calculation, we use the following form of exchange-correlation potential (for spin-up electrons) in a magnetic system, proposed by von Barth, etc. and parametrized by Janak:[9-10]

$$v_{xc}^{u}(\mathbf{r}) = (\mu_x^P + v_c)\,(2\rho_u/\rho_c)^{1/3} + \mu_c^P - v_c + \tau_c\, f(\rho_u/\rho_c), \text{ for spin-up electrons;}$$

where: ρ_u is the spin-up charge density; for spin-down electrons, ρ_u needs to be replaced by ρ_d. $\rho_c=\rho_u+\rho_d$ is the total charge density. Other function are defined as:

$$\mu_x^P = -1.96949\,\rho_c^{1/3},\ \mu_c^P = -0.045\ln(1+33.85183\,\rho_c^{1/3});$$

$$v_c = \gamma(\varepsilon_c^F - \varepsilon_c^P),\ \gamma = \frac{4}{3}\frac{2^{-1/3}}{1-2^{-1/3}}$$

$$\varepsilon_c^F = -\frac{0.045}{2} F[(2^{4/3}\times 33.85183\ \rho_c^{1/3})^{-1}],\ \varepsilon_c^P = -0.045\ F[(33.85183\ \rho_c^{1/3})^{-1}];$$

$$\tau_c = (\mu_c^F - \mu_x^P) - \frac{4}{3}(\varepsilon_c^F - \varepsilon_x^P),$$

$$\mu_c^F = -\frac{0.045}{2} \ln(1 + 2^{4/3}\times 33.85183\ \rho_c^{1/3}),\ \varepsilon_x^P = \frac{3}{4}\mu_x^P;$$

$$f(x) \equiv (1 - 2^{-1/3})^{-1}[x^{4/3} + (1-x)^{4/3} - 2^{-1/3}],$$

$$F(x) \equiv [(1+x^3)\log(1+x^{-1}) - x^2 + \frac{x}{2} - \frac{1}{3}].$$

Note that by definition the exchange-correlation energy is the difference between the many body total energy of the ground state and the kinetic energy of a non-interacting system + classical Coulomb interactions + external energy of the ground state of the system. For ground state calculations, the LSDA is generally a good assumption since one uses the ground state wave functions in the evaluation of the above formula. On the other hand, for the calculation of excited states it is uncertain whether the LSDA is still good. If the exchange-correlation functional is approximately the same for the ground and excited states, it may be safe to use it; otherwise, it will introduce a large amount of error in the results of the calculations due to a wrong model of the exchange and correlation. Whether this is the case very often depends upon the characteristics of the electronic structure of the system; for example, calculations of the optical gap in semiconductors give wrong results using straightforward LSDA.

The task for total energy calculations in density functional theory is to minimize the energy functional $E[\rho_c,\rho_s]$. The global minimum in this energy functional always corresponds to the ground state of the system. In our case, the global minimum of the total energy corresponds to one of several magnetic states of iron; in bcc iron, for example, the ground state is ferromagnetic.[11] On the other hand, this energy functional will also have a number of local minima in density space which in most cases do not correspond to excited states of the interacting electronic system; vice versa, the excited states of the system may

not always correspond to local minima in the energy functional. In metallic systems, fortunately, there are many excited states for which the correlation energy is very similar to that in the ground state. In our calculations for bcc iron, for instance, we do find a number of local minima which correspond to antiferromagnetic states and which are excited states of the system. One must keep in mind, however, that not all antiferromagnetic states are associated with a local minimum.

2.1.4 Self-Consistent Calculations

Self-consistent calculations are very frequently used methods in almost every branch of physics, especially in computational physics, when general analytical results are impossible to obtain and some numerical approaches have to be applied. In solid state physics, this method is extremely effective, particularly when used with other approximations; in our case, the latter are the density functional theory with the local density approximation. Consider the following Schrödinger equation for a crystal structure:

$$(-\Delta + V(\rho)) \psi = E \psi;$$

where $V=V(\rho)$ because in DFT, everything can be expressed as a functional of ρ; ρ should now be considered as a generalization of total charge and spin density. We also have :

$$\rho_c = \sum_{u,d} |\psi|^2 , \quad \rho_s = \sum_{u} |\psi|^2 - \sum_{d} |\psi|^2 ;$$

then we will have the following loop to complete the self-consistent calculations:

$$\rho_{in} \text{ --> } V(\rho) \text{ --> Solving Schrödinger Equation to get } \psi \text{ --> } \rho_{out} (= \sum |\psi|^2).$$

ρ_{out} can be used to improve the values of ρ_{in} and to start the process again. We often use the results of other calculations to make an initial guess of ρ_{in}. The first step in the loop may involve LSDA for the form of $V(\rho)$. The self-consistent process can be stopped with success if ρ_{in} and ρ_{out} are within a satisfactory range. In most cases the process is fairly

efficient, and again, it will give good results about the ground state and excited states if the local minima indeed correspond to physical states of the system.

In contrast to the simple theoretical formalism, the self-consistent process must be performed very carefully, mainly because of the following two reasons. First, we have to consider numerical stability and convergence. In any computation performed on a computer, there will be round-off and truncation errors added into the final output (numerical) results. Also, in our self-consistent process the charge density tries to overcompensate the errors in the input charge density, resulting in a larger deviation (but in the opposite direction) from the self-consistency in the output charge density. This is related to the physical nature of the systems under investigation. As mentioned in the previous sections, for calculations of an excited state, our goal is to find the corresponding local minima of the system. In this case there is another instability, especially in the first few iterations when the calculation is further away from the minimum, leading us either to the ground state (global minimum) or to an unintended local minimum we are not interested in.

Thus, if we take the output charge densities ρ_{out} as input for the next iteration, all these errors will introduce a great amount of instability, causing rapid divergence of the total energy calculations in most cases. In fact, in all calculations we have to mix the input and output charge densities to compose a new charge density for the input of the next iteration, with a larger weight factor on the input side. It turns out that taking about 10-30% of the output of charge and higher percentage of output spin densities is a good choice in our calculations. If evidence shows that the calculation is still unstable, one can either reduce this percentage, or mix the input and output densities with those of previous iterations to increase the stability.

In each of the iterations in our calculation, we calculated the difference in the charge and spin densities, $\Delta\rho_c$ and $\Delta\rho_s$, between the input and output. At small values of these differences, the total energy behaves as a quadratic function of $\Delta\rho_c$ and $\Delta\rho_s$:

$$E = E_0 + a\,(\Delta\rho_c)^2 + b\,\Delta\rho_c\,\Delta\rho_s + c\,(\Delta\rho_s)^2 .$$

After several iterations, we have enough data to determine the converged values of total energy (E_0 in above equation) using extrapolation. It is important to note that this procedure is only valid when one uses a small mixing between input and output densities.

2.1.5 FLAPW Method

Consider the Schrödinger equation of the form:

$$(-\Delta + V(\rho))\,|\psi\rangle = E\,|\psi\rangle.$$

If we choose $|\varphi_n\rangle$ to be a set of basis functions, we have :

$$\sum_m \langle\varphi_n|\,(-\Delta + V(\rho))|\varphi_m\rangle\langle\varphi_m|\,\psi\rangle = E\,\langle\varphi_n|\,\psi\rangle, \quad \text{for all possible n;}$$

i.e., $$\sum_m H_{nm}\,\psi_m = E\,\psi_n,$$

where H is a matrix and ψ is a vector in the space of $\{\,|\varphi_n\rangle\}$.

In the process of total energy calculations, we need to choose the right approximation for the exchange-correlation potential, choose the appropriate set of basis functions, then transfer the Schrödinger equation into a matrix problem as described above which a computer can solve very effectively. We need to apply numerical techniques to solve for the eigenvectors ψ_n, and eigenvalues $E_n(\mathbf{k})$, known as energy bands, which depend on the wave vector **k** and band index n.

In our studies we use the Full-potential Linearized Augmented Plane Wave (FLAPW)[12] method to obtain the kinetic energy of the non-interacting reference system. In

a crystal, we expect the potentials to be rather spherical near the nuclei, and relatively flat in the interstitial regions, due to the fact that the core electrons are dominant near the atomic nuclei and the valence electrons are the most important in the interstitial region. So it is natural that we can expand the potential by spherical functions inside a carefully chosen sphere centered at each nucleus, with a radius large enough to contain most of the core electrons but limited by requiring that the spheres do not overlap each other. On the other hand, in the interstitial region between these spheres we approximate the potential by a set of plane wave functions, expecting that this set will converge rather rapidly so we only have to include the first few terms in the calculations. Note although the radius of the sphere is usually called the "muffin-tin" radius of the muffin-tin sphere, our approximation is different from the conventional muffin-tin approximation, in which, the potential is purely spherical inside the sphere and is precisely constant between the spheres. Rather, in our case, the potential will be expanded in $Y_{lm}(\theta,\varphi)$ functions inside the sphere and in $\exp(i\mathbf{k}\cdot\mathbf{r})$ outside it:

$$V(\mathbf{r}) = \sum_{lm} A_{lm}(r)\, Y_{lm}(\theta,\varphi); \quad l,m = 0, 1, 2, \ldots \quad (\text{ inside muffin-tin })$$

$$V(\mathbf{r}) = \sum_{\mathbf{k}} B_{\mathbf{k}} \exp(i\mathbf{k}\cdot\mathbf{r}); \quad \mathbf{k} = \{ \text{ reciprocal lattice vectors } \} \ (\text{ outside muffin-tin })$$

On the muffin-tin boundary these potentials have to satisfy a continuity condition. The approximation will be the same as the muffin-tin approximation only if we restrict the summations to l=m=0 and k=0 in the above equations. Although the muffin-tin approximation gives reasonable results for close-packed metals, it results in a large error for open structure and for materials with directed covalent bonds. Our full-potential approach, on the other hand, does not contain any implicit numerical approximations and gives very accurate results. In fact, the only influences on our final results are virtually related to the effects caused by the application of the LDA.

The augmented plane wave (APW) method suggests the following way to expand the wave function: 1. In the interstitial region, choose plane waves $\phi_{\varepsilon\mathbf{k}}(\mathbf{r})=\exp(i\mathbf{k}\cdot\mathbf{r})$ as basis functions; 2. Find the solutions of the following atomic Schrödinger equation and use that as basis functions within muffin-tin radius r_{mf} in the atomic region centered at **R**:

$$(-\Delta + V(|\mathbf{r}-\mathbf{R}|)) \phi_{\varepsilon\mathbf{k}}(\mathbf{r}) = \varepsilon \phi_{\varepsilon\mathbf{k}}(\mathbf{r}), \text{ for } |\mathbf{r}-\mathbf{R}| < r_{mf} \text{ (V is the atomic potential);}$$

3. The basis function is continous at the boundary between the interstitial and atomic regions. This APW basis also has to satisfy the orthogonality and completeness conditions.

In order to perform the band calculations by using limited computing resources, in practical, we must use energy-independent basis functions. Therefore, the linearized augmented plane wave (LAPW) method was proposed to construct a basis from the partial waves (i.e., the plane waves in the interstitial region and the atomic wave functions within the muffin-tin sphere) in the above APW method and first energy derivatives at an energy value E_l, known as energy parameter. This linearized method is only accurate within a certain energy range, thus the values of E_l are always chosen at the center of the occupied bands in our calculation to obtain the maximum accuracy.

In our full-potential linearized augmented-plane-wave (FLAPW) calculation, we go a few steps further than the LAPW. The most important aspect of the FLAPW method is the implementation of a second variation technique, which is within the framework of the LAPW approach. For the valence electrons in a given potential, we first perform a semi-relativistic "warped" muffin-tin calculation, in which we include the full-potential in the interstitial region (as stated above), but only the spherical contribution to the potential inside the muffin-tin spheres, as to solve the following semi-relativistic Dirac equation where all semi-relativistic corrections are embodied in $v^{mt}(\mathbf{r})$:

$$\{ -\Delta + v^{mt}(\mathbf{r}) \} \psi_{n\mathbf{k}}{}^{mt}(\mathbf{r}) = \varepsilon_{n\mathbf{k}}{}^{mt} \psi_{n\mathbf{k}}{}^{mt}(\mathbf{r}).$$

In the above equation, $\psi_{nk}^{mt}(\mathbf{r})$ is the large component of the Dirac wave function and "mt" indicates "warped muffin-tin" calculations. Note that the spin-orbit coupling is excluded from the above calculation, due to the semi-relativistic treatment. In the second step, we use the wave functions obtained from the first calculation as basis functions for the second variation to bring back the contribution of all non-spherical terms we have left out inside the muffin-tin sphere in the previous calculation. It is accomplished by the following linear transformation, to the l-m representation inside the muffin-tin spheres:

$$\psi_{nk}(\mathbf{r}) = \sum_{lm} \{ a_{nk}(l,m)\, R_l(E_l,r) + b_{nk}(l,m)\, R_l'(E_l,r) \}\, Y_{lm}(\theta,\varphi),$$

where **R** denotes the atomic site; R_l and R_l' are the radial solutions to the above semi-relativistic equation and its energy derivative; the coefficients a and b can be obtained from their counter parts in the plane-wave expansion of the wave functions in the interstitial region; $\psi_{nk}(\mathbf{r})$ is our FLAPW basis function. Therefore, the matrix elements of our full-potential Hamiltonian inside muffin-tin spheres will be:

$$H_{mn} = \varepsilon_n^{mt}\, \delta_{mn} + \langle \psi_{mk}(\mathbf{r}) \mid v^{ns}(\mathbf{r}) \mid \psi_{nk}(\mathbf{r}) \rangle.$$

The calculation of the last term is very time consuming. Since the second term, the non-spherical contribution in a "spherical basis", is relatively small, it is expected that the Hamiltonian is already close to diagonal, resulting in an enormous increase in speed for the FLAPW process. Typically, one needs about 200 (atomic) basis functions per atom in the first calculation but only about the order of 20 (warped-muffin-tin) basis in the second variation. The whole process of second variation is equivalent to solving the following self-consistent single-particle equations:

$$\{ -\Delta + v^{mt}(\mathbf{r}) + v^{ns}(\mathbf{r}) \}\, \psi_i(\mathbf{r}) = \varepsilon_i\, \psi_i(\mathbf{r}).$$

Two points need to be emphasized: First, the core and valence electrons are treated separately and differently. While the valence electrons are treated semi-relativistically with a second variation as described above, the core electrons are calculated fully relativistically to

include spin-orbital coupling, but use only the spherical contribution as in an atomic potential. The resulting core-valence overlap is usually very small and negligible in most transition-metal systems.

2.1.6 Band Structure Fitting Procedures

As described in the last section, $E_n(\mathbf{k})$ forms an energy band if we can obtain its continuous behavior in **k** space. In numerical calculations we can only perform the tasks at a number of discrete points of the energy band. Fortunately, theoretical methods of band structure calculations provide us with many ways to interpolate our results in order to plot the whole band structure over **k** space.[13] The tight-binding method is one of the most effective means for such an interpolation. Although such schemes are generally used for insulators and impurity states, the application to a transition metal such as iron is also very natural and useful, since it is simple and fast. It is only used as an interpolation method rather than direct band structure calculation, so the bands will be pinned down by points calculated using the FLAPW method. In most systems, the characteristics are determined by only a few out of many bands. Band interpolation methods are based on the following two facts: 1. In the interpolation process, we use only a small number as the size of the secular Hamiltonian matrices, typically 9×9, including s, p, d orbitals, verses hundreds by hundreds in a full band structure calculation; 2. By construction, the symmetry properties of the interpolated energy bands and their corresponding wave functions will be exactly the same as those of the direct band calculation.

Yet one has to pay a price in the following two aspects: first, one has to derive the basic parameters in a fitting process, and the number of the parameters grows rapidly as the order of fitting (the number of neighbors included in the model) increases; second, although typically each matrix element depends linearly on the interpolation parameters, the

dependence of the bands on these parameters is in a very nonlinear fashion, which in turn creates many local minima in the parameter space. One has to be careful not to be trapped in those local minima during the fitting process.

Our basic purpose is to minimize the error functional in the equation:

$$\varphi(\beta, f) = \sum_i (y_i - f(x_i,\beta))^2$$

where in our case, $\{y_i\}$ are the calculated points of an energy band, $\{f(x_i,\beta)\}$ are the eigenvalues of the model Hamiltonian, and β is the set of fitting parameters. In the vicinity of the current value **b** of the parameter, we have :

$$f(x_i,\mathbf{b}+\varepsilon) = f(x_i,\mathbf{b}) + \frac{\partial f(x_i,\mathbf{b})}{\partial \beta} \cdot \varepsilon + \ldots$$

The value of ε is determined by minimizing $\varphi(\mathbf{b}+\varepsilon, f)$, and this can be done easily by substituting the above formula into φ. The solution is found by evaluating ε from the matrix equations:

$$A\varepsilon = g;\ A_{mn} = \sum_i \frac{\partial f(x_i,\mathbf{b})}{\partial \beta_m} \cdot \frac{\partial f(x_i,\mathbf{b})}{\partial \beta_n},\ g_n = \sum_i (y_i - f(x_i,\mathbf{b})) \cdot \frac{\partial f(x_i,\mathbf{b})}{\partial \beta_n}.$$

A modified version of the above equation, the Marquart algorithm, uses :

$$\sum_m (A_{nm} + \lambda \delta_{nm})\, \varepsilon_m = g_n;\ \text{for } n=1, 2, \ldots$$

The advantage of the modified form is that it can handle the case when **b** is far away from the minima, by using the gradient (down-hill) method. One should increase λ if φ is getting larger (closer to down-hill scheme), and decrease it when φ is becoming smaller (closer to Taylor expansion), respectively.

In our cases, the interpolations are performed in three steps. First of all, we apply the tight-binding method to set up the model Hamiltonian. In the tight-binding method, a matrix element has the following form which has to be restricted by symmetry:

$$H_{mn} = \sum_{j} A_{mn}(j) \cdot \exp(i\mathbf{k}\cdot\mathbf{R}_j)$$

where $A_{mn}(j)$ is our interpolation parameter set. We determine the order of fitting by the number of neighbor "shells" included in the summation, starting from the 1st nearest and truncating at a certain "order" of neighbor shell, based on the reasonable assumption that the further away a pair of atoms are, the smaller the interaction will be between them.

Second, we have to look for a set of parameters as our initial guess of input, run through a self-consistent process by evaluating ε in each iteration, and stop when we end up with a minimum (within a satisfied error limit). The easiest way for an initial guess is just taking an existing set for the closest material, structure, etc., if that is available. For example, we can take the results of bcc iron to fit the band of face-centered tetragonal iron close to bcc structure. The final step is taking the calculated set of parameters to plot the band structure along a particular direction in **k** space.

2.2 Specific Descriptions About the Material (Iron)

2.2.1 Electronic Structure of Iron

The atomic configuration of iron is [Ar] $3d^6 4s^2$, in terms of the language of "atomic orbitals". The band structure of bcc iron is shown is Figure 2.1. The solid lines show the spin-up band and the dashed lines indicate the spin-down band. The magnetic phase of the whole system is ferromagnetic, because the Fermi level in both spin-up and spin-down states has to be the same. In a self-consistent calculation, on the other hand, one can start with a nonmagnetic band structure with the same spin-up and -down band structure; in the next step, one can shift the spin-down band upward relative to spin-up band by transferring some spin-down electrons to spin-up states. The relative motion of the Fermi energies is important for the stable magnetic phases: it shows the (meta)stability of the nonmagnetic

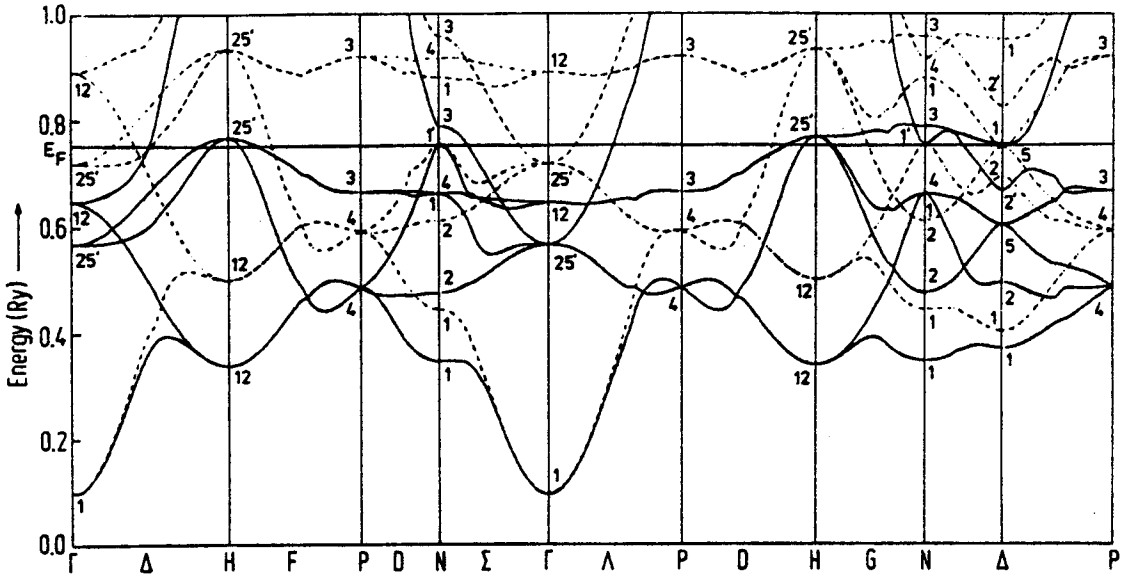

Figure 2.1 Band Structure of Iron at Zero Temperature

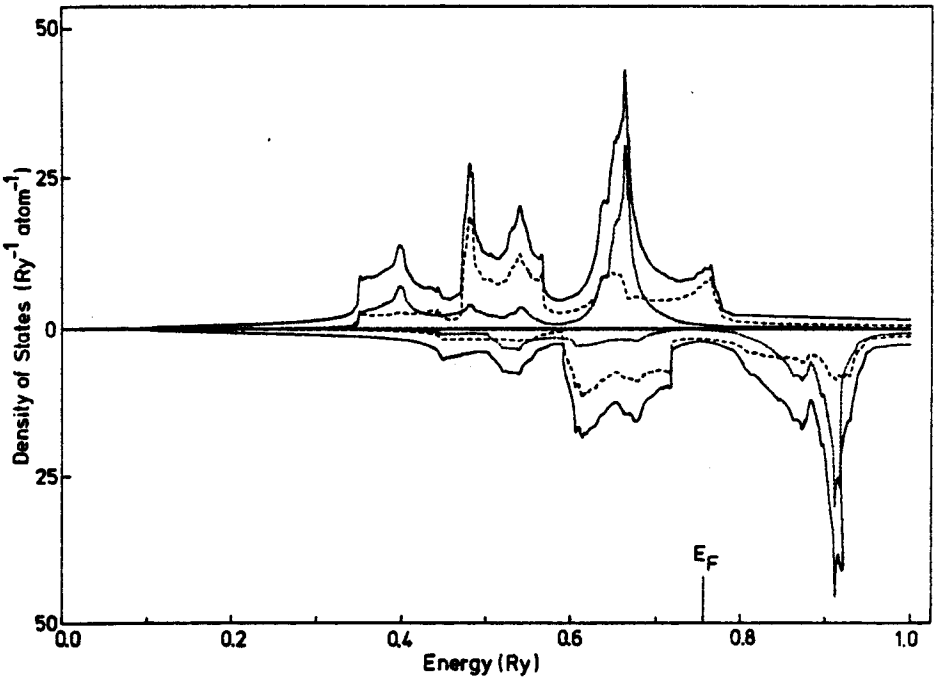

Figure 2.2 Density of States of Iron at bcc Structure

phase. If the calculated spin-down Fermi level has shifted downwards, it is metastable; otherwise, the nonmagnetic phase is a stable state. Both of them are self-consistent solutions of the system. In bcc iron, the irregular density of states makes the ferromagnetic phase more favorable.

Although it is in general hard to distinguish the atomic orbitals in a band structure, in iron such a characteristic is relatively easy to see. As indicated in the band plot, the major spin (spin-up) partially occupies the s and d bands; the partially filled d-band plays a significant role in magnetism in iron (or in other transition metals). According to Hund's rule, the occupation of atomic states with a particular L value will be such to make the net spin maximal. In this case, the d-band only has 6 electrons out of 10 in a filled status. An independent iron atom has a total angular momentum of 4.0 μ_B. In the crystal structure, the interactions between iron atoms will make that value much smaller (~ 2.2 μ_B). Since in ferromagnetic iron, the valence electrons are mainly s and d electrons, the interactions among them are much larger than others. If we consider the problems in terms of atomic orbitals, e.g., when we use the tight-binding method to fit the calculated band-structure, we must first incorporate all interactions between s and d-electrons. For a complete consideration, we can also include the p-electrons, because both the majority and minority spin electrons also partially occupy the p-orbital. In the band fitting process using the tight-binding method, for instance, the s-, d-electron-only consideration will result in a secular problem of a 6×6 matrix (s:1; d:5); in a complete calculation involving all the s, p, and d electrons we need to solve a 9×9 matrix problem.

The density of states (DOS) is given by the following formula:

$$N(E) = \frac{\Omega}{(2\pi)^3} \sum_{n\sigma} \int \delta(E - E(n\mathbf{k}\sigma))\, d\mathbf{k} ,$$

where Ω is the volume of the Wigner-Seitz cell. If N(E) is known, then many observable quantities O can be calculated by:

$$O = \int dE\, N(E)\, O(E)\, f(E),$$

where f(E) is the Fermi-Dirac distribution function. The DOS of iron at room temperature is shown in Figure 2.2. An experimental measurement of the DOS can be obtained by X-ray emission spectra. The upper part of the plot is the contribution of spin-up (majority spin) electrons, and the lower part is that of minority spin electrons. Notably in the plot are two peaks: A sharp peak near the Fermi level and a broader peak at lower energy. These structures are important for the stability of the ferromagnetic phase of the material. Suppose we are moving a portion of electrons from the majority spin state to the minority spin state. Due to the low value of the DOS near the Fermi surface, one soon will be transferring the electrons from well below the Fermi energy to high above the Fermi energy, resulting in a sharp energy increase. The high energy cost of this process stabilizes the ferromagnetic phases.

2.2.2 Magnetic Phases

In this section, we will describe some features which are common to most magnetic materials, especially the transition metals. Among them are Fe, Ni, and Co, the most common ferromagnetic materials. Cr is also a magnetic material; at room temperature, its ground state is antiferromagnetic. Rare earth elements are other types of magnetic materials often used in permanent magnets. We will concentrated our discussion on the transition metals, but some of our remarks are also applicable to other systems.

As mentioned in the last section, the partially filled d-band is the basic cause of magnetism in transition metals. The core electrons are all the same as Ar; the valence electrons are, in Fe, $3d^6 4s^2$; in Co, $3d^7 4s^2$; in Ni, $3d^8 4s^2$. Due to Hund's rule, there is net spin (local moment) associated with each atom of these elements. At room temperature, the crystal structures of these elements are different (Fe: bcc; Co: hcp; Ni: fcc), but they are

all ferromagnetic in their ground states. For Cr, the magnetism is associated with the detailed form of the Fermi surface. In a material like Cr, there is still a local moment linked with each atom, but there is alternate long-range order in the crystal in such a way that the macroscopic magnetism is totally lost. It is a so called spin-density-wave antiferromagnetic state. If the macroscopic magnetism is not totally lost but the long range order is still present, the material is in a "ferrimagnetic" phase. Another possibility, even when there is a local moment associated with each atom, is that one sees no long-range ordering at all in the crystal: we call it paramagnetic. Because the local spin in this case cannot be ignored, it is quite different from the state of nonmagnetic materials. Although a particular material will have a certain phase at room temperature, we can force it to adapt any magnetic phase which we are interested to calculate. For instance, we can force the majority and minority spin densities to be exactly the same for a nonmagnetic calculation, and we can also exchange the majority and minority spins at certain atomic sites for an antiferro- or ferrimagnetic state in our calculations. Because the spin-orbit coupling is small, both L and S are good and independent quantum numbers, which allows us to consider only two possible spin directions of electrons: spin-up and -down.

2.2.3 Heisenberg Hamiltonian

The Heisenberg Hamiltonian is known as the following form :

$$H = -\ 2 \sum_{i<j} J_{ij}\, S_i \cdot S_j + H_o$$

where H_o contains all non-magnetic contributions -- it can depend on the magnitudes of the spin but not on its directions; S_i indicates the magnetic moment at atomic site i. J_{ij}, the interaction parameters, represent the energy of magnetic interaction between atom i and j per atom. There is an important assumption in our calculation: We assume that there are only two possible directions for the spin of an iron atom, spin-up and spin-down. This

would reduce the above Hamiltonian to an Ising-like model. However, there are two reasons for us to keep the three dimensional nature of atomic spins: 1. In order to be able to look at some spin waves and related properties; 2. Quantum mechanical corrections are added later for the results to include three dimensional effects (i.e. factors like S(S+1)).

Although many attempts have been made, there are no analytical solutions available for general cases, only for a few extreme cases (e.g., under very low temperatures). Therefore, one has to apply some kind of approximations. Two possibilities lead to two famous theories in this area: the theory of spin wave excitations, a quantum mechanical treatment of the Heisenberg Hamiltonian, and the molecular field theory, a single-particle statistical mechanical approach.

Ground State (T=0 K)

Let us consider the first nearest neighbor contribution only; later we can extend our discussion to a general case by simply adding other neighbor "shells" one by one. We are assuming that these different shells of neighbors can be considered separately, i.e., they are only "two shell" interactions. Hence, we only consider one J instead of all J_{ij}'s.

In the case of J>0, the ground state solution is obvious: all the spins will line up along the same direction to get a ferromagnetic state. If there is no external field, the ground state is infinitely degenerate, because the space is isotropic so that the direction of spins (the same direction for all !) is arbitrary. Usually, this direction is affected by the shape, size, and other geometrical aspects of the crystal.

In the case of J<0, the situation is more complicated. There will be no exact solution for the ground state unless the crystal structure can be mapped onto a two sub-lattice model. In this model, the whole crystal can be divided into two sub-lattices, which are identical in geometry (not necessary in physics), but one is shifted from the other at

some direction by an amount so that one atom's nearest neighbors belong to the other sub-lattice, and 2nd nearest neighbors belong to the same sub-lattice. For example, in a unit cell of the bcc structure the corner atoms belong to a different sub-lattice than the center atoms. An antiferromagnetic state will exist for those crystals having J<0, with each of the two sub-lattices being ferromagnetic, but spins pointing in opposite directions on the two sublattices.

Excitation of a spin wave mode (T>0 K)

J>0: At a low temperature T≠0, there will be a few spins excited to a different orientation, creating pseudo particles called spin-wave modes, or magnons, an energy eigenstate of such an excitation. Just as lattice waves (phonons) are the collective modes pertaining to the motion of atoms in a crystal, spin waves (magnons) are a certain kind of collective motion of spins in a magnetic material. A particular magnon is such a state in a magnetic material that all neighboring spins have certain phase differences and each individual spin is moving at a particular frequency, as indicates in Figure 2.3.

Some detailed calculations show that for small wave vector k, the dispersion relation is $w \sim k^2$, corresponding to the acoustic branch of a spin wave. The gap between ground and excited state of the system will be proportional to the external field present.

J<0: Under the two sub-lattice model, the dispersion relation is $w \sim k$ in contrary to $w \sim k^2$ in the ferromagnetic case, and specific heat behaves as $C_v \sim T^3$, the same as in phonon contribution. In this case, an external field called an "anisotropic field" is assumed to be present in such a way that it stabilizes the crystal structure, since the interaction beyond the nearest neighbors is unknown. Usually, the gap induced by this field is much smaller than kT.

2.2.4 T_c - Mean Field Approach

The previous discussion of the spin wave solution is a beautiful quantum mechanical theory, but it is quite complicated and therefore not so easy to apply. For instance, the quantum mechanical approach cannot give a direct relationship between total energy and critical temperature, one of several basic quantities to describe a magnetic material. A much simpler and more useful approach based on a semi-quantum-mechanical approximation is mean field theory which was introduced many years ago by Pierre Weiss et al.[8-14] By applying mean field theory and statistical mechanics, one can get some physical quantities such as the critical temperature quite easily and directly.

The basic idea of mean field theory (also known as molecular field theory) is that each spin will behave exactly the same if all other atoms were replaced by an effective field (mean field), which is proportional to the magnetization of the crystal. Let us consider the interaction between an atom and its neighbors. By using the Heisenberg Hamiltonian, atom i interacts with its neighbors by a one-body Hamiltonian H_1, which is :

$$H_1 = -\ 2\,J\,\mathbf{S}_i \cdot \sum_j \mathbf{S}_j = -\ g\beta\,\mathbf{S}_i \cdot \mathbf{H}_e\,, \quad \mathbf{H}_e \equiv \frac{2J}{g\beta}\sum_j \mathbf{S}_j\,,$$

where $\mathbf{H}_e$ is called the effective magnetic field, g is the gyromagnetic ratio (g-factor), and ß is the Bohr magneton. The mean field theory implies that, the effective field $\mathbf{H}_e$ can be written as an expression related to the average value of S_j , $\langle S_j \rangle$, rather than the value of S_j itself:

$$\mathbf{H}_e = \frac{2J}{g\beta}\sum_j \mathbf{S}_j = \frac{2J\ Z}{g\beta}\langle \mathbf{S}_j \rangle = \frac{2J\ Z}{Ng^2\beta^2}\mathbf{M} = r\,\mathbf{M},$$

where N is the number of spins per unit volume. Using this form of one-body interaction, we can apply statistical mechanics and compare the results with Curie-Weiss law ($\chi \sim C/(T-T_c)$, describing the paramagnetic susceptibility of a ferromagnet when T is greater than T_c (the critical temperature), to get a formula for the transition temperature :

$$T_c = \frac{2J\,ZS(S+1)}{3k}.$$

Note that here we just include the interaction with first nearest neighbors. A more detailed calculation by W. Jones[8] shows that T_c can be expressed in the following form:

$$T_c = \frac{2J(0)ZS(S+1)}{3k},$$

where J(0) is the k-->0 limit of $J(\mathbf{k}) = \sum_{\mathbf{R}} J_{\mathbf{R}} \exp(i\mathbf{k}\cdot\mathbf{R})$. In this case J(0) includes any order of neighbor interaction within the crystal.

For the case of an antiferromagnetic system, the basic idea is the same except that once again we have to apply the two sub-lattice model to handle the crystal structure. Let $\mathbf{K}_p$ to be the reciprocal primitive translation of the magnetic lattice (which is one of the two sub-lattices), because $\mathbf{K}_p\cdot\mathbf{t} = \pi$ and $\mathbf{K}_p\cdot\mathbf{R} = 2\pi$ ($\mathbf{R}$ is the primitive translation of the magnetic lattice and $\mathbf{t}$ is a non-primitive translation between the two sub-lattices), we only need to modify the formulas of T_c for the ferromagnetic case by changing J(0) --> $J(\mathbf{K}_p)$. Note at this time, T_c is the Neel temperature at which an antiferromagnetic ($T<T_c$) to paramagnetic ($T>T_c$) phase transition will occur, when $T>T_c$, the Curie-Weiss law for antiferromagnets is $\chi \sim C/(T-T_c)$. We have then the following:

$$T_c = \frac{2J(\mathbf{K}_p)ZS(S+1)}{3k},$$

$$J(\mathbf{k}) = \sum_{\mathbf{R}} (J_{\mathbf{R}} + J_{\mathbf{R}+\mathbf{t}} \exp(i\mathbf{k}\cdot\mathbf{t})) \exp(i\mathbf{k}\cdot\mathbf{R}).$$

We can combine the formulas of T_c for either ferro- and antiferromagnetic cases, as:

$$T_c = \frac{2J(\mathbf{K}_m)ZS(S+1)}{3k},$$

where $J(\mathbf{K}_m)$ is the maximum value of $J(\mathbf{k})$. We can see that if $J(\mathbf{k})$ takes its maximum at $\mathbf{k}=0$, we will expect the system to be ferromagnetic below T_c; whereas if the maximum is elsewhere, we will expect that some kind of antiferro- or ferri-magnetic states may exist.

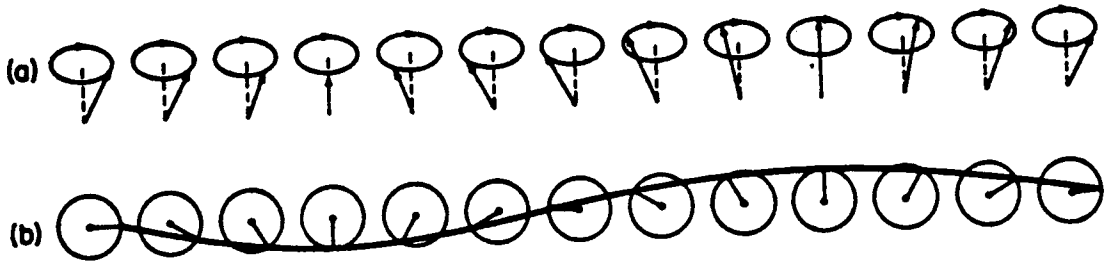

Figure 2.3 Classical Picture of Spin Waves. (b) Same as (a), but seen from above.

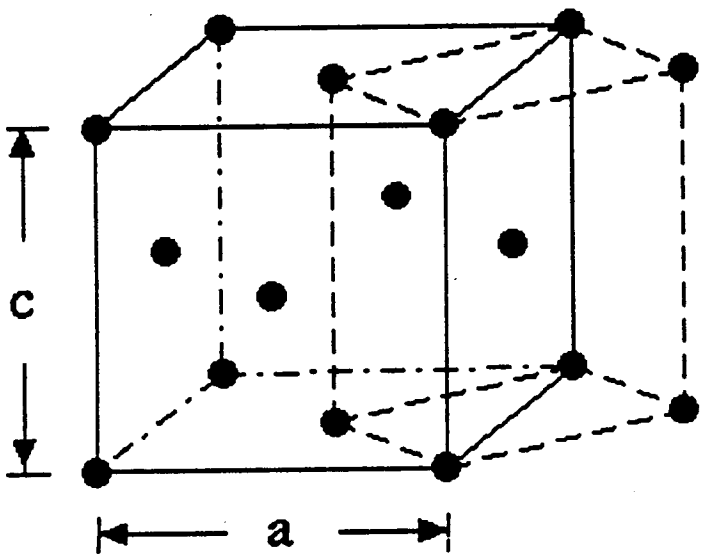

Figure 2.4 Face-Centered-Tetragonal Structure

2.2.5 Spin Waves

Spin waves describe the collective motion of spins in a magnetic material. Figure 2.3 shows a classical picture associated with an array of precessing spins (Ref.8, page 330) in a ferromagnetic material. Like many other forms of waves, or collective motions, spin waves will contribute to the internal energy, specific heat, and many other physical quantities; they exist in any kind of magnetic materials. For convenience, the concept of its own quasi-particles, magnons, was introduced; they can be created (excitation of a spin wave mode) and annihilated (broadening the spin wave mode to a resonance), and these quasi-particles will also have interactions between them. From the model for our total energy calculation -- Heisenberg Hamiltonian, one can see very easily how the spin wave is associated with an excitation mode of spin systems. Rewriting the Heisenberg Hamiltonian by using the operators a and $a^\dagger$, and only leaving the quadratic terms in these operators, we will have:

$$H = 2JSZ\sum_{\mathbf{n}} a_{\mathbf{n}}^\dagger a_{\mathbf{n}} - 2JS\sum_{\mathbf{nm}} \{a_{\mathbf{n}} a_{\mathbf{m}}^\dagger + a_{\mathbf{n}}^\dagger a_{\mathbf{m}}\};\quad \text{where } \mathbf{n} \text{ denotes the atomic site.}$$

Introducing: $b_{\mathbf{q}} = \frac{1}{\sqrt{N}}\sum_{\mathbf{n}} \exp(-i\mathbf{q}\cdot\mathbf{n})a_{\mathbf{n}}$, and $b_{\mathbf{q}}^\dagger = \frac{1}{\sqrt{N}}\sum_{\mathbf{n}}\exp(i\mathbf{q}\cdot\mathbf{n})a_{\mathbf{n}}^\dagger$, the spin wave behavior becomes clear in the following resulting equation:

$$H = \sum_{\mathbf{q}} E(\mathbf{q})b_{\mathbf{q}}^\dagger b_{\mathbf{q}},\ \text{where } E(\mathbf{q}) = 2JSZ\{1-\gamma_{\mathbf{q}}\} \text{ and } \gamma_{\mathbf{q}} = \frac{1}{Z}\sum_{\mathbf{R}} \exp(-i\mathbf{q}\cdot\mathbf{R})$$

As part of our result, we will show the behavior of the quantity $L(\mathbf{q})$, the Fourier transform of J's, which is also directly related to $E(\mathbf{q})$:

$$L(\mathbf{q}) = \sum_{oj} J_{oj}(1-\exp(-i\mathbf{q}\cdot\mathbf{R}_{oj})),\ \text{including up to j-th nearest neighbor "shell".}$$

When $\mathbf{q} \to 0$, it can be written as $L(q) \approx D\,q^2$. The D is defined as spin-stiffness constant, which often describes the behavior at q=o of the acoustic branch of a spin wave. Very

similar to the calculation for phonons, we can also obtain the internal energy and then the specific heat by applying Boson statistics as follows:

$$U = \sum_{q} \frac{h\omega_q}{[\exp(h\beta\omega_q)-1]} \longrightarrow C_v \sim T^{3/2} \text{ (FM) and } C_v \sim T^3 \text{ (AF).}$$

The spin wave excitations relate to our calculation in a fashion that in the bcc structure the total energy differences between the several antiferromagnetic configurations and their ferromagnetic counter parts are assumed to be the corresponding spin wave energies. We also assume in our calculations that the inter-atomic correlation energy is the same for the ferromagnetic and anti-ferromagnetic states, meaning that there is no change in many-body effects between the two cases: only the hybridization effects embodied in the changes of the kinetic energy of the effective non-interacting reference system drive the change of total energy. While practically the total charge density is about the same in both ferro- and antiferro-magnetic iron, the spin density is very different: the regions of zero spin density change their shape in the interstitial region, and on the atoms, the value of the moment is reduced due to its antiferromagnetic environment in which the moment on a number of atoms will point in the opposite direction to form an antiferromagnetic state. This spin density change is the only important difference between the FM and AF cases.

2.2.6 Thin Films and FCT Iron

Thin films are of great interest both in theoretical importance and practical applications.[15-18] In two dimensional cases, e.g., thin films, surfaces, and interfaces, some quantum-mechanical effects can be seen and explained easily by applying simple quantum mechanical theory; this low-dimensional physics usually loses its characteristics and becomes more complicated theoretically in a three dimensional crystal. On the other hand, the term "crystal" we often see in a solid state book, meaning a lattice without limit in

space, seems impractical. In the real world, any crystal has its own boundary; it is a practical problem how to explain the associated low-dimensional phenomena. Moreover, thin films are very interesting because of their own applications as new techniques develop, although the complexity in making low-dimensional devices seems to be inversely proportional to the complexity to analyze them in theory.

For instance, thin film technology is very important in magnetic recording media. Due to the magnetic anisotropy, it is very likely that in a thin film the spins have a tendency to be parallel to the surface, because the shape makes such a configuration more favorable by reducing the magnetic dipole energy. In this case, we need a large in-plane magnetic anisotropy for the recording media, to avoid the information stored in the media being easily destroyed by a weak field. Current experimental investigations focus on obtaining films with a perpendicular moment, which would allow for a larger density of bits on the medium.

A thin film is typically grown on an appropriate substrate. Although such a substrate is often chosen to match the lattice constant of the thin film, they will never fit perfectly. Thus a distortion between the film and the substrate is present. In the case of an iron thin film grown on copper, such a distortion is believed to be face-centered-tetragonal (fct) like: the film will adopt the lattice constant in the surface because of the stress the substrate applies on the film, and "eventually" will have its own lattice constant in the direction perpendicular to the surface. By "eventually", we mean that after the transition region, typically about 1~2 atomic layers, the vertical lattice constant will stabilize. The transition region is determined by the screening length in iron: it is on the order of several angstroms in a metal. An iron thin film is normally grown with a thickness up to ~10 atomic layers. Except for the first few layers being distorted, the rest of the thin film is similar to a bulk system of face-centered-tetragonal iron. In this sense, a calculation for the bulk fct iron system will be very meaningful to investigate the electronic properties of iron

thin films. Thick iron films all have defects near the interfaces in order to transform to the bcc structure.

At room temperature, iron has a bcc structure (α-Fe, from 0-1184 K) until at higher temperature it becomes fcc (γ-Fe, from 1184-1664 K). At even higher temperatures until the melting point, it is in a bcc structure again (δ-Fe, from 1664-1809 K). At normal pressure, iron is never in a fct structure unless it is grown on a proper substrate as described in the last section. Fct is a fcc structure which has been stretched or squeezed along the z direction, as shown in Figure 2.4. It has the same lattice constants in two dimensions and a usually different lattice constant in the third. Bcc and fcc are just two special cases of fct structures: when a=c, it becomes fcc; when $a=\sqrt{2}\,c$, it will be bcc. This is why sometimes fct is also refereed as body-centered-tetragonal, since the two are equivalent (just different choice of the unit cell). In our calculations, we cannot change the pressure, but change the dimensions of the unit cell. All the values of the volume are relative to the experimental value.

Since bcc and fcc are two major interesting structures in iron system, we choose our calculated points in a way that these points will: 1. concentrate more or less on the bcc and fcc region with a volume near the experimental thin film value; 2. they will also be dispersed over the whole fct c-vs-a plane to expose any interesting behavior other than high symmetry region, and concentrate our attention on regions with an extremum in the total energy if any of them are found in the calculations. This way to locate the points for our *ab initio* calculations is of course not optimal. The strategy to obtain the maximum amount of information out of the minimum number of points is non-trivial in our case, since it has to depend on the physical information involved. However, our method turns out to be practically very feasible, economical, and effective. In iron, we will not expect many fast-varying local structures in the total energy behavior on the c-vs-a plane; rather, it will be quite smooth and insensitive to the changes of c and a values. It is because we expect that

each of the matrix elements of the Hamiltonian will have rather smooth dependency on c and a values.

2.2.7 NM vs FM, LS vs HS Phases

As we mentioned before, a ferromagnetic (FM) state is a state in which all spins are aligned along the same direction. In iron, however, there exists evidence that these spins could have different values. When the local moment is large it is called high-spin (HS) FM state, or with a low local moment it is called a low-spin (LS) state. In the language of density functional theory, if these spin states correspond to the global or local minima in E-ρ space, they are relatively independent and well isolated. In other words, if one starts from one particular FM state to calculate a neighboring structure in the c-a plane and proceeds very carefully (i.e, small mixing percentage and a small change in c and a values), one is able to end up with the same type of FM state. Some of the local minima, however, may be very shallow, and if one is not very careful in the calculations, it is possible that the calculation ends up with the global minimum and transfers to a different FM state; in some cases, the calculations do not converge at all. Therefore, we follow a strategy that we used many times: first, we use an available FM charge density for iron, perform the calculations for a fct structure, and obtain the ground state (global) total energy and charge density of that structure, which could be in either a HS or LS phases. This step does not have to be handled carefully, although one still has to ensure the calculation does not diverge. Then in the next step, we expand the calculations CAREFULLY to neighbor points, in order to guarantee that the calculation is for the same FM state.

As we perform the calculations for the nonmagnetic (NM) phase, we force the major and minor spins to be exactly the same so there is no net moment associated with each atom and in the interstitial region, although that does not imply we totally ignore the

spin freedom. In E-ρ space, NM could either correspond to a global or local minimum, or even to a maximum, depending on its energy compared to other phases.

Along the boundary between the NM and FM region (by which we mean the regions where the NM or FM, respectively, is the ground state of the system), there is a phase transition from NM to FM. Yet there is also a phase transition from the HS-FM to the LS-FM state. Because the spin wave contribution to the specific heat, $C_v = \kappa T^{3/2}$ and the constant κ depends upon the values of S, both of these phase transition are first order due to the discontinuity of S.

Most of the recent work on iron shows that the FM state is the ground state for bcc iron and the NM (or AF, being essentially degenerate with the NM) state is more favorable for the fcc structure (Wang; Moruzzi; Hathaway)[3-4,19]. By using a general-potential LAPW method which is very similar to ours, Wang, etc.[3] also found the evidence for the coexistence of two FM metastable states: a small-volume, low-spin, large-bulk-modulus state, and a large-volume, high-spin, small-bulk-modulus state with higher total energy values. In their work on transition metals, Moruzzi, etc.[4] support the idea of the coexistence of two spin states using a nonrelativistic augmented-spherical-wave calculation and a fix-spin-moment technique, in which dependence of the total energy on the moments can be studied thoroughly. With increasing volume from the equilibrium value of the NM state, the system undergoes two successive phase transitions, from NM to LS to HS. In our calculation, we performed the calculation for the LS phase in the fcc region as well as a few points for the HS phase, and the results are consistent with these previous studies.

2.2.8 AF vs. FM in FCT Structure

In antiferromagnetic calculations, the procedure is slightly different. In this case, we always start with a FM calculation for a fct structure from an available charge density.

Since the FM phase could now be either the ground or excited states (in the latter case, it then corresponds to a local minimum), this step should be performed very carefully, i.e., the structure should be very close to the starting structure. In the second step, we flip the spin to the opposite direction at some desired atomic sites by exchanging the major and minor spins, to set up the initial charge/spin density for the antiferromagnetic calculation. For a fct structure, the flipping is performed at the site of the center atom of the equivalent bct structure, so that the two-sublattice model holds near the bcc region. The rest of the task is to bring the AF calculation to self-consistency and calculate the total energy differences between the FM and AF configurations. Unlike in the bcc structure, in general, the AF phase can in this case be either the ground or an excited state (corresponding to global or local minimum respectively) of the fct system.

The symmetry is an interesting point in the AF calculations. After spin flipping, the original bct (it is convenient to consider fct as bct in this discussion) structure becomes a tetragonal structure with two atoms in a unit cell, one is a spin-up atom and the other is a spin-down atom. The crystal symmetry is exactly the same tetragonal group as in general cases. However, it is interesting to see the situation in the cubic cases. For bcc (when $a = \sqrt{2}\, c$), the symmetry is still the same cubic O_3 for both the FM (bcc) and the AF (simple cubic) phases. On the other hand, for fcc (when $a = c$), the situation is different: the symmetry is still cubic in the FM phase (fcc), but is NOT cubic anymore for the AF phase (still tetragonal), because the AF 'magnetic lattice' no longer has a cubic structure and therefore the two-sublattice model no longer holds. In our calculations, we have indeed seen features associated with a broken symmetry phenomenon.

There has been a lot of research on the exploration of the antiferromagnetic phases in iron, although these studies are basically concentrated on the cubic structures.[3,20-22] In the bcc case, all the calculations using different methods are quite consistent, confirming that the antiferromagnetic state is unstable around the ferromagnetic equilibrium volume. In

the fcc case, on the other hand, Wang, etc.[3] found that the AF phase is nearly degenerate with the NM phase, having almost the same equilibrium volume and bulk modulus. Their calculation is in contrast to Kübler's work[20] using the ASW method, in which the AF total energy of fcc iron is found lying 1183 K (~7.5 mRy) below the NM counterpart at zero pressure.† However, by using the same ASW method, with the fixed spin moment procedure, Moruzzi, etc.[21] showed recently that the AF total energy is indeed essentially degenerate with the NM phase at equilibrium, in agreement with Wang, etc.. Both calculations imply that at larger volume the AF ordering is more favorable for fcc iron. Some discrepancy between these studies stem from the use of different lattice constants, different choice of exchange-correlation potential, or different use of the muffin-tin approximation. Despite of these differences, most of these calculations are in agreement with the recent experimental results[22] showing that the fcc-Fe(100) films grown on Cu(100) surfaces are antiferromagnetic.

2.3 Numerical Approaches

In our calculations, we perform some numerical tests to tune the parameters to appropriate values. Among the most important are the test of kmax and nkpt as discussed as follows, and we will give some examples for that in the chapter 3.

2.3.1 Test of kmax and nkpt

As seen in our theoretical formalism, the calculations involve the evaluation of integrals in three dimensions over the Brillouin zone to obtain the total energy and other physical quantities. One has to choose a number of discrete points in k-space to evaluate

---

† Computational errors were found later in this work, and after correction the results are consistent with Moruzzi's.

these integrals in a numerical computation. In principle, using more points yields more precise results. For economical reasons, however, one cannot afford calculations with a very large number of k-points (nkpt) since the computing time T is proportional to nkpt. Hence we have to trade off between the two and find the minimum acceptable value of nkpt to perform the calculation. This is the main reason we have tested our calculations with a number of different values for nkpt. A second test one has to perform is changing the number of basis functions used to describe the wave functions of the non-interacting particles in the reference system. This number of basis functions is determined by the value of a parameter called kmax, where kmax is the maximum value of the momentum of the plane wave part of the basis function (only in this reference system). Obviously, for more precise results one has to choose more basis functions and larger value of kmax. Again, there is a limit due to numerical reasons, because the computer time increases like the ninth power of kmax (we are solving the eigenvalue problem of $N \times N$ matrices, where the number of basis functions N is proportional to the third power of kmax).

When we choose the k-points to evaluate the integral, we followed a scheme called maximization of the minimal distance, i.e., maximizing the distances to surrounding k-points which are already there, to ensure that our chosen k-point are near-randomly, non-discriminatively, and as completely as possible distributed to cover the whole Brillouin zone. For related calculations, by which we mean those calculations for which we are only interested in their total energy differences, such as FM calculations for fct structures, the way to arrange these k-points must be in exactly the same relative locations within the Brillouin zone to avoid any possible induced errors. The dimension of the Brillouin zone might change, but its topology will remain the same.

2.3.2 Convergence of E and μ

In §1.1.4, we have already mentioned some convergence properties on iterations of self-consistent calculations, and how we can get converged total energy values from the last few iterations. Now we will focus our attention to more physical convergence problems: the total energy dependence on parameters nkpt and kmax.

In the last section, we explained why we should carry our calculations for a number of nkpt and kmax values to see which value is sufficient for the calculation. Just as the same idea as we used for the iterational convergence, we try the following formula for the nkpt convergence:

$$E = E_{\infty} + f(\text{nkpt}),$$

where f must be in the form of inverse polynomial of nkpt, as:

$$f(\text{nkpt}) \sim (\text{nkpt})^{-p}\,(1 + (\text{nkpt})^{-1} + (\text{nkpt})^{-2} + \ldots)$$

since when nkpt = ∞, E should be equal to E_{∞}. As nkpt is sufficient large, we can ignore the higher order term, and p=2/3. Therefore:

$$E = E_{\infty} + c * (\text{nkpt})^{-2/3}$$

if everything else remains the same. And similarly, we will have the following formula for the kmax convergence, if everything other than the changes of kmax remains the same:

$$E = E_{\infty} + c' * (\text{kmax})^{-12}.$$

Although the above are very useful to obtain the converged values of total energy, one should be very careful in using them, as they are not good at all if the nkpt / kmax parameters are not large enough, and can introduce a large error or inaccuracy. If necessary, the powers in the above equations could also serve as parameters rather than be specified. The price one has to pay is the increase of the computational complexity, because more data points are needed to determine these parameters.

Chapter 3. Critical Temperature of Iron Derived From Total Energy Calculations

3.1 Abstract

We have performed total energy calculations for iron in the ferromagnetic and in several antiferromagnetic configurations. It is assumed that the functional describing exchange and correlation is the same for the ferromagnetic ground state and the anti-ferromagnetic states. The calculated total energies are used to obtain the interaction parameters in a Heisenberg model. From this Heisenberg model we derive excited state properties, where one has to keep in mind that the model parameters are directly based on the ground state *ab initio* results. The nearest neighbor interaction is ferromagnetic and a model which includes only nearest neighbor interactions yields a transition temperature of 1685 K. The next-nearest neighbor interaction, however, is anti-ferromagnetic and reduces the critical temperature to 895 K. Several other physical quantities derived from our model Heisenberg Hamiltonian are discussed.

3.2 Introduction

Although the basic mechanisms giving rise to magnetism in solids are well understood, *ab initio* calculations of many important properties have not yet been performed. Local spin-density functional calculations for iron show that the ground state of bcc iron is indeed ferromagnetic and they yield values for the magnetic moment close to the experimental values.[11] These calculations do, however, not give any information about the excited states in this system. An especially interesting question pertains to the nature of the spin-waves in iron and nickel.[23] Above T_c the atoms still have a local moment associated with them, but these moments have lost their long range order. The amount of short range order is unknown, and this is responsible for the current debate whether above T_c spin

waves still can be seen as collective excitations or if they have lost their identity and are broadened into resonances. Also, the *ab initio* calculations themselves do not predict a realistic value for the critical temperature. Several theoretical methods describing the ferromagnetic phase transition in iron do exist,[24] and parameter values can be derived from band structure calculations.[25-27] These combined approaches give good results for the transition temperature in iron and nickel. They rely, however, on the values of the band energies, and interpret these energies as excitation energies. Although self energy effects in metals are small, this still gives rise to questions. Therefore we follow a different approach to obtain the parameters in a model Hamiltonian description of magnetism in iron and base our results on total energies only, essentially constructing a magnetic alloy similar to the chemical alloys in the work of Connolly and Williams.[28] At this point we need to emphasize that we are not attempting to improve the simple model description, but that we only want to eliminate possible errors in the derivation of the values of the model parameters. One has to keep in mind that only the total energy in density functional theory incorporates many body effects! Obviously, in the local density approximation this is not complete true anymore.

3.3 Total energy calculations of para-, ferro- and anti-ferromagnetic iron

Ab initio total energies for the different spin structures of bcc iron are obtained within density functional theory. We use the local approximation to the exchange and correlation potential, as formulated by von Barth-Hedin and parametrized by Janak.[9-10] Total energy differences change only by about a mRy when we replace this functional with a different local approximation.[29] It is, of course, unknown how these differences in total energy would change using the real exchange-correlation functional. The total energy calculations are performed using the Full potential Linearized Augmented Plane Wave method.[12] All calculations are performed for a value of the lattice constant of 5.40 a.u.,

which is close to the experimental value. Changing the value of the lattice constant will affect the differences in total energy. The value of J_1, for example, will change by about 30% when we perform the calculations at 5.25 a.u., which is close to the theoretical value of the lattice constant.

The main objective in density functional calculations is to minimize the energy functional $E[\rho_\uparrow, \rho_\downarrow]$ representing the total energy of the interacting electrons. The global minimum corresponds to the ground state of the system, and the corresponding densities are the ground state densities of the system. In general, this energy functional will have a number of local minima which in most cases do not correspond to excited states of the interacting electron system. In magnetic metallic systems, however, there are cases where the energy differences between the local minima are small. In iron the global minimum of the energy corresponds to the ferromagnetic state of iron. A local minimum is found for antiferromagnetic iron, but the total charge density is almost the same in both cases. The only important differences between ferro- and anti-ferromagnetic iron are seen in the spin-density in the interstitial region, where the regions of zero spin density change shape, and in the spin-density on the atoms, which is reduced from 2.30 μ_B to 1.93-1.91 μ_B.

The basic crystal structure we are concerned with is a bcc lattice. The 'magnetic lattice', however, can be different. This means that even though all iron atoms are located at bcc lattice points, they can have different spin configurations. The two anti-ferromagnetic structures we have considered so far are shown in Figs. 3.1(a) and 1(b). Our calculations proceed in two steps. First, we perform a ferromagnetic calculation for the crystal symmetry corresponding to the structures we try to obtain as local minima. In the next step, we construct a trial spin-density by inverting the spin-density for the sites which have spin down, and we average the interstitial spin-density in order to start with zero magnetization in the interstitial region. For the two cases shown in Figs. 3.1(a) and 1(b) the calculations

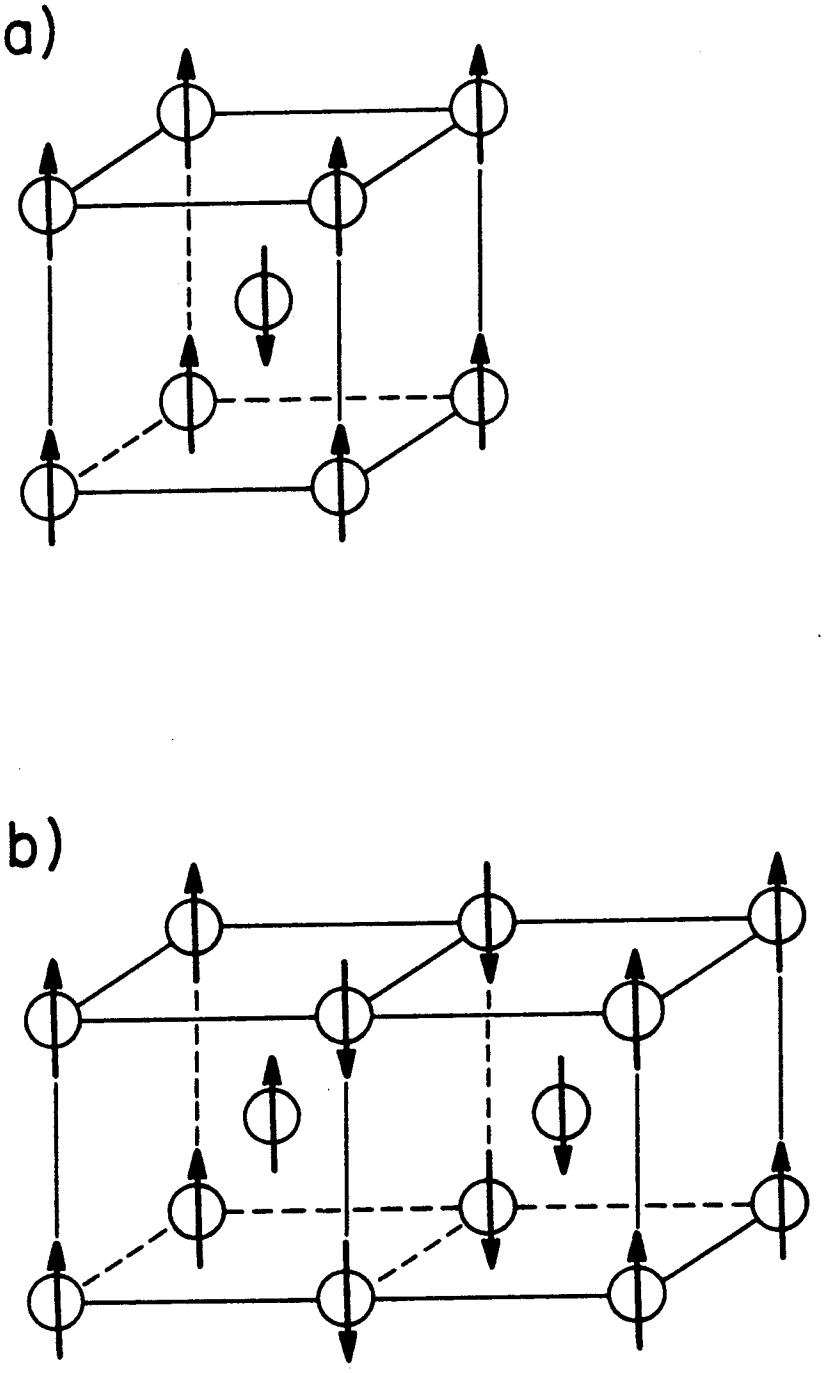

Figure 3.1 Spin structure for the first (a) and second (b) anti-ferromagnetic configuration discussed in this paper.

then converge to a local minimum, although one has to be very careful. The mixing between input and output charge densities in the self-consistent cycle cannot be too large, because it is very easy to set up oscillation in charge density between non-equivalent atoms.

In Table 3.1 we list our results of the total energy calculations. For the total energy and the exchange-correlation energy we have chosen the energy of ferromagnetic iron as a reference point. Additionally, we show in Table 3.1 the magnetic moments of the different sublattices and the interstitial, indicated by m_a, m_b, and m_{int}. The total energy difference between the different spin configurations is smaller than the difference in exchange-correlation energy (Table 3.1), confirming that there is an opposite change in the kinetic energy.

Table 3.1 Total energy per atom (mRy, with 1 mRy of error) relative to the ferromagnetic state, exchange-correlation energy per atom (mRy) relative to the ferromagnetic state, and spin magnetic moment on each site (Bohr magneton).

	E_{tot}/atom	E_{xc}/atom	m_a	m_b	m_{int}
Ferromag.	0	0	2.30		-0.04
Antiferro I	32	58	1.93	-1.93	0.00
Antiferro II	10	39	1.91	-1.91	0.00
Paramag.	34	140			

3.4 Model Hamiltonian

We assume that our calculated total energies are the eigenvalues of a model Hamiltonian of the form:

$$H = -2 \sum_{i<j} I_{ij} \mathbf{S}_i \cdot \mathbf{S}_j + H_0$$

where H_0 contains all non-magnetic effects and S_i pertains to the magnetic moment on site i. We assume that the expectation value of H_0 is the same for all three states we have considered and further simplify our discussion by ignoring the change in magnitude of the magnetic moment between the ferromagnetic and antiferromagnetic results. This reduces the Hamiltonian to the form:

$$H = -2 \sum_{i<j} J_{ij} \hat{\mu}_i \cdot \hat{\mu}_j + \varepsilon_0$$

where μ_i is the direction of the local magnetic moment. By making these assumptions we can directly compare our results with those of reference 25.

3.5 Discussion

Since at this time we have only three data points available, we can derive values for ε_0, the nearest neighbor coupling J_1, and the next-nearest neighbor coupling J_2. The results are ε_0= 8.5mRy, J_1= 2.0mRy, and J_2= -1.25mRy. Compared to the values in reference 26 (J_1 = 1.65 mRy and J_2 = -0.25 mRy) we see that J_2 is different by a factor of 5; it is important, however, that the sign is the same. They are very different from the results in reference 25 (J_1 = 0.65 mRy and J_2 = 0.71 mRy). Within mean field theory one is able to derive a value for the critical temperature of this model Hamiltonian from:

$$kT_c = \frac{2}{3} \sum_{j \neq 0} J_{0j}$$

The conversion factor is 1mRy≡158K. Since this basically corresponds to an extrapolation of our data, our values will be very sensitive to the inclusion of additional coupling constants and our results at this point are only qualitative. Using only J_1 we find a value T_c= 1685K, but including J_2 reduces this value to 895K. This result is consistent with the calculations in reference 25 (see Table 3.2). Additionally, one should add a factor (S+1)/S

in a quantum mechanical treatment. This factor is 1.87 in our case; we did not include it in order to be able to compare directly with reference 25.

Table 3.2 Transition temperature (K) and spin-wave stiffness constant (meVÅ^2)

T_c^{mfa}	T_c^{mf1a}	T_c^{mf2a}	T_c^{Gfa}	T_c^{b}	T_c^{exp}	D^a	D^b	D^{exp}
1220	1420	1250	1051	895	1043	560	145	330

[a]Reference 25; [b]Present Work.

Once we know the values of the coupling constants J we can also derive a value for the spin stiffness constant D.[25] As can been seen in Table 3.2 our results again compares well with the previous results and with experiment, but there is a clear need for including more J_{ij} values.

Finally, in Figure 3.2 we show our curve for the quantity

$$L(q) = \sum_j J_{0j} \left(1 - \exp(iqr_{0j}) \right),$$

which was also calculated in reference 25. We only show data along the [100] direction, since we do not have sufficient information for all directions (our spin structures are both modulated along [100]). The results are similar, the main difference arises from the value of J_2 which is negative (anti-ferromagnetic coupling) in our case but not in reference 25. Again, including more data points might change this value.

3.6 Conclusion

From our results we conclude that obtaining the values of the parameters in a model Hamiltonian, describing the magnetic order in solids, from *ab initio* total energy ground state calculations is a feasible procedure. This offers a realistic approach to understand the excited state properties of magnetic materials, ranging from the spin wave stiffness constant

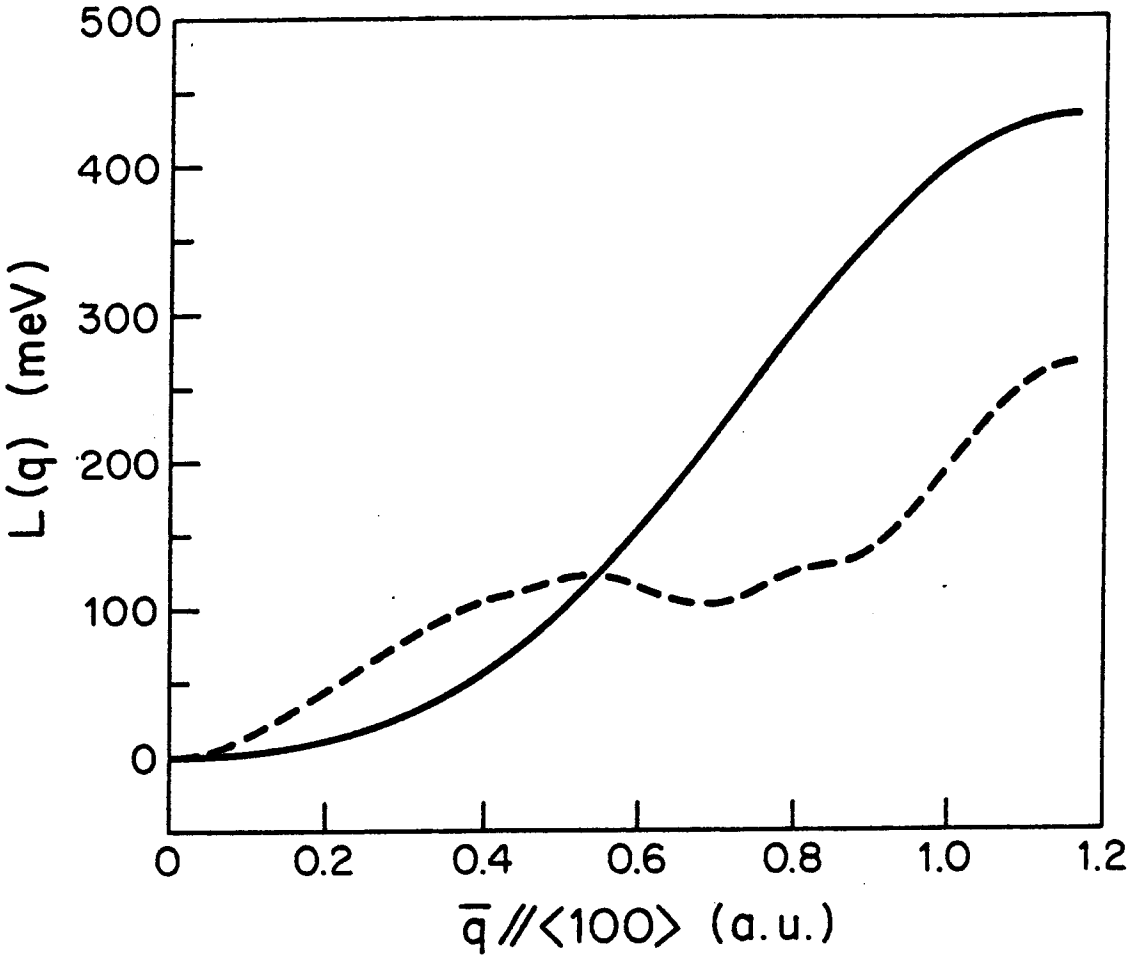

Figure 3.2 Fourier transform L(**q**) of the coupling constants along the [100] direction. The dashed result is from reference 25.

D and the spin wave dispersion relation to the critical temperature T_c and the susceptibility. At this point our results are still very limited and the main conclusion is that we are in agreement with some of the earlier work based on single-particle band-structure calculations.

Our evaluation of the interaction parameters involves a large number of configurations of ferrimagnetic and/or antiferromagnetic states and such calculations can be quite tedious mainly for numerical reasons. At this moment we are extending our calculations to include more configurations, which will allow us to study the convergence of the results as a function of the number of neighbor shells. Obviously, this is very important in order to determine whether our approach makes any sense at all.

Acknowledgement

This research was supported by Office of Naval Research under Contract No. N00014-86-K-0294.

Chapter 4. Inter-atomic Magnetic Interactions in Iron

4.1 Abstract

We have performed total energy calculations for bcc iron in several magnetic structures using density functional theory. The lattice constant was fixed at its experimental value. We have considered the ferromagnetic and several anti-ferromagnetic configurations and used the calculated total energies to obtain the interaction parameters up to sixth nearest neighbors in a Heisenberg model. We assumed that the local density functional describing exchange and correlation is the same for the ferromagnetic ground state and the antiferromagnetic states, with the latter corresponding to local minima of the energy functional. In this approach, the inter-atomic magnetic interactions are pure hybridization effects, due to the kinetic energy term in the total energy. Our parametrized model Heisenberg Hamiltonian yields realistic values of the spin stiffness constant and the critical temperature.

4.2 Introduction

The theories of quantum mechanics and relativity, both essential for an explanation of the basic mechanisms of magnetism in solids, are very old. A number of models describing magnetic solids has been proposed since the development of these fundamental theories and they can be found in several text books[1-2]. The Hubbard model, for example, incorporates an intra-atomic Coulomb correlation and inter-atomic hopping terms. The Stoner model, on the other hand, uses a molecular field approach to relate the magnetic properties of the interacting many-body system to corresponding quantities of a non-interacting system. Although our qualitative understanding of magnetic properties of solids has increased dramatically, all quantative calculations always have to resort to some approximations in order to be feasible.

Density functional theory [5-7] offers a computationally efficient approach to obtain the total energy of the ground state of an interacting electron gas. The total energy is the sum of the many-body kinetic energy, the many-body Coulomb energy, and the external energy (due to the atomic nuclei and external fields). In density functional theory, the first term is approximated by the kinetic energy of a non-interacting reference system with the same charge and spin density, and the second term is approximated by the classical Coulomb energy due to the electronic charge density. The correction term is called the exchange-correlation energy, which is a misnomer since this term also contains contributions from the kinetic energy. This correction term certainly includes all many-body effects and hence it is only possible to give approximate expressions for this term. The standard Local Spin-Density Approximation (LSDA) is based on the results for a homogeneous interacting electron gas. LSDA calculations show that the ground state of bcc iron is ferromagnetic and that the calculated values of magnetic moment are close to the experimental data[11]. These LSDA calculations, however, do not give any information about the excited states in this system. A particularly interesting question concerns the spin waves in a magnetic material. For $T>T_c$ the atoms still have a local moment associated with them, but these moments have lost their long-range order. The amount of short range order is unknown[30], which makes it hard to answer the question whether above T_c spin waves can still be seen as collective excitations or if they have lost their identity and are broadened into resonances.

The presence of spin waves breaks the translational symmetry of a solid. This effect is very similar to the formation of random alloys. A standard computational technique to investigate the electronic structure of alloys within the framework of density functional theory uses the coherent potential approximation. This technique has been applied to the problem of spin waves in iron[27]. In the calculations the directions of the moments on individual atoms are constrained and the corresponding Lagrange multipliers are evaluated.

The same functional form of the exchange-correlation potential is used for all configurations and hence differences in the inter-atomic correlation effects are ignored. This work yields good results for iron, and somewhat larger differences for nickel, which can be explained.

The electronic structure of alloys can also be obtained from a series of simple ordered alloys[28]. In that case the total energy is interpolated as a function of structure and the parameters needed in the interpolating function are obtained by fitting this function to the values of the total energy of the simple reference alloys. A similar technique can be applied for spin waves in iron, where one treats different (anti)ferromagnetic structures in the same way as different alloys[31]. A simple interpolation scheme is based on a Heisenberg model Hamiltonian, and the interaction parameters can be obtained from density functional calculations[25-26]. These latter calculations rely, however, on the bandstructure of the non-interacting reference system and therefore possibly ignore many-body effects. Although self energy effects in metals are small, this still remains a questionable point. In this paper, in contrast to the previous work[25-26] we derive the values of the interaction parameters directly from our calculated total energy data, essentially constructing a magnetic alloys similar to the chemical alloys in the work of Connolly and Williams[28]. Because we only use the values of the total energy, we definitively stay within the limits of validity of density functional theory. Preliminary results were published before[32]. At this point we need to emphasize that we are not attempting to improve the simple model description, but only want to eliminate possible errors in the derivation of the values of the interaction parameters. Also, one has to keep in mind that only the total energy in density functional theory incorporates many body effects and that this is only approximately true in the LSDA theory.

4.3 Details of the Total Energy Calculations

The main objective in density functional calculations is to minimize the energy functional $E[\rho_\uparrow, \rho_\downarrow]$, representing the total energy of the interacting electrons. The global minimum corresponds to the ground state of the system, and the corresponding densities are the ground state densities of the system. In general, this energy functional will also have a number of local minima which in most cases do not correspond to excited states of the interacting electron system. The exchange-correlation potential is defined as the difference between the true ground state energy and the ground state kinetic energy of a non-interacting system plus the Hartree Coulomb energy. If the electron correlation is very different in the excited states, the exchange-correlation energy will be different too. A well-known example is the calculation of the optical gap in semiconductors, where straightforward LDA calculations give wrong results because of this difference in correlation energy[33]. In metallic systems on the other hand there are many excited states for which the correlation energy is very similar. In our case, the global minimum of the total energy corresponds to the ferromagnetic state of iron. In our calculations, however, we do find a number of local minima which correspond to antiferromagnetic states. Figure 4.1 represents this situation in a schematic way. On the other hand, not all antiferromagnetic states are associated with a local minimum.

We use the total energies obtained in calculations for several antiferromagnetic structures and assume that they are representative for the corresponding spin wave energies. Therefore, in this paper we, too, ignore differences in inter-atomic correlation energy and only take into account the changes in total energy due to hybridization effects, embodied in the changes of the kinetic energy of the effective non-interacting reference system. In other words, we assume that there is no change in many-body effects between the ferromagnetic and anti-ferromagnetic states. The total charge density is almost the same

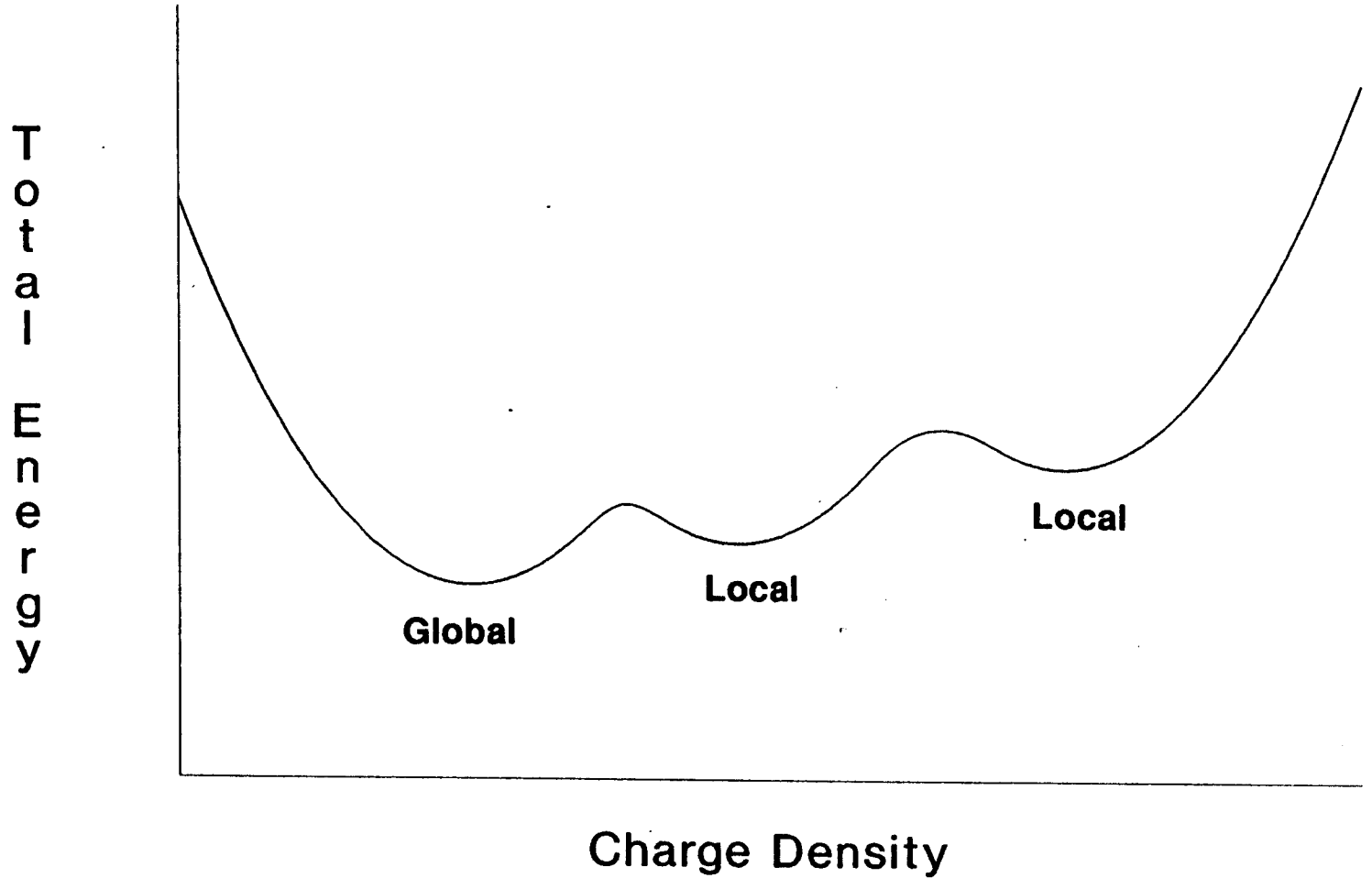

Figure 4.1 Global and local minima in E-ρ space, where the global minimum corresponds to the FM state and local minima correspond to AF states.

in both ferro- and antiferro-magnetic iron. The only important differences between the two cases are seen in the spin-density in the interstitial region, where the regions of zero spin density change shape, and in the spin-density on the atoms, of which the value is reduced from 2.30 μ_B to 1.81-2.14 μ_B. Obviously, the moment on a number of atoms will point in the opposite direction to form an antiferromagnetic state.

The crystal structure of iron at room temperature is bcc. The 'magnetic lattice' , however, can be different. The 'magnetic lattice' is defined when we treat atoms with different spin directions as different types of atoms. The antiferromagnetic structures we have considered are shown in Figure 4.2. In order to include more interaction parameters, one has to find more anti-ferromagnetic configurations for which the calculations converge to a local minimum. Additional configurations will give new information only under the following two conditions: 1. the configuration must have an anti-ferromagnetic state as a local minimum of the total energy (the self-consistent calculations have to converge); 2. the energy of this configuration as a function of the parameters in the model Hamiltonian must be linear independent of all existing configurations. Including a dependent configuration is still useful, since it will reduce the error in the interaction parameters. In our calculations, only 4 out of 5 configurations are independent when using the lowest order interactions and fixed moments.

Our calculations proceed in two steps. First, we perform a ferro-magnetic calculation for the crystal symmetry or the 'magnetic lattice' pertaining to the structure for which we try to obtain a local minimum. The energy value of this calculation will serve as a reference for the total energy of the anti-ferromagnetic state. By only calculating relative energies this way, we reduce errors because systematic errors cancel. In the next step, we construct a trial spin-density by inverting the spin-density for the sites which have spin down, and we average the interstitial spin-density in order to start with zero magnetization in the interstitial region. For all cases shown in Fig. 4.2 the calculations then converge to a

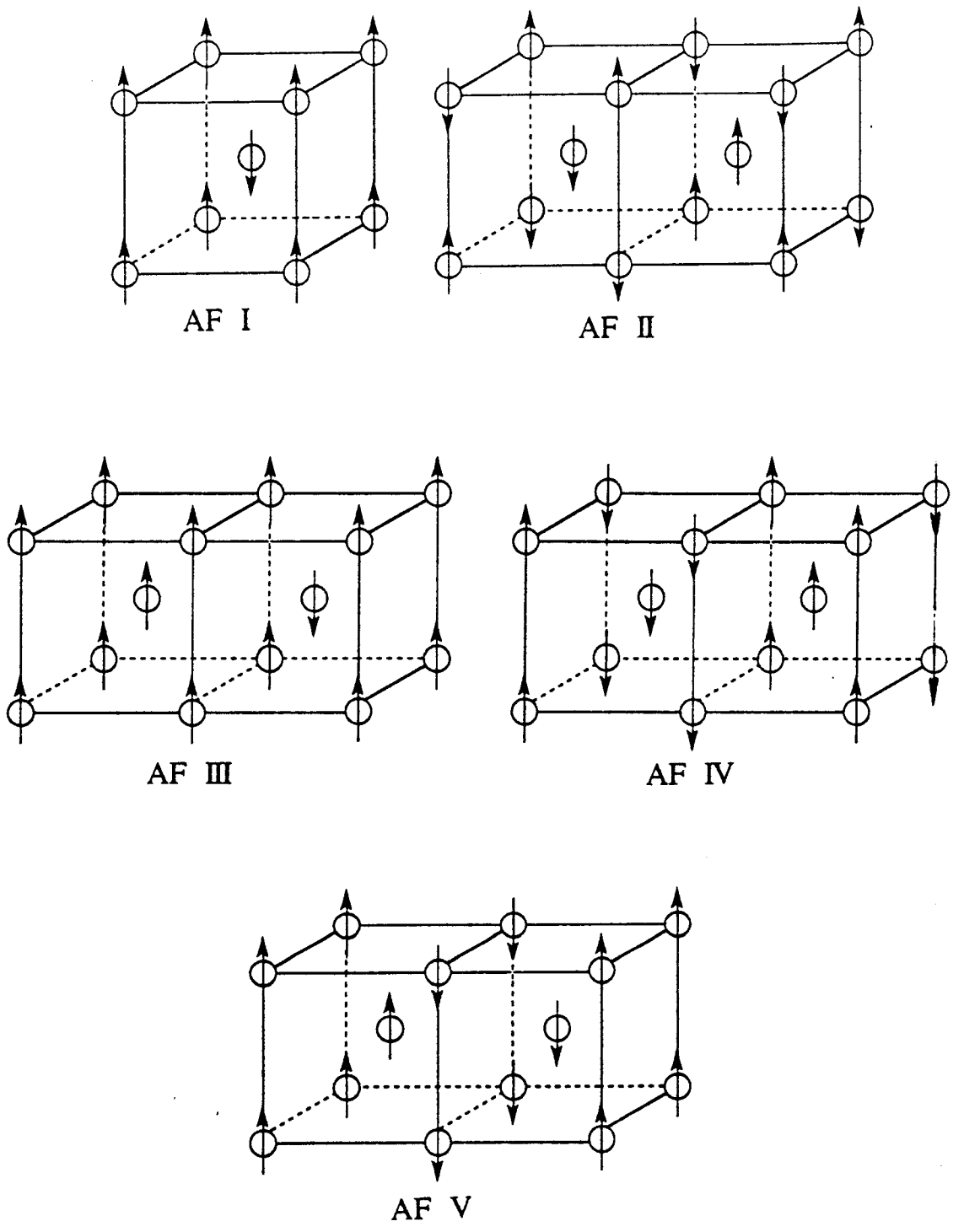

Figure 4.2 Antiferromagnetic configurations (AF-I to AF-V) calculated in this work

local minimum, although one has to be very careful. The mixing between input and output charge densities in the self-consistent cycle cannot be too large, because it is very easy to start oscillations in charge density between non-equivalent atoms.

In our studies we use the Full-potential Linearized Augmented Plane Wave method[12] to obtain the kinetic energy of the non-interacting reference system. The calculations involve the evaluation of integrals in three dimensions over the Brillouin zone to get the total energy and other physical quantities. One has to choose a number of discrete points in k-space to evaluate these integrals. In principle, using more points yields more precise results. For economical reasons, however, one cannot afford calculations with a very large number of k-points (nkpt) since the computing time T is proportional to nkpt. Hence we have to find the minimum acceptable value of nkpt to perform the calculation. This is the main reason we have tested our calculations with a number of different values for nkpt. A second test one has to perform is changing the number of basis functions used to describe the wave functions of the non-interacting particles in the reference system. This number of basis functions is determined by the value of a parameter kmax, where kmax is the maximum value of the momentum of the plane wave part of the basis function. Obviously, for more precise results one has to choose more basis functions. Again, there is a limit due to numerical reasons, because the computer time increases like the ninth power of kmax (we are solving the eigenvalue problem of N×N matrices, where the number of basis functions N is proportional to the third power of kmax).

Table 4.1 Total energy for ferromagnetic and simple antiferromagnetic iron, per atom, in mRy, as a function of kmax. A constant term of -2,541 Ry has been omitted.

kmax	FM	AF	AF-FM
3.5	-83.48	-71.02	12.46
4.0	-91.60	-79.53	12.07
4.5	-92.70	-80.28	12.42

Table 4.1 shows the results of the total energy for different choices of kmax for configuration AF V (at this point, nkpt=30). Table 4.2 shows the effect of changing nkpt at different configurations. The numbers in these tables show that the calculations are sufficiently precise only when nkpt is equal to 30 or more, because the differences between 30 and 60 nkpt are within the estimated error range of our calculations, which is about 1 mRy. Based on similar considerations, a sufficiently large value for kmax for AF V is 4.50. For structures with fewer atoms in the unit cell this value of kmax is also more than sufficient.

Table 4.2 Total energy of the various antiferromagnetic configurations of bcc iron with respect to the ferromagnetic configuration in mRy as a function of the number of k-points in the Brillouin zone.

nkpt	AF I	AF II	AF III	AF IV	AF V
10	31.2	10.9	10.2	25.0	8.4
20	29.4	10.6	11.6	14.6	11.1
30	30.8	10.2	14.0	7.1	12.4
60	29.8	12.0	13.0	6.6	12.4

There is one thing we would like to emphasize here. Although the absolute values of total energy of ferro- and anti-ferromagnetic may be very different for different values of nkpt or kmax, as shown above, we are only interested in the differences between these energies rather than the absolute values. Structure dependent errors, mainly induced by the different ways to divide the Brillouin zone into small tetrahedrons to evaluate the three dimensional integrals or by differences in the basis functions, will cancel each other if we only consider the differences between ferromagnetic and anti-ferromagnetic configurations.

The convergence of the iterations towards a self-consistent solution is not always straightforward. For the anti-ferromagnetic calculations instabilities in this iteration towards

self-consistency often prevent the use of a large mixing between input and output densities used in the construction of the charge and spin densities for the next step in the iterations. In each of iterations of our calculations, we calculated the difference of charge and spin densities, $\Delta\rho_c$ and $\Delta\rho_s$, between the current and previous iterations. At small values of these differences, the total energy behaves as a quadratic function of $\Delta\rho_c$ and $\Delta\rho_s$:

$$E = E_o + \alpha\Delta\rho_c^2 + \beta\Delta\rho_c\,\Delta\rho_s + \gamma\Delta\rho_c^2$$

After several iterations, it is possible to determine the converged values of total energy (E_0) using this extrapolation. This procedure is only valid when one uses a small mixing between input and output densities.

4.4 Model Hamiltonian

Standard local density calculations only yield the total energy of a solid for a relatively small number of geometries. An interpolation between these geometries in necessary. If we only vary the volume of a solid, but keep the symmetry the same, this is easy. Near the minimum of the total energy one can use an expansion in polynomials, or for a larger range of volumes one can use some equation of state, like Murnaghan's equation. Matters are more complicated when more degrees of freedom are involved, especially when these degrees of freedom are related to the electrons, like in our case. One important reason to perform density functional calculations is to improve upon simple models, because the electronic effects can be very subtle! Nevertheless, simple models are very useful since it is not feasible to perform calculations for large unit cells. Our situation is completely analogues to that in alloy theory[28], where an expansion of the total energy in pair- and triplet-potentials is used in order to extrapolate to larger unit cells. These larger cells are needed to reliably calculate the entropy and hence any thermodynamic quantity.

A number of model Hamiltonians exist for magnetic systems. Here we assume that our calculated total energies are the eigenvalues of a model Hamiltonian of the form:

$$H = -2 \sum_{i<j} I_{ij} \mathbf{S}_i \cdot \mathbf{S}_j + H_0$$

where H_0 contains all non-magnetic effects and $\mathbf{S}_i$ pertains to the magnetic moment on site i. All magnetic effects are found in the first term and the expectation value of H_0 is the same for all (anti)-ferromagnetic states we have considered.

In a second model, we further simplify our discussion by ignoring the change in magnitude of the magnetic moment between the ferromagnetic and antiferromagnetic configurations. This reduces the Hamiltonian to the form

$$H = -2 \sum_{i<j} J_{ij} \hat{\mu}_i \cdot \hat{\mu}_j + \varepsilon_0$$

where μ_i is the direction of the local magnetic moment. By making these assumptions we can directly compare our results with those of reference 25 and 26. The use of this simplified model Hamiltonian is justified in reference 25. Although our data could also be interpolated by an Ising like Hamiltonian, we prefer to keep the three dimensional nature of

Table 4.3 Contribution to total energy from different nearest neighbors

	$J_1(111)$	$J_2(200)$	$J_3(220)$	$J_4(311)$	$J_5(222)$	$J_6(400)$
FM	-8	-6	-12	-24	-8	-6
AF I	8	-6	-12	24	-8	-6
AF II	0	6	-12	0	8	-6
AF III	0	-4	-4	0	0	-6
AF IV	0	2	4	0	-8	-6
AF V	0	-2	4	0	8	-6

the spins in the model in order to be able to look at spin waves. The contributions to the terms in the model Hamiltonian from the states we have considered are given in Table 4.3. The linear dependence of J_1 and J_4 is clearly seen, and we only determine the combination J_1+3J_4 from our calculations.

4.5 Discussion

Table 4.4 Total Energy in mRy, and exchange correlation energy in mRy for the antiferromagnetic states, with respect to the corresponding value for ferromagnetic iron. m_a, m_b and m_c denote the integrated value of the magnetic moment in a value of radius 2.25 a.u. around each atom. m_{int} is the corresponding value in the remainder of the unit cell.

	nkpt	E_{tot}/atom	E_{xc}/atom	m_a	m_b	m_c	m_{int}
Ferromag.	30	0	0	2.25			-0.06
	60	0	0	2.30			-0.04
AF I	30	31	58	1.93	-1.93		0.00
	60	30	56	1.81	-1.81		0.00
AF II	30	10	39	1.91	-1.91		0.00
	60	12	38	1.95	-1.95		0.00
AF III (Ferri)	30	14	5	2.31	-2.01	1.99	0.03
	60	13	19	2.37	-1.99	1.95	-0.05
AF IV	30	7	11	2.06	-2.06		0.00
	60	7	27	2.08	-2.08		0.00
AF V	30	12	5	2.17	-2.17		0.00
	60	12	15	2.14	-2.14		0.00
Paramag.	30	34	140	/	/	/	/

The results of our calculations are summarized in Table 4.4. The total energy of the ferromagnetic state is taken as a reference and all other states have a higher value of the energy. The magnetic moments at the different atomic sites refer to the values integrated over muffin tin spheres of radius 2.25 a.u. and the interstitial moment pertains to the

remaining region in the unit cell. The exchange-correlation energy also shows the difference of this quantity with that in the ferromagnetic state. Unfortunately, for the more complicated systems this difference depends on the convergence in reciprocal space and on the convergence to self-consistency and has larger errors (only the total energy is variational). The only conclusion we can draw from this entry is that the change in exchange-correlation energy is large enough to drive the differences in total energy, but that the system also shields these changes, which leads to a reduced value of the change in total energy as compared to the change in exchange-correlation energy. The values of the magnetic moments are generally reduced in the anti-ferromagnetic structures. In the ferri-magnetic structure AF III we find a moment close to that in the ferromagnetic state for the central layer which has nearest neighbors with the same spin direction.

Table 4.5 Interaction parameters with different nkpt (using fixed magnetic moments), in mRy.

nkpt	E_o	J_1+3J_4	J_2	J_3	J_5	J_6
10	16.14	1.95	0.75	0.22	-0.85	0.05
20	13.01	1.84	-0.03	0.01	-0.23	0.03
30	10.51	1.93	-0.66	-0.19	0.17	-0.00
60	10.60	1.86	-0.54	-0.25	0.22	0.02

In Table 4.5 we present our results for the interaction parameters up to the sixth neighbor shell for the model in which the changes in the magnetic moments are ignored. Using 30 points in the Brillouin zone gives an acceptable coverage of the Fermi surface, and we expect that the difference between the values based on 30 and on 60 points gives a measure of the error in the derived values of the parameters. Using less than 30 points is clearly insufficient. Since calculating six parameters based on six data points is not very satisfactory in terms of error propagation, we have also fitted our data to the model

Hamiltonian with a fewer number of nearest neighbors. The results of this procedure are given in Table 4.6 for 30 and 60 points in the Brillouin zone. As we see, adding more parameters does not alter the values of the old parameters significantly.

Table 4.6 Interaction parameters with different nearest neighbors (nkpt=30,60),using fixed values of the moment, in mRy.

nkpt	E_o	J_1+3J_4	J_2	J_3	J_5	J_6
30	12.43					
30	12.43	1.93				
30	11.47	1.93	-0.58			
30	10.62	1.93	-0.52	-0.18		
30	10.54	1.93	-0.66	-0.19	0.17	
30	10.51	1.93	-0.66	-0.19	0.17	-0.00
60	12.31					
60	12.31	1.86				
60	11.63	1.86	-0.41			
60	10.50	1.86	-0.34	-0.23		
60	10.39	1.86	-0.52	-0.25	0.21	
60	10.60	1.86	-0.54	-0.25	0.22	0.02

In Tables 4.7 and 4.8 we show our results using the Heisenberg Hamiltonian including the changes in the size of the magnetic moments. In order to be able to compare with our previous results, we have divided I_{ij} by <S>(<S>+1), with the average magnetic moment <S>=2.30. The results are slightly different, in large part due to a rather arbitrary choice of the scaling with <S>.

Table 4.7 Interaction parameters with different nkpt (using variable magnetic moments), in mRy.

nkpt	E_o	J_1+3J_4	J_2	J_3	J_5	J_6
10	16.59	2.26	0.62	0.23	-1.04	0.06
20	13.09	2.19	-0.27	-0.07	-0.28	0.04
30	10.71	2.36	-0.94	-0.31	0.15	-0.01
60	10.82	2.27	-0.78	-0.38	0.22	0.02

Table 4.8 Interaction parameters with different nearest neighbors (nkpt=30,60), using variable magnetic moments, in mRy.

nkpt	E_o	J_1+3J_4	J_2	J_3	J_5	J_6
30	12.43					
30	13.28	2.11				
30	11.82	2.30	-0.97			
30	10.87	2.37	-0.84	-0.28		
30	10.80	2.36	-0.96	-0.30	0.15	
30	10.71	2.36	-0.94	-0.31	0.15	-0.01
60	12.31					
60	13.15	2.05				
60	12.00	2.20	-0.77			
60	10.79	2.29	-0.60	-0.35		
60	10.69	2.27	-0.77	-0.39	0.22	
60	10.82	2.27	-0.78	-0.38	0.22	0.02

Our result for J_1+3J_4 is similar to the value found in reference 26 for J_1 (1.65mRy), but the value of J_2 is different by a factor of 2 (reference 26 gives J_2=-0.25 mRy). It is important, however, that the sign is the same, which means both calculations indicate that the second-nearest-neighbor interaction is anti-ferromagnetic. On the other hand, our results are very different from reference 25, which gives J_1+3J_4=2.71 mRy, J_2=0.71 mRy, J_3=-0.4mRy, J_5=-0.17mRy, and J_6=0.07mRy. The signs of J_2 and J_5 are opposite, and the value of J_1+3J_4 is somewhat larger. It remains questionable whether such a comparison makes sense, since we only use the model Hamiltonian to interpolate our total energy data, and since the other papers derive the interaction parameters from a different type of calculation. Another interesting point is that the values of interaction parameter decrease quite rapidly as a function of the neighbor distance. The exact dependency of these parameters on the distance R-vector is not known, and can probably only be interpolated by a simple formula at large distances. We did therefore not attempt to fit our data for J_i to such a formula.

Within mean field theory one is able to derive a value for the Curie temperature of this model Hamiltonian. If we take the magnetic moments fixed, the following formula holds:

$$kT_c = \frac{2}{3} \sum_{j \neq 0} J_{0j}$$

Note that in this formula only the combination J_1+3J_4 appears, and that there are no ambiguities due to the fact that we cannot separate these terms. If we include the variation of the magnetic moments this formula is modified and includes <S>, the average magnetic moment:

$$kT_c = \frac{2}{3} \sum_{j \neq 0} I_{0j} \langle S \rangle (\langle S \rangle + 1)$$

The conversion factor is 1mRy=158 K. Since in this situation we basically extrapolate our data away from zero temperature properties, we expect inaccuracies due to the small number of configurations we could include. Also, we neglect changes in the exchange-correlation energy as a function of temperature. We find that the value of T_c is very sensitive to the inclusion of additional coupling constants and that a precise prediction is impossible. Table 4.9 summarizes our results for different choices of number of k-points and number of parameters. We find a value for T_c of about 1100K, which is close to the experimental value. Without a model for the dependency of $J_i(R)$ on the distance R it is not possible to give an error for this result and therefore one cannot draw any firm conclusions. The best one can say is that our results are consistent with experiment, which in itself not something to be expected on obvious grounds. Our results are very similar to those of reference 25, indicating that it is very hard to determine the interaction parameters in an absolute way. They are constructed in a different context in reference 25, but do give similar results for the critical temperature.

Table 4.9 Results for the critical temperature and spin stiffness constant for 30 and 60 k-points, including different number of parameters J_i.

Results with fixed moments			
nkpt	parameter	T_c(K)	D(meV Å^2)
30	1	1624.2	372.0
30	2	1260.4	260.9
30	3	1072.2	135.8
30	4	1108.5	228.0
30	5	1107.3	225.5
60	1	1572.1	360.1
60	2	1312.6	280.8
60	3	1060.6	113.3
60	4	1107.2	231.5
60	5	1116.1	250.0
Results with variable moments			
nkpt	parameter	T_c(K)	D(mev Å^2)
30	1	1780.6	407.8
30	2	1322.2	255.9
30	3	1111.8	79.5
30	4	1129.9	155.8
30	5	1127.8	148.8
60	1	1731.2	396.5
60	2	1369.9	276.8
60	3	1104.2	54.0
60	4	1130.5	164.8
60	5	1139.8	180.3
Results of Reference 25			
Method		T_c(K)	D(mev Å^2)
mfa		1220	
mf1a		1420	
mf2a		1250	
Gfa		1051	
			560
exp.		1043	330

The Fourier transform

$$L(q) = \sum_j J_{0j} \left(1 - \exp(iqr_{0j}) \right),$$

which was also calculated in reference 25 is a useful quantity to analyze, since it can be related to T_c in various approximations. The curvature of this function near q=0 is related to the spin-wave stiffness. Obviously, in this formula one has to separate the contributions from J_1 and J_4. At first we will assume J_4=0. In Figure 4.3 we show how L(q) along a <100> direction changes by including more k-points in the Brillouin zone integration. Figure 4.4 depicts how L(q) changes when including more interaction parameters. The dominant shape of this curve is determined by the nearest neighbor interaction J_1, and subsequent parameters mainly change the features on a more local scale. The previous figures are based on our results for fixed magnitudes of the magnetic moments. In Figures 4.5, 4.6, and 4.7 we compare the results for fixed and variable moments along <100>, <110>, and <111>; the change in J_1 gives a slightly different shape of L(q).

The spin-wave stiffness constant D can be derived from the curvature of L(q) near the origin and the values we found, assuming J_4=0, are given in Table 4.9. They vary dramatically, because the effects of higher order neighbors are multiplied by the square of the distance. In order to determine this parameter better, we need the coefficients I_i up to a much higher order. Nevertheless, our results do have the correct order of magnitude, which again is not an obvious result.

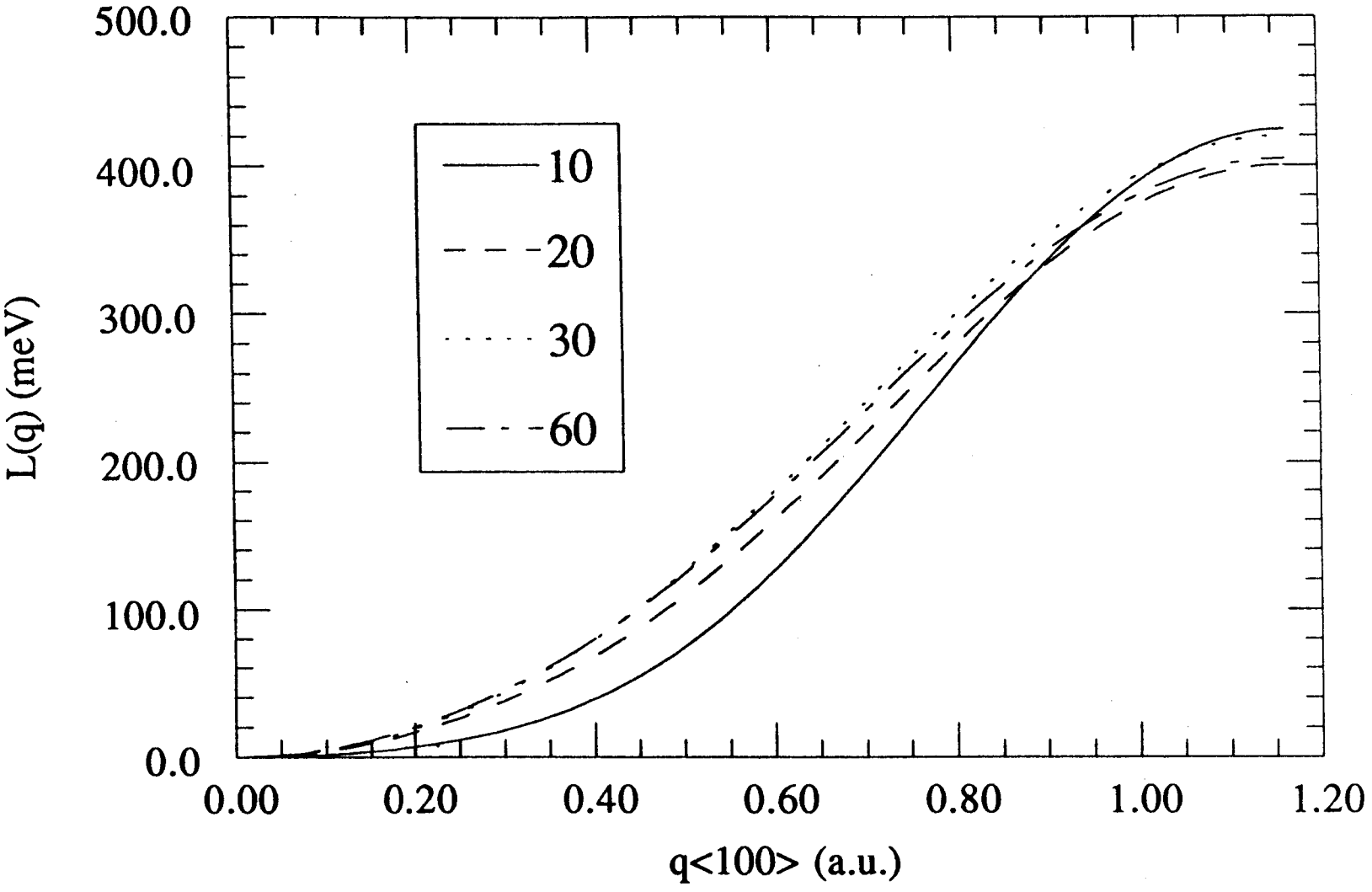

Figure 4.3 L(q) along the ⟨100⟩ direction with different nkpts, using fixed moments.

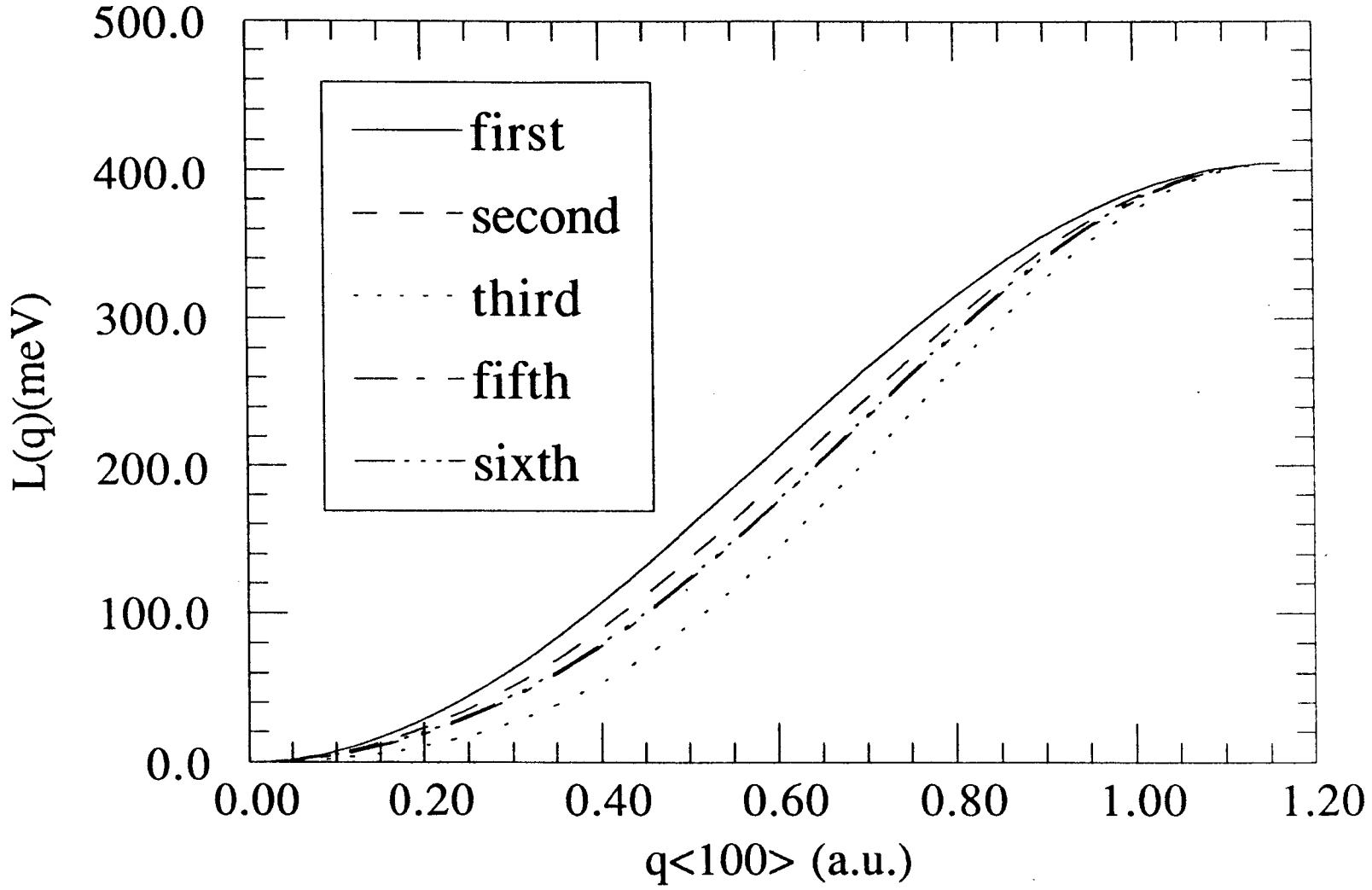

Figure 4.4 L(q) along the <100> direction including different number of interaction parameters, using fixed moments.

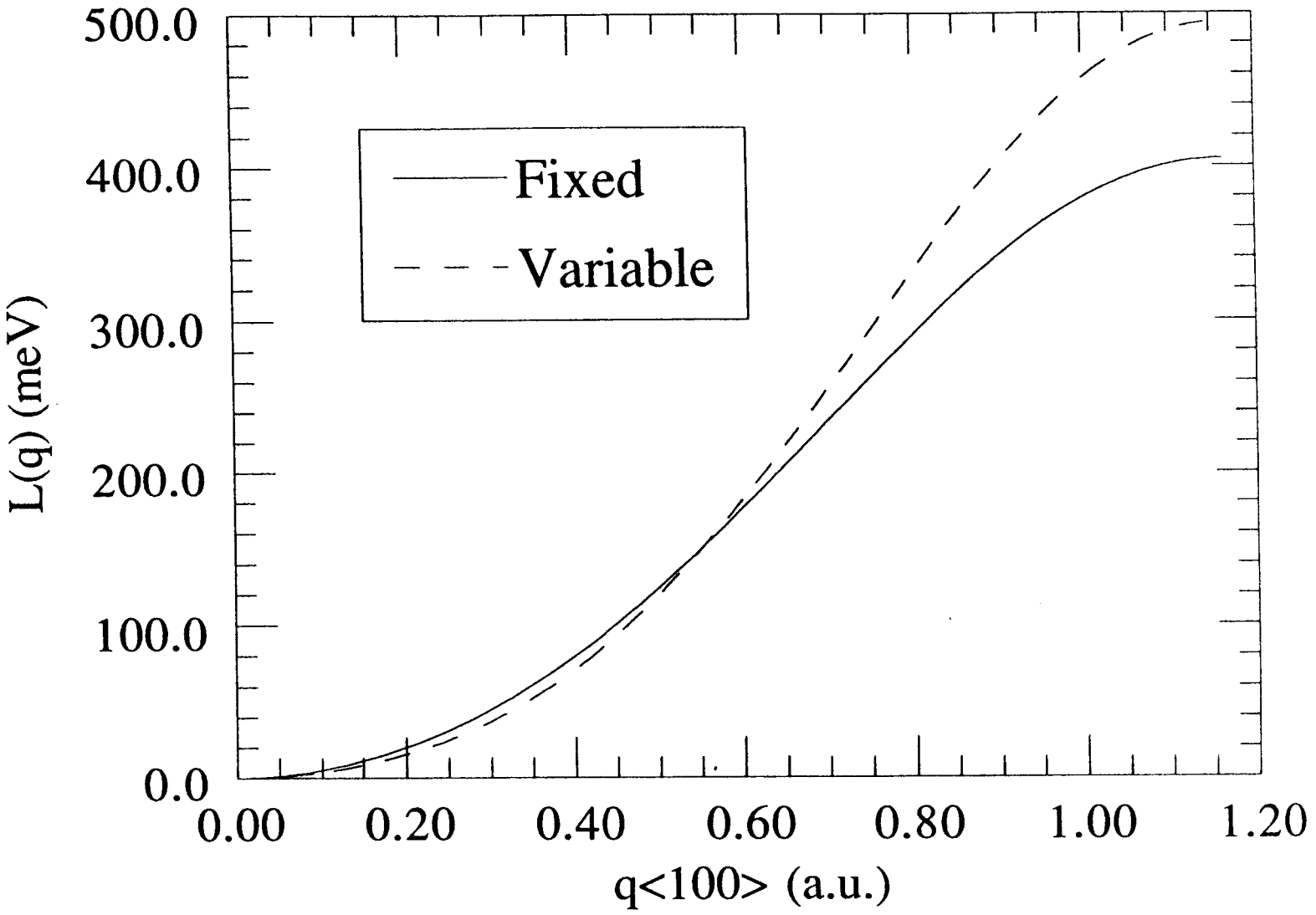

Figure 4.5 L(q) along the <100> direction with fixed moment vs. variable moment (60 nkpt).

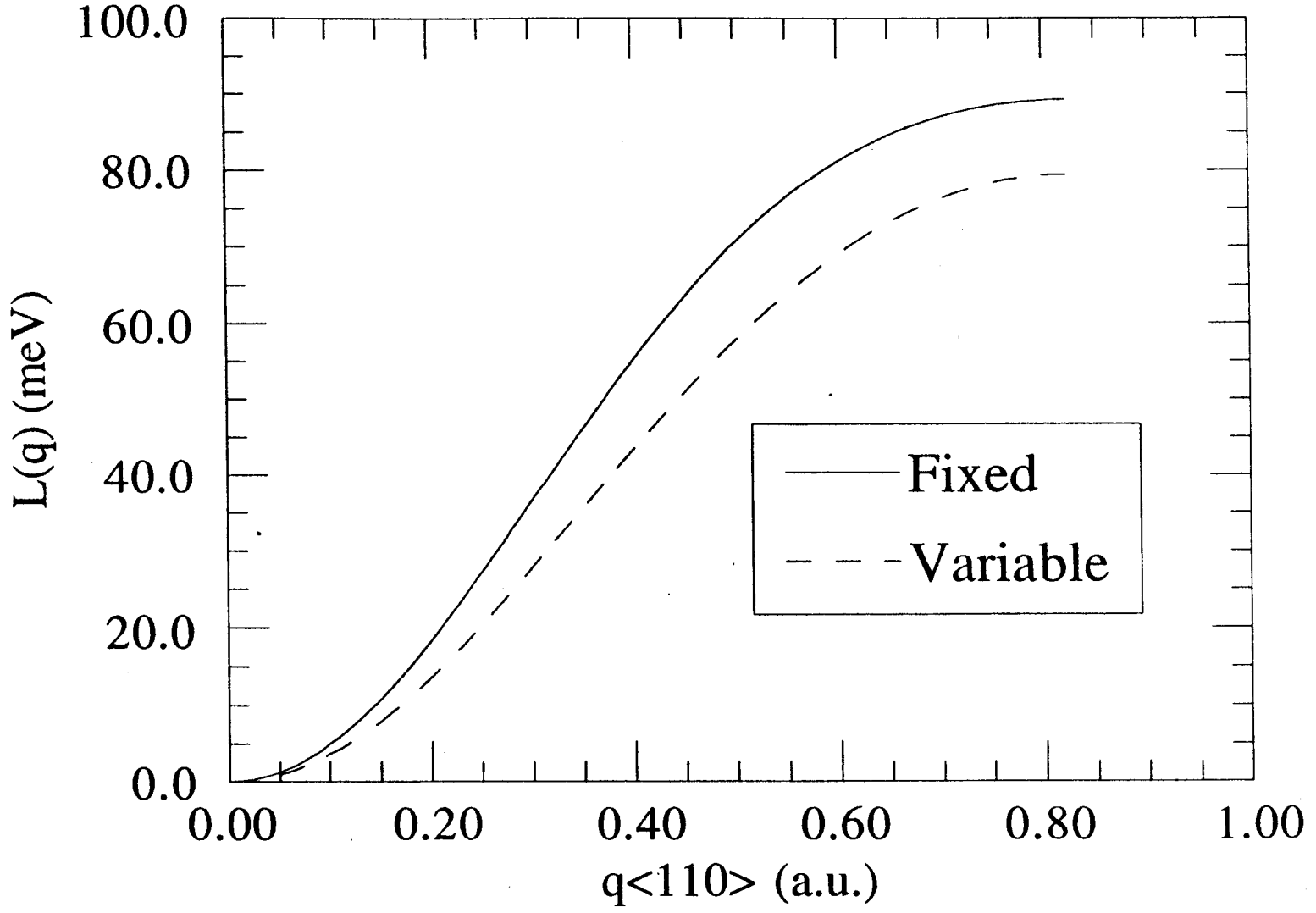

Figure 4.6 Similar to Figure 5, but along <110>.

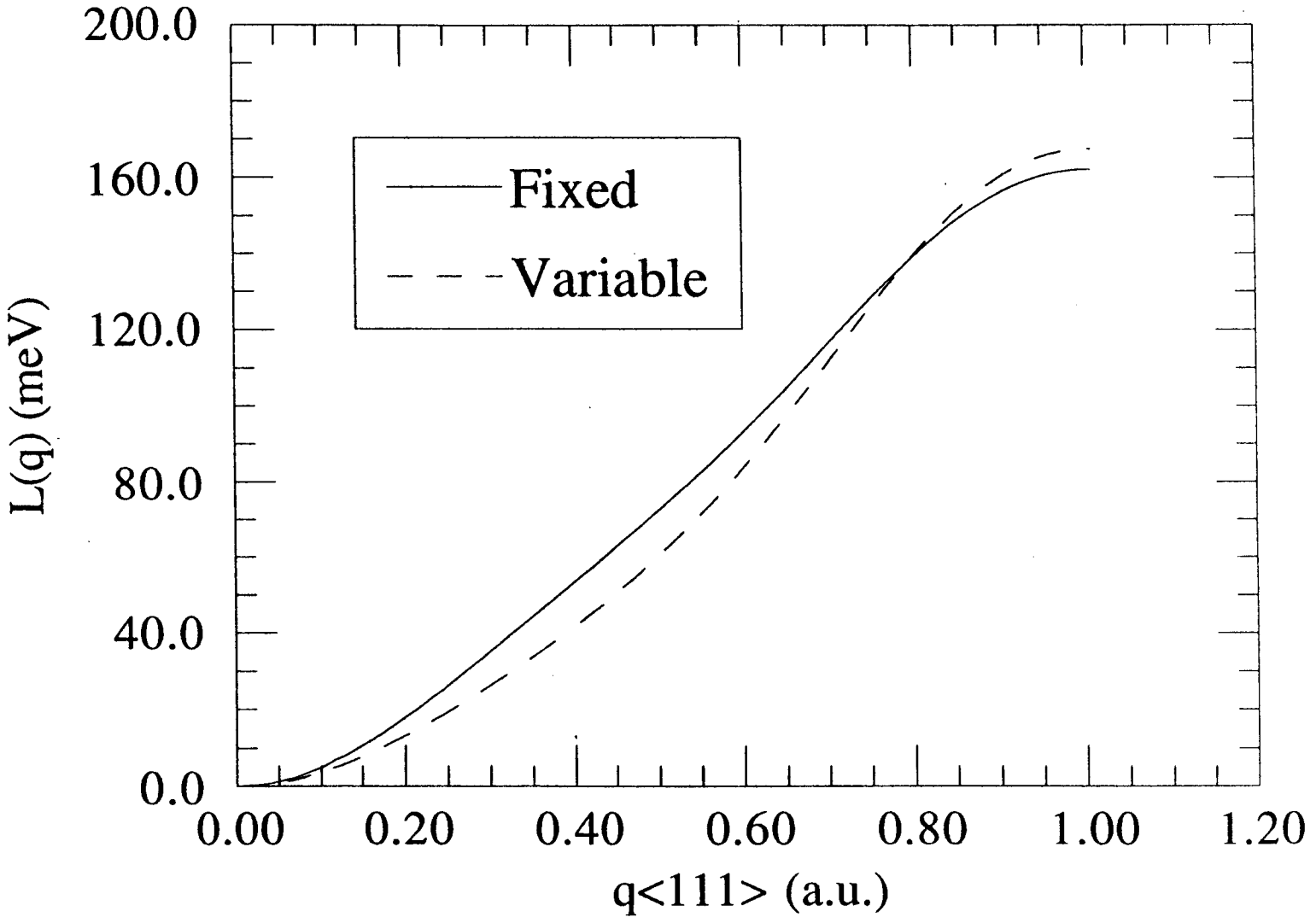

Figure 4.7 Similar to Figure 5, but along <111>.

Finally, we investigate the effects of including non-zero values of J_4. A reasonable range for J_4 is [-0.2, 0.2], and we have chosen five values in this range. J_1 is then determined from the fitted value of J_1+3J_4 for fixed moments. Figure 4.8 shows the results. It is clear that the curvature near the origin varies dramatically, and the corresponding results are given in Table 4.10.

Table 4.10 J_4's Contribution to Spin-Stiffness Constant (using fixed magnetic moments)

	J_4=-0.2	J_4=-0.1	J_4=0.0	J_4=0.1	J_4=0.2
D(mev Å^2)	-58.8	95.6	250.0	404.4	558.8

4.6 Conclusion

From our results we conclude that obtaining the values of the parameters in a model Hamiltonian, describing the magnetic order in solids, from *ab initio* total energy ground state calculations is a feasible and promising procedure, leading to realistic predictions of experimental quantities. This offers a realistic approach to understand some excited state properties of magnetic materials, ranging from the spin wave stiffness constant D to the critical temperature T_c.

These calculations do depend on the specific form of the model Hamiltonian, however, and have to be taken in the context of such a model Hamiltonian. This situation is the same as that in attempts to calculate phase diagrams from first principles and our work is an extension of these schemes to magnetic properties. These calculations of the interaction parameters involve a large number of configurations of ferri-magnetic and/or antiferromagnetic states and are naturally limited to relatively small unit cells, since a high precision of the total energy is needed. It will require a large amount of computer time to include a substantially larger number of interaction parameters in the type of calculation we

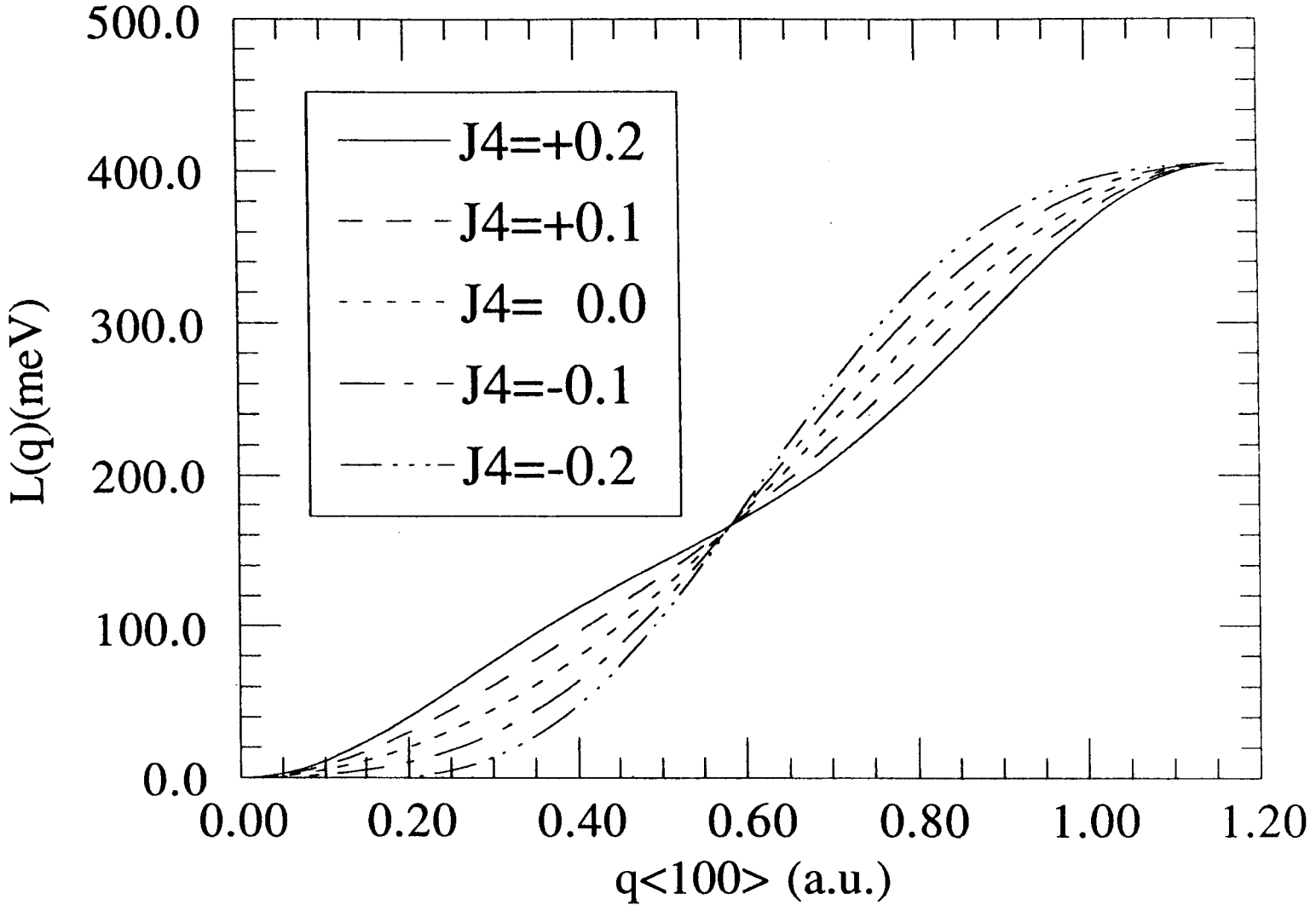

Figure 4.8 J_4's contribution to L(q), along the <100> direction .

have performed, and therefore the errors in the theoretical predictions will remain large. But it is very important that the approach to study low temperature excitations we followed in this paper leads to qualitatively correct results. Therefore, local density calculations along these lines are very meaningful.

Acknowledgement

This work was supported by the Office of Naval Research under contract N00014-86-K-0294 and grant N00014-89-J-1165. This work was made possible by a grant of computer time obtained through the College of Science on the Oregon State University Floating Point system.

Chapter 5. Electronic Structure of Face-Centered Tetragonal Iron

5.1 Abstract

Thin films of iron can be grown in either the bcc or fcc structure when using an appropriate substrate. Since the two lattices never match perfectly, it is to be expected that tetragonal distortions are present. Therefore, we have performed total energy calculations for face-centered tetragonal iron in both the ferromagnetic and para-magnetic states. The standard bcc and fcc structures are two special cases of the face-centered tetragonal space group. There are two minima in the total energy, one near the bcc line and one near the fcc line. The fcc minimum has the lowest total energy. Near the fcc minimum we find a region in the c vs. a plane where our calculations have trouble converging. We associate it with the existence of a low-spin metastable state in this region. We also study the values of the magnetic moments as a function of crystal structure.

5.2 Introduction

The motivation for total energy calculations of face centered tetragonal (fct) iron stems from thin film growth of iron on different substrates. Results of the first experiment in which fcc iron was grown on copper were reported a long time ago[34]. Recent investigations focus on the structural and magnetic properties of such films[15]. Although these studies increased our understanding of the properties of the thin films, there are still questions pertaining to the lattice constant misfit between the film and the substrate. This misfit is believed to produce a fct type of distortion of iron[15]. Thus, a calculation of the electronic structure and total energy of bulk fct iron will give useful information to assist the interpretation of the experimental results.

5.3 Total Energy Calculations of FCT iron

Our total energy calculations are based on density functional theory. In this theory, the energy functional, including exchange and correlation, is used to construct an effective potential in an equivalent set of non-interacting Schrödinger equations. We used the local density approximation, as formulated by von Barth-Hedin and parametrized by Janak[9-10], for the exchange-correlation potential. The semi-relativistic Schrödinger equations are solved using the full potential linearized augmented plane wave method (FLAPW)[12].

The main task in total energy density functional calculations is to minimize the energy functional ($E[\rho\uparrow,\rho\downarrow]$ in the FM-phase or $E[\rho]$ in the NM phase) representing the total energy of the whole electronic system. The global minimum corresponds to the ground state of the system, and it's corresponding densities are the ground-state densities. Local minima of the total energy functional do exist and correspond to metastable states of the system. If the correlation in such a metastable state is very different from the ground state, the local densities approximation will give rise to large relative errors between these states. For fct iron this is fortunately not the case.

In iron, two ferromagnetic phases appear, i.e., a high spin phase (HS, with a high net moment) and a low spin phase (LS, with a low net moment)[4]. In other words, the two ferromagnetic minima, corresponding to the two ferromagnetic phases, are independent (or well isolated) in E-ρ space in terms of the density functional language. Which one is the global minimum of the system depends on the values of c and a. This gives rise to the following interesting situation. If one has the charge and spin densities for a given state of a certain geometry, one can use these densities to start a calculation at neighboring values of c and a. In this new geometry this spin state might not be the ground state, but if one carefully proceeds to self-consistency, it is possible to converge to a metastable state at higher energy! This does not always work, however, because the

metastable minimum might become very shallow (or disappear completely) . For example, using the densities of the low-spin phase for c=4.0 Å and a=3.2 Å to start the calculations for a low spin phase at c=4.2 Å and a=3.4 Å, our calculations did not converge. Going in the opposite direction (from high c,a to low c,a) to perform calculations for the high spin phase did not give any trouble.

Table 5.1 Dependence of the results on nkpt (kmax=4.5) for the reference and point B.

nkpt	E (Ry)	E_B (Ry)	E_B-E (mRy)	μ	μ_B
30	-2541.0675	-2541.0420	25.5	2.181	2.540
60	-2541.0823	-2541.0556	26.7	2.164	2.621
90	-2541.0794	-2541.0531	26.3	2.118	2.658
120	-2541.0808	-2541.0543	26.5	2.115	2.660
150	-2541.0819	-2541.0554	26.5	2.121	2.674

We have tested our calculations for a number of different values of the number of k-points in the Brillouin zone integrations, as shown in Table 5.1. From Table 5.1 we can conclude that the calculations are good enough only when nkpt is larger than 90, since the differences between 90 and 120 nkpt are within the estimated error range of our calculations, which is about 1 mRy. We can also extrapolate our data to get the values of total energies corresponding to infinite number of k-points, using the fact that the total energy is proportional to $(nkpt)^{-2/3}$ when nkpt is large enough. The next test we have performed is to investigate the dependency of the total energy on kmax (Table 5.2), where kmax determines the number of APW basis functions. Based on the data shown in Table 5.2, we conclude that a value of 4.5 for kmax will be sufficient.

Table 5.2 Dependence of the results on kmax (nkpt=30) for the reference and point B.

kmax	E (Ry)	E_B (Ry)	E_B-E (mRy)	μ	μ_B
3.5	-2541.0586	-2541.0322	26.4	2.180	2.541
4.0	-2541.0664	-2541.0407	25.7	2.183	2.542
4.5	-2541.0675	-2541.0420	25.5	2.181	2.540

We are not interested in the absolute values of total energies, but only in the energy differences with respect to a reference point (point O). Many systematic errors will cancel if we only consider energy differences. One important source of random errors is the Brillouin zone integration. The way to divide the Brillouin-zone into small tetrahedrons to evaluate these integrals should be the same for all values of c and a.

Finally, we also investigated the convergence of the iterations to self-consistency. Our programs calculate the norm of the difference between the input and output charge and spin densities ($\Delta\rho_c$ and $\Delta\rho_s$, respectively). Near self-consistency, for small values of these differences, the total energy behaves as a quadratic function of $\Delta\rho_c$ and $\Delta\rho_s$, which looks like:

$$E = E_0 + \alpha\Delta\rho_c^2 + \beta\Delta\rho_c\Delta\rho_s + \gamma\Delta\rho_s^2$$

This is only a good approach if one uses some mixing of input and output densities to start the next iteration. After several iterations, one has enough data to determine the converged values of total energy (E_0) through extrapolation. This technique is important when one can only use small values of the mixing parameter. Most of our results in this paper, however, are well converged.

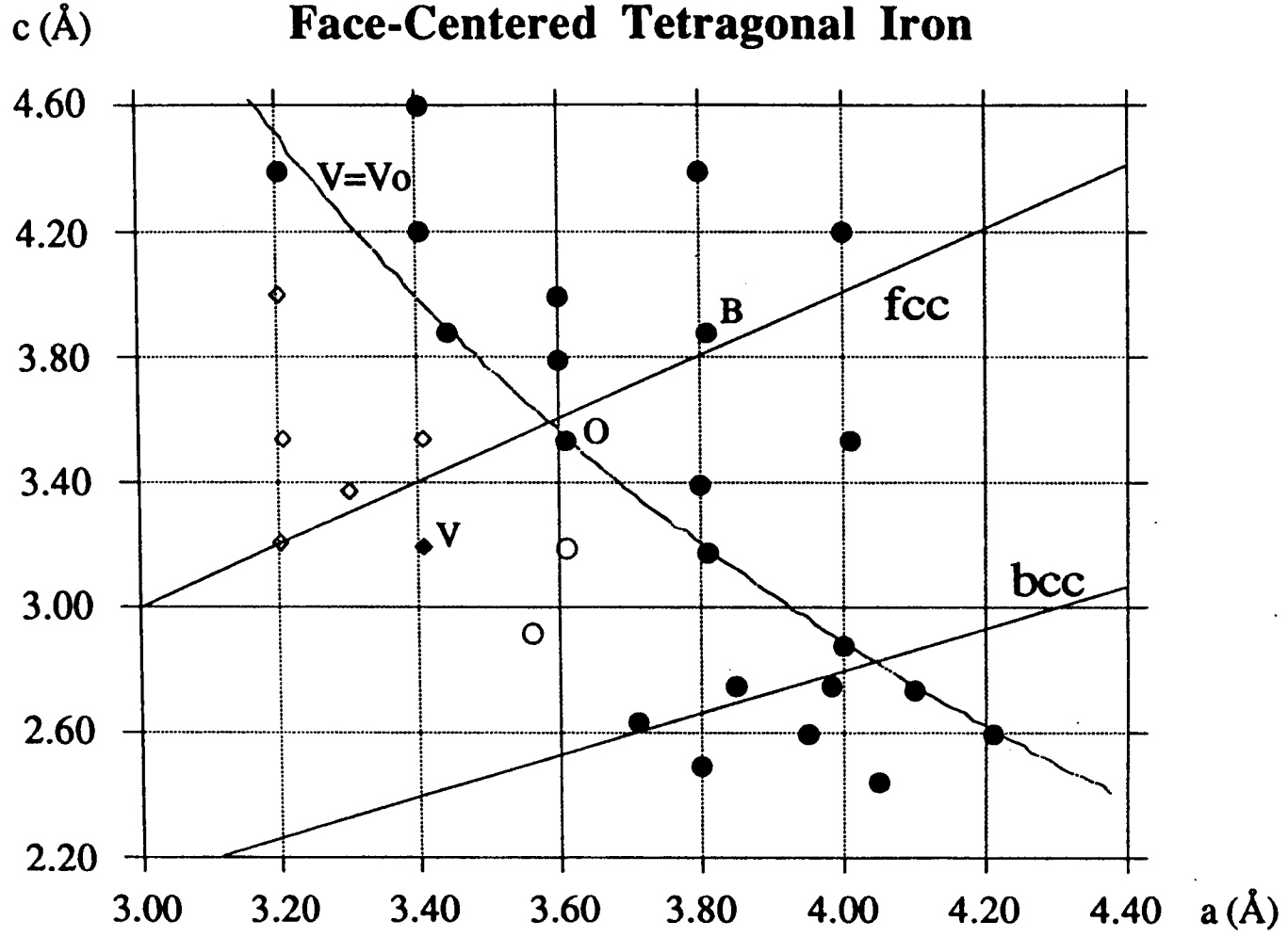

Figure 5.1 Points at which we performed our calculations. The solid lines correspond to the fcc and bcc phases respectively; the dashed line is the experimental equal-volume line. Calculated fct structures include those at which: (•)High Spin phase exists and EM<ENM,(o)HS phase exists and EM>ENM,(♦)Low Spin phase exists and EM<ENM,(◇)LS phase exists and EM>ENM.

5.4 Results and Discussions

The lattice constants of the fct structures at which we performed our calculations are shown in Figure 5.1. We also draw the fcc line, on which a=c, the bcc line, on which $a=\sqrt{2}\,c$, and the equal-volume line corresponding to the experimental value. We performed a calculation of the total energy and the magnetic moment for at least one ferromagnetic phase at every point on this plane; also we performed calculations in the non-magnetic phase for a few points with small volumes.

Figure 5.2 shows contours of constant energy in the plane defined by the volume and the c/a ratio. These contours are constructed from our data points using the Kriging fitting method. As one can see, there are two minima: one is near the fcc line and the other is near the bcc line. The fcc minimum has the lowest total energy, which is consistent with reference 3. These two minima correspond to two (meta) stable states of the ferromagnetic face-centered tetragonal system. At T=0 K, the system will occupy the lowest energy state; at high temperatures, entropy will play a role. The energy barrier between the two minima corresponds to about 1200 K per atom, but this number cannot be related directly to the fcc-bcc transition. Without considering entropy (and phonons) at high temperature the system would have the opportunity to jump back and forth between the two states, making the system unstable.

At present, we do not have enough data points near these minima for the precise locations of them. Therefore, we can only state that our data are consistent with the cubic fcc and bcc phases being (meta) stable. More calculations are needed in order to find possible tetragonal distortions at these minima.

Figure 5.3 shows contours of constant magnetic moment in the same plane. There is a clear separation of the non-magnetic and ferromagnetic region. The transition region is broad because of two reasons: (a) we do not have enough data points to pin down this

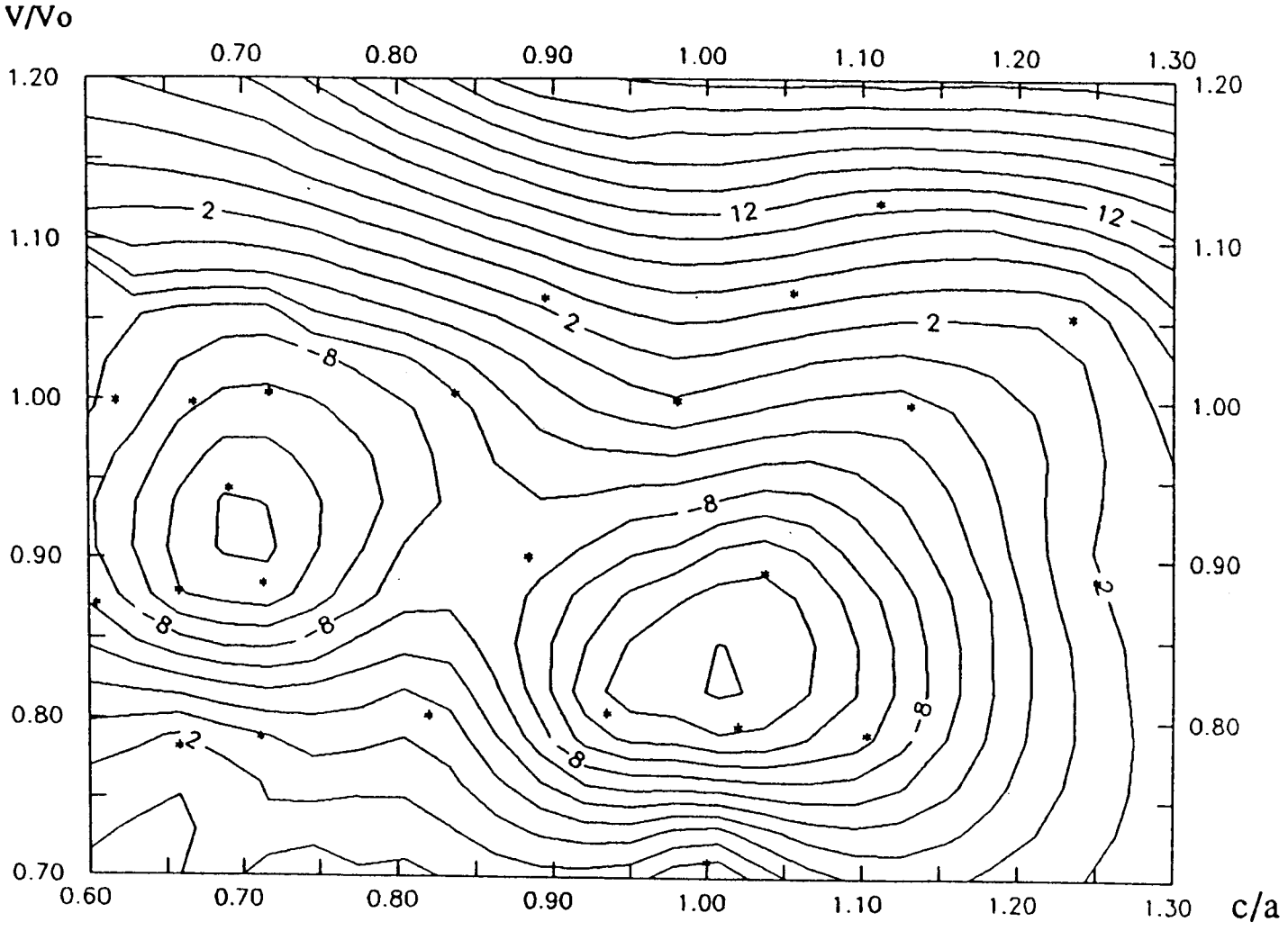

Figure 5.2 Contours of constant energy differences with respect to the reference point (O in Fig.1) on the volume (relative to the experimental value) vs. c/a plane. Data points are indicated by stars.

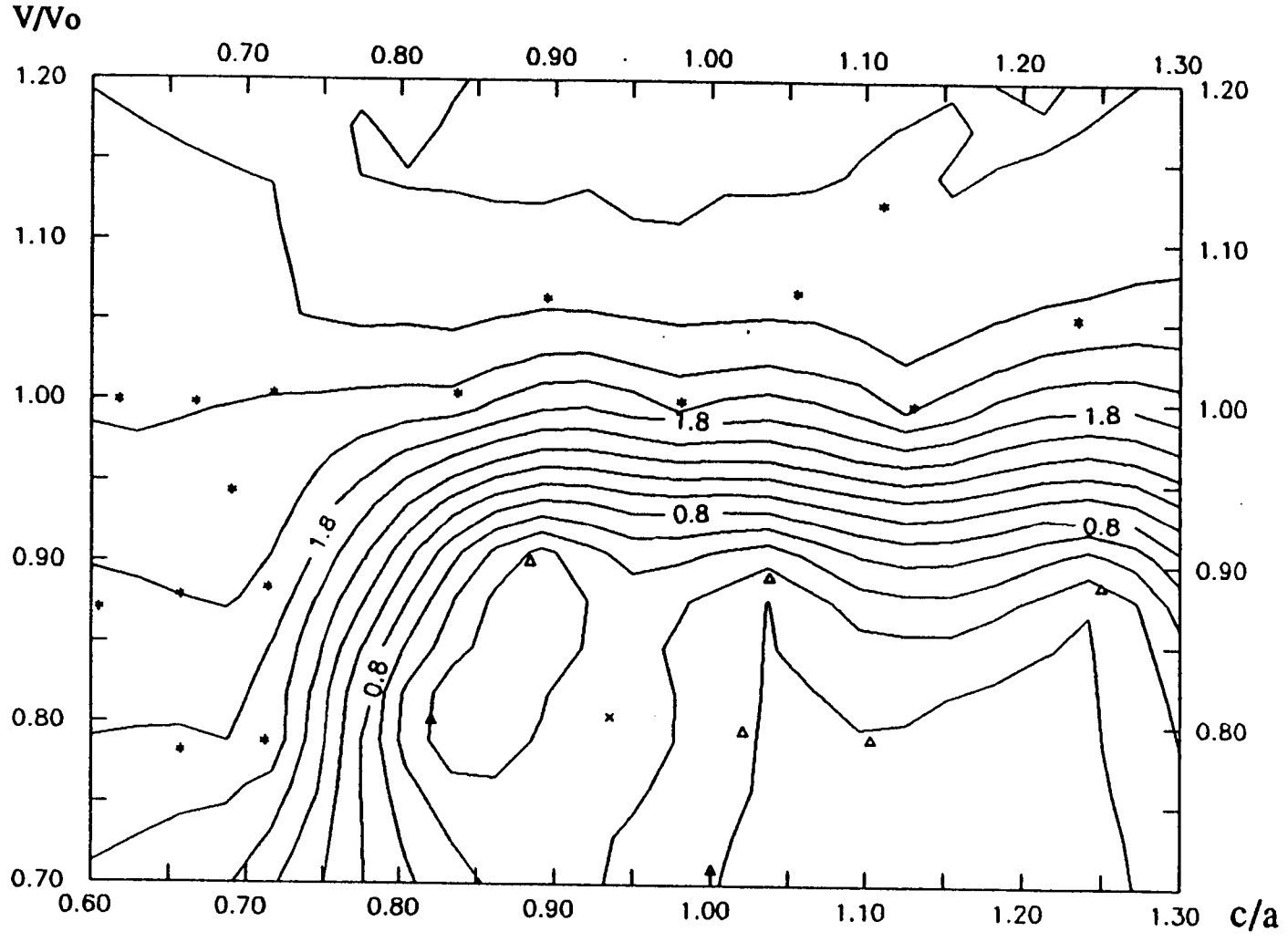

Figure 5.3 Contours of constant magnetic moment on the same plane as in Fig.2.
Calculated points are: (*) high spin phase; (×) low spin phase; (Δ) non-magnetic phase (μ=0).

sharp transition; (b) the error range of 1 mRy for the total energy values will also smooth this transition in a numerical sense. It is possible that near point V the stable state of the system is a low spin state. The difference in energy between this state and the non-magnetic state is very small, however, and calculations with many k-points have to decide which state is stable. Also note that the fcc minimum is near the dividing line between the non-magnetic and ferromagnetic states, again consistent with reference 3.

Because we do not have enough data near the minima, we cannot make quantitative comparisons with earlier work[3,19]. It is important, however, that the locations of the minima are consistent: in Wang's results[3], the fcc minimum is at a=c=3.39 Å, the bcc minimum is at a=3.90 Å, c=2.76 Å; in Hathaway's results[19], the minimum is at a=3.91 Å, c=2.77 Å; both of them are very close to ours, within an error range of about 1 mRy. Also, our results for the magnetic moments are consistent with the results of these two references: in the fcc case we found the same transition behavior from LS to HS as found in reference 3. Our values (μ=2.05) at the bcc minimum compares well with Wang's μ=2.08 and Hathaway's μ=2.07.

Two interesting phenomena are found in our calculations: (a) a phase transition of non-magnetic to ferromagnetic iron, and (b) a transition from a low spin to high spin phase. The non-magnetic to ferromagnetic phase transition line lies close to the experimental equal-volume line at large values of the c/a ratio. Since the total energy differences between two phases at the same structure is often very small and does not change much when the structure changes, it is difficult to precisely determine the position of this transition line. Our results indicate, however, that one could probably not only grow thin films of ferromagnetic iron but also of non-magnetic iron on a proper substrate.

5.5 Conclusion

Based on our preliminary results we can conclude that calculations of total energies and magnetic properties of bulk face-centered tetragonal iron are helpful in understanding the nature of these magnetic materials and the physics of thin film growth. In these calculations, we found two total energy minima (near the fcc and the bcc line), non-magnetic to ferromagnetic, and low-spin to high-spin phase transitions. At this point the calculations are still incomplete, but it is important that we are in good agreement with earlier work for the locations of the two total energy minima, the values of magnetic moments, and the phase transition behavior.

So far the choice of points in the c vs. a plane is more or less arbitrary, based on considerations of physical importance or interest. We fit our results by the Kriging method, which is, of course, not a satisfactory fitting function based on physics. Possible further work includes a more careful choice of structure points which can give maximal information of the system, and a realistic fitting function to the total energy data points. The latter may not be easy. Also, and more importantly, we should have more physical understanding of the results, in relation to questions like whether the minima are exactly (or should be) on the fcc/bcc lines.

Chapter 6. Antiferromagnetism in Face-Centered-Tetragonal Iron

6.1 Abstract

The total energy of face-centered-tetragonal iron is calculated within density functional theory. We have obtained results for nonmagnetic, ferromagnetic, and antiferromagnetic iron. In the range of tetragonal structures we have studied our total energy calculations for the ferromagnetic phase give just two minima: one is nearly bcc (c/a=0.71) and one is nearly fcc (c/a=1). The antiferromagnetic phase yields only one minimum near the fcc structure, but is unstable near the bcc structure. The global minimum in total energy is antiferromagnetic. The difference in total energy between ferromagnetic and antiferromagnetic iron shows an oscillatory behavior as a function of c/a. Our results show that it might be possible to grow iron films with a large in-plane lattice constant that have an antiferromagnetic ordering.

6.2 Introduction

A study of thin films of iron grown on appropriate substrates is very meaningful, both experimentally and theoretically, to understand the nature of magnetism in this old material[34]. Recent research has focussed on structural and magnetic properties of these thin films[15-17]. Very thick films of iron grown this way are bcc with many defects near the interface. For films of about ten monolayers, however, there is not enough energy available to create these defects and the in-plane lattice constants of the film are determined by the substrate. Ideally, one would be able to grow fcc iron, but due to the mismatch between film and substrate there is always a face-centered-tetragonal (fct) type of distortion in the iron films. The screening length in iron is rather short and beyond the first two interface layers the iron film can be considered as bulk iron. Hence total energy calculations for bulk iron will be very helpful because they predict the perpendicular lattice constant as a function

of the in-plane lattice constant, and the energy difference between this strained structure and the ground state.

Our preliminary results for ferromagnetic fct iron have been reported earlier[35]. Since then we completed our ferromagnetic calculations by carefully choosing more points in the c vs.a plane and, more importantly, we also calculated the total energy of a number of points in the antiferromagnetic phase. We found evidence of interesting phenomena we believe are useful in obtaining more knowledge about the magnetic properties of these thin films. Our results are consistent with the work done earlier by V. L. Moruzzi *et al* for antiferromagnetic cubic iron[21,36].

6.3 Theory

Our total energy calculations are based on density functional theory in the local-density approximation[9-10]. We use the full-potential linearized augmented-plane-wave method[12] to calculate the total energy of fct iron. In total energy density functional calculations, the essential task is to minimize the energy functional ($E[\rho_\uparrow,\rho_\downarrow]$ in the (anti)ferromagnetic phase or $E[\rho]$ in nonmagnetic phase) describing the total energy of the interacting electronic system. Here $\rho_\uparrow$ and $\rho_\downarrow$ are the charge densities of spin-up electrons and spin-down electrons; in the nonmagnetic calculations they are forced to be the same. The global minimum corresponds to the ground state energy of the system at the corresponding ground-state densities. In general, this total energy functional will have a number of local minima. In our calculations these local minima correspond to metastable states. In the case of bcc iron near the experimental volume the global minimum corresponds to the ferromagnetic ground state but the antiferromagnetic state is associated with a local minimum in electron-density space. If the correlation in a metastable (excited) state is very different from the ground state, the exchange-correlation functional will be also very different. In that case, a straightforward local-density approximation will give fairly

large relative errors between the energy of the ground state and the excited state. For fct iron this is fortunately not the case because the difference between the ferromagnetic and antiferromagnetic state is mainly due to a difference in hybridization between the electrons on neighboring atoms.

Our calculations are accomplished in two steps: first, we perform a calculation for the ferromagnetic state, which will later serve as a reference point for the total energy of the antiferromagnetic state. In the second step, we construct an initial spin density for the antiferromagnetic calculation by inverting the spin density for the sites which are spin down, and by averaging the interstitial spin density in order to start with zero magnetization in the interstitial region. The calculations then converge to an antiferromagnetic minimum, although one has to be very careful. The mixing between input and output charge densities in each self-consistent cycle cannot be too large, since it is very easy to start oscillations in charge density between non-equivalent atoms.

6.4 Review of our previous work.

We have performed a calculation of the total energy and magnetic moment for at least one ferromagnetic phase at a large number of points in the c/a versus volume plane[35]. We also performed calculations for the nonmagnetic phase for a few points with small volumes. For small volumes near the fcc structure the nonmagnetic phase has a lower energy than the metastable low spin ferromagnetic phase. Figure 6.1 shows that there are two minima in the total energy for the ferromagnetic phase, one is near the fcc line and the other is near the bcc line. The fcc minimum has the lowest total energy, which is consistent with reference 3. These two minima correspond to two (meta)stable structures of the ferromagnetic fct system. At T=0 K, the system will occupy the lowest energy state; at

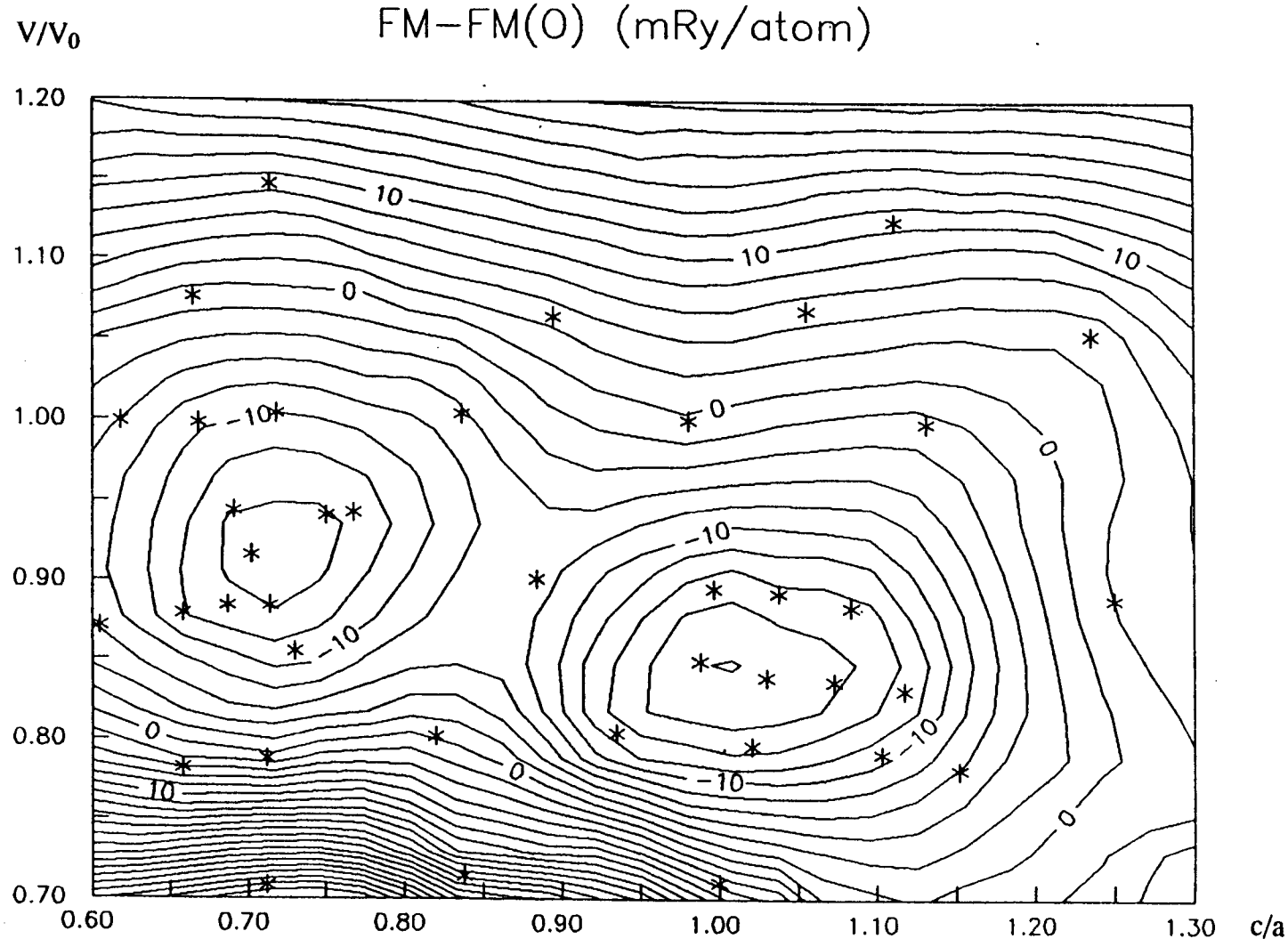

Figure 6.1 Contours of constant energy (in mRy/atom) with respect to the reference point at c/a=0.98, v/v_0=1.00 in the volume (relative to the experimental value) vs. c/a plane for ferromagnetic iron. Data points are indicated by stars.

high temperatures, entropy will play a role. The energy barrier between the two minima corresponds to about 1200 K per atom, but this number cannot be related directly to the fcc-bcc transition. Without considering entropy and phonon contributions, however, the phase transition at finite temperature cannot be determined.

6.5 Antiferromagnetic calculations.

The results for the total energy of the antiferromagnetic phase are presented in Table 6.1. At present, the amount of information obtained in our calculations is still too limited to give a complete picture of antiferromagnetism for the whole fct structure. We are, however, able to compare the data for the antiferromagnetic phase with our previous results near the fcc and bcc minima as well as along the equal-volume line corresponding to the experimental volume for the fct iron films[15-17]. Around the fcc minimum the total energy of the antiferromagnetic phase is 1 mRy below that of the nonmagnetic phase; our relative error is also 1mRy. This fact implies that near the fcc minimum the electronic structure of iron is very likely to favor a phase without a net macroscopic moment, either with or without local ordering, and not a ferromagnetic phase. Hence our calculations still find fcc iron to have a lower energy (by about 4 mRy/atom) than bcc iron, as found in earlier full-potential calculations[3]. In the bcc region, on the other hand, the total energy of the antiferromagnetic phase is far above that of the ferromagnetic state. The difference is about 30 mRy/atom. This result is consistent with our earlier work on total energy calculations for cubic iron[32].

In Figure 6.2 we show the total energy of both the ferromagnetic and the anti-ferromagnetic phase as a function of the c/a ratio for the experimental volume of the fct films. The lines in this figure are just guides for the eye obtained from polynomial fits to the data. At this volume, the total energy of ferromagnetic iron has a minimum for the bcc

Table 6.1 Total energy results (in mRy/atom) for ferromagnetic, anti-ferromagnetic, and nonmagnetic iron as a function of a and c. The values of the magnetic moments (in μ_B) are integrated within a muffin radius R_{mt} =2.10 a.u. around the atoms.

a(Å)	c(Å)	E_{FM}	E_{AF}	E_{NM}	M_{FM}^{sp}	M_{AF}^{sp}
4.00	4.20	67.1	79.8		2.84	2.73
3.81	3.89	29.5	38.4		2.70	2.39
4.01	3.54	29.1	47.7		2.68	2.40
4.40	3.00	28.4	58.4		2.64	2.51
3.20	4.40	6.6	15.0		2.22	1.98
3.44	3.89	-3.0	-5.8	4.7	2.31	1.80
3.61	3.54	0.0	-2.8	0.8	2.13	1.82
3.81	3.19	-6.6	11.8		2.26	1.59
4.01	2.88	-10.3	22.0		2.27	1.60
4.21	2.60	-5.9	13.1		2.26	1.55
4.40	2.38	3.7	12.6		2.15	1.68
3.61	3.19	-4.1	-7.2	-7.2	2.00	0.97
3.95	2.60	-11.7	4.6		2.01	0.83
3.30	3.37	-16.4	-16.4		0.10	0.28
3.41	3.19	-14.6	-15.6	-14.6	0.58	0.46
3.56	2.92	0.1	-2.8	-2.2	0.21	0.40
3.80	2.50	3.8	10.9		1.74	0.52

structure, a maximum for the fcc structure, and a second, local, minimum at a larger value of c/a. This is consistent with the data in Figure 6.1. The bcc minimum occurs at a volume closer to the experimental value than the fcc minimum, and as a result at the experimental volume the bcc phase has the lowest energy. In addition, the structure around the fcc minimum is not elliptic, and the minimum as a function of c/a is pushed to larger values. Between these two minima there has to be a maximum, but it is remarkable that in Figure 6.2 this maximum occurs at the fcc structure. Figure 6.1 shows that this is probably the

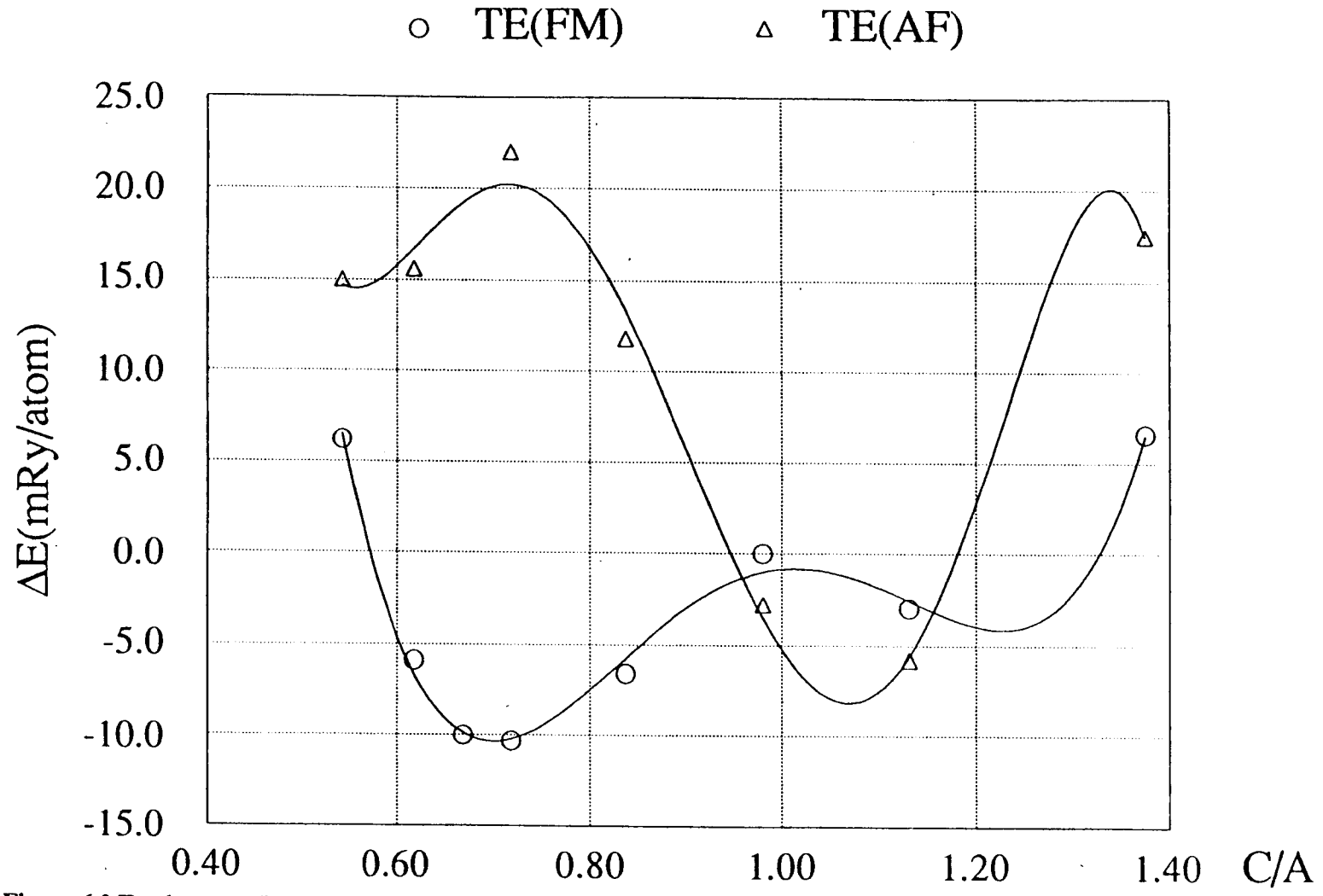

Figure 6.2 Total energy (in mRy/atom) of ferromagnetic and antiferromagnetic iron as a function of the c/a ratio. The volume is fixed at the experimental value. The ferromagnetic total energy at c/a=0.98, v/v_o=1.00 is used as a common reference point.

case for a larger range of volumes. Therefore, if one would modify the exchange-correlation potential to include a stronger internal magnetic pressure, pushing the volume to a larger value, one would also obtain the correct ground state for iron.

The total energy of antiferromagnetic iron shows the opposite behavior. In this case there is a minimum near the fcc structure and a maximum for bcc iron. As a result, the difference in energy between the ferromagnetic and the antiferromagnetic structure shows oscillations as a function of c/a. The antiferromagnetic phase has a lower energy than the ferromagnetic phase in the fcc structure. These calculated results are in agreement with the fact that films of Fe grown on Cu(001) are antiferromagnetic[15-18,22].

When the c/a ratio is very large, the crystal consists of two-dimensional atomic layers with a very small inter-layer interaction. On the other hand, if the c/a ratio is very small, the system is one-dimensional with a very small inter-chain interaction. In both cases, the electron density near the atoms is very high, and both systems will be nonmagnetic. This means that in Figure 6.2 at small and large values of the c/a ratio the two curves will merge together into a single curve representing nonmagnetic iron.

In Figure 6.3 we present preliminary results on the difference in total energy between ferromagnetic and antiferromagnetic iron as a function of c/a and volume (normalized with respect to the experimental value of the equilibrium volume of the fct films). The contour lines have only a qualitative meaning and should be considered guides to the eye only. When the relative volume is very small, iron is nonmagnetic and the difference shown in Figure 6.3 is zero. At smaller values of c/a the oscillatory pattern of the contour lines indicates that an antiferromagnetic state is possibly more favorable again at normal volumes. It would be interesting to grow films of iron with a large in-plane lattice constant and to see whether these films are antiferromagnetic. Whether the antiferromagnetism in this case comes from the in-chain or inter-chain interaction is not clear.

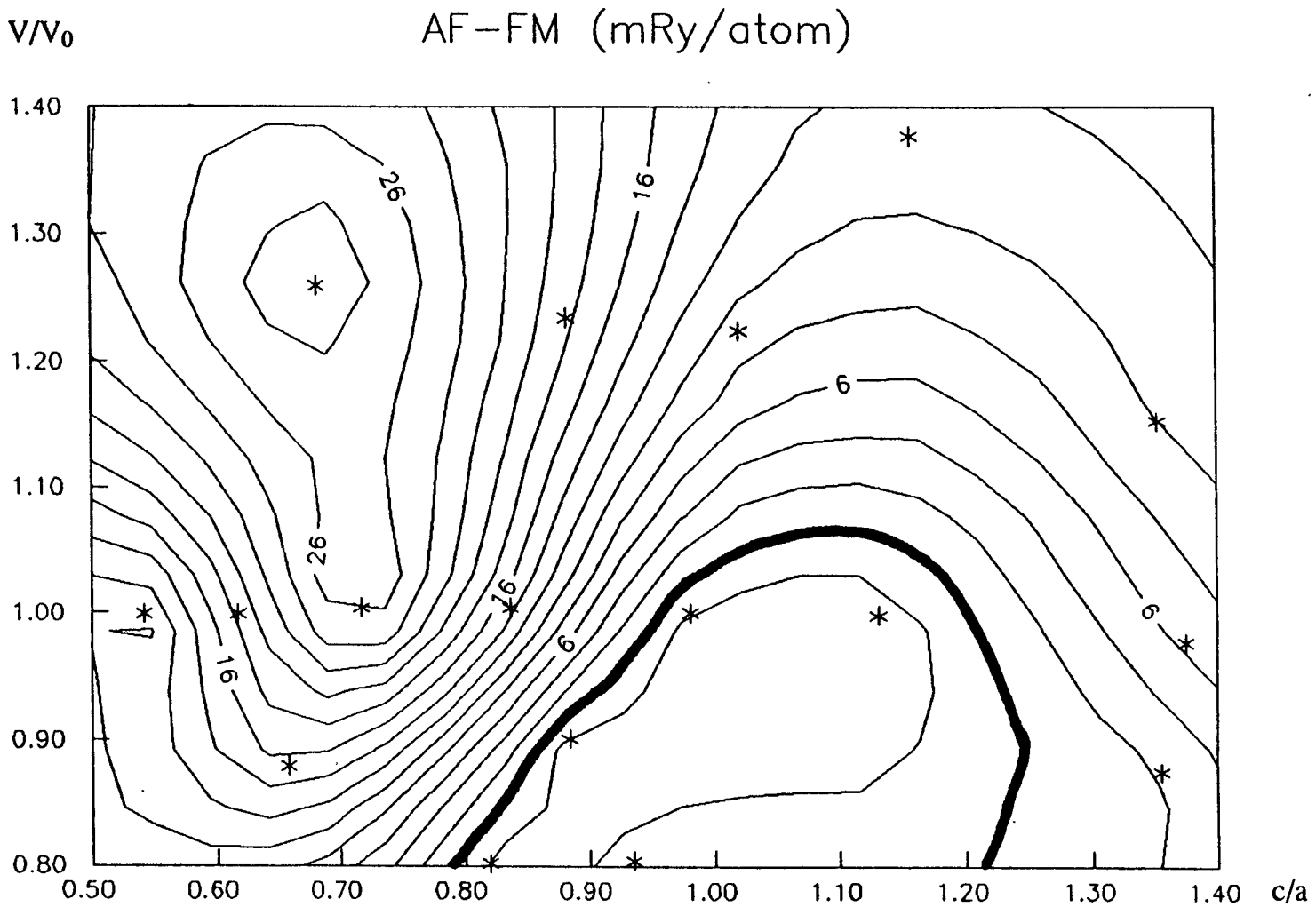

Figure 6.3 Contours of constant energy differences between the antiferromagnetic and ferromagnetic phase, in mRy/atom, in the volume(relative to the experimental value) vs. c/a plane. The bold contour line represents a zero energy difference.

Figure 6.3 shows an oscillatory pattern, which one would like to understand in terms of a Heisenberg model with exchange parameters that depend on distance like

$$J(R) \propto \frac{\cos(\alpha R)}{R^3}$$

The nearest-neighbor distance of the iron atoms is approximately the same in the bcc and the fcc structure at the same value of the volume. Our work on antiferromagnetic bcc iron[32] has shown that the exchange parameter corresponding to the nearest neighbors is large and positive, favoring ferromagnetism. Since we expect this parameter to have the same value in the fcc structure, this argument shows that fcc iron at the experimental volume is expected to be ferromagnetic if the exchange parameters are only a function of distance. It is, of course, possible that the values of the exchange parameter for further neighbors become negative and positive in just the right way to make fcc iron antiferromagnetic, but this is unlikely. At this point we conclude that a formula of the exchange parameter which depends only on the distance between the atoms is too simple, and that it also has to depend on the direction of the vectors **R**.

Acknowledgement

This work was made possible by a grant of computer time obtained through the College of Science on the Oregon State University Floating Point system.

References

1. R.M. White, "*Quantum Theory of Magnetism*", Springer-Verlag Berlin, Heidelberg, New York, 1983.
2. D. C. Mattis, "*The Theory of Magnetism*", Springer-Verlag, New York, 1965.
3. C. S. Wang, B. M. Klein, and H. Krakauer, Phys. Rev. Lett. **54**, 1852 (1985).
4. V. L. Moruzzi, P. M. Marcus, K. Schwarz, and P. Mohn, Phys. Rev. **B34**, 1784 (1986).
5. P. Hohenberg and W. Kohn, Phys. Rev. 136, B864 (1964).
6. W. Kohn and L. J. Sham, Phys. Rev. 140, A1133 (1965).
7. "*Theory of the Inhomogeneous Electron Gas*", edited by S. Lundqvist and N. M. March, Plenum, New York, 1983.
8. W. Jones and N. H. March, "*Theoretical Solid State Physics* ", Dover, 1973.
9. U. von Barth and L. Hedin, J. Phys. C5,1629 (1972).
10. J. F. Janak, Solid State Commun. **25**,53 (1978).
11. V. L. Moruzzi, J. F. Janak, and A. R. Williams, "*Calculated Electronic Properties of Metals*", Pergamon, New York, 1978.
12. H. J. F. Jansen and A. J. Freeman, Phys. Rev. B30, 561 (1984).
13. H. J. F. Jansen and F. M. Mueller, Phys. Rev. B20, 1426 (1979).
14. Pierre Weiss, et al, J. Phys. **6**, 661(1907).
15. S. H. Lu, J. Quinn, D. Tian , F. Jona, and P. M. Marcos, Surf. Sci. **209**, 364 (1989).
16. C. Liu, E. R. Moog, and S. D. Bader, Phys. Rev. Lett. **60**, 2422 (1985).
17. D. Pescia, M. Stampanoni, G. L. Bona, A. Vaterlaus, R. F. Willis, and F. Meier, Phys. Rev. Lett. **58**, 2126 (1985).
18. P. A. Montano, G. W. Fernando, B. R. Cooper, E. R. Moog, H. M. Naik, *et al*, Phys.Rev. Lett. **59**, 1041 (1987).

19. K. B. Hathaway, H. J. F. Jansen, and A. J. Freeman, Phys. Rev. B **31**, 7603 (1985).

20. J. Kübler, Phys. Lett., **81A**, 81 (1981).

21. V. L. Moruzzi, P. M. Marcos, and J. Kübler, Phys. Rev. B**39**, 6957 (1989).

22. W. A. A. Macedo and W. Keune, Phys. Rev. Lett. **61**, 475 (1988).

23. See, e.g., Bull. Am. Phys. Soc. **29**,328 (1984).

24. D. M. Edwards and R. Bechara Muniz, J. Phys. F: Met. Phys. **15**, 2339-2356 (1985); R. Bechara Muniz, J. F. Cooke and D. M . Edwards, J. Phys. F: Met. Phys. **15**, 2357-2363 (1985); M. V. You, V. Heine, A. J. Holden and P. J. Lin-Chung, Phys. Rev. Lett. **44**, 1282 (1980).

25. C. S. Wang, R. E. Prange and V. Korenman, Phys. Rev. B **25**, 5766 (1982).

26. A. I. Liechtenstein, M. I. Katsnelson, and V. A. Gubanov, J. Phys. F14, L125 (1984)

27. J. Staunton, B. L. Gyorffy, G. M. Stocks, and J. Wadsworth, J. Phys. F16, 1761 (1986)

28. J. W. D. Connolly and A. R. Williams, Phys. Rev. B27, 5169 (1983).

29. H. J. F. Jansen and S. S. Peng, Phys. Rev. B **37**, 2689 (1988).

30. G. Shirane, P. Boni, and J. P. Wicksted, Phys. Rev. B33, 1881 (1986); J. W. Lynn, Phys. Rev. Lett. 52, 775 (1984).

31. T. Jarlborg, Solid State Comm. 57, 683 (1986).

32. S. S. Peng and H. J. F. Jansen, J. Appl. Phys. 64, 5607 (1988).

33. M. Alouani, L. Brey, N. E. Christensen, Phys. Rev. B37, 1167 (1988), and references therein.

34. O. Haase and Z. Naturforsch. A**14**, 920 (1959)

35. S. S. Peng and H. J. F. Jansen, J. Appl. Phys. **67** (9), 4567 (1990)

36. V. L. Moruzzi and P. M. Marcus, to be published in Phys. Rev. **B**

Appendix

Appendix

A.1 Iterational Total Energy Convergence for T_c Calculations

A.1.1 Simple Cubic Structure

Table I. (a) nkpt=10, k_{max}=4.5, R_{mf}=2.25 a.u.

Ferromagnetic			Antiferromagnetic		
$\Delta\rho_c$(a.u.)	$\Delta\rho_s$(a.u.)	E_{total}(-5082Ry-)	$\Delta\rho_c$(a.u.)	$\Delta\rho_s$(a.u.)	E_{total}(-5082Ry-)
3.64	4.50	.1667929	4.69	5.17	.1131413
7.37	6.65	.1362751	4.45	4.68	.1132780
8.11	5.78	.1296836	4.22	4.25	.1133777
8.08	6.72	.1287166			

Table I. (b) nkpt=20, k_{max}=4.5, R_{mf}=2.25 a.u.

Ferromagnetic			Antiferromagnetic		
$\Delta\rho_c$(a.u.)	$\Delta\rho_s$(a.u.)	E_{total}(-5082Ry-)	$\Delta\rho_c$(a.u.)	$\Delta\rho_s$(a.u.)	E_{total}(-5082Ry-)
1.17	1.03	.1754821	0.54	5.41	.1167127
2.33	1.71	.1727081	0.49	5.17	.1167922
2.77	1.95	.1710202	0.44	4.93	.1168608
2.90	2.00	.1705954	0.40	4.71	.1169242

Table I. (c) nkpt=30, k_{max}=4.5, R_{mf}=2.25 a.u.

Ferromagnetic			Antiferromagnetic		
$\Delta\rho_c$(a.u.)	$\Delta\rho_s$(a.u.)	E_{total}(-5082Ry-)	$\Delta\rho_c$(a.u.)	$\Delta\rho_s$(a.u.)	E_{total}(-5082Ry-)
1.79	2.20	.1832	5.68	10.8	.1227
.862	2.06	.1852	5.42	10.1	.1234
.814	1.99	.1853	5.29	9.02	.1236
.802	1.91	.18533	4.99	8.82	.1240
1.98	1.59	.18534	4.13	8.40	.1239
1.32	1.17	.1854	4.27	7.89	.1194
.840	.705	.1871			
.728	.575	.1880			

Table I. (d) nkpt=60, k_{max}=4.5, R_{mf}=2.25 a.u.

Ferromagnetic			Antiferromagnetic		
$\Delta\rho_c$(a.u.)	$\Delta\rho_s$(a.u.)	E_{total}(-5082Ry-)	$\Delta\rho_c$(a.u.)	$\Delta\rho_s$(a.u.)	E_{total}(-5082Ry-)
0.52	0.39	.1871384	2.52	6.29	.1260946
0.47	0.36	.1871452	2.31	5.87	.1262642
0.43	0.34	.1871485	2.11	5.49	.1264117
0.41	0.33	.1871494	1.92	5.14	.1265438
0.39	0.32	.1871499			

A.1.2 Diamond Structure

Table II. (a) nkpt=10, k_{max}=4.5, R_{mf}=2.25 a.u.

Ferromagnetic			Antiferromagnetic		
$\Delta\rho_c$(a.u.)	$\Delta\rho_s$(a.u.)	E_{total}(-10164Ry-)	$\Delta\rho_c$(a.u.)	$\Delta\rho_s$(a.u.)	E_{total}(-10164Ry-)
3.27	0.20	.3581116	2.59	4.63	.3158607
3.02	0.15	.3591135	2.45	4.21	.3150089
2.86	0.14	.3592526	2.32	3.84	.3151361
2.71	0.10	.3593669	2.20	3.50	.3152479

Table II. (b) nkpt=20, k_{max}=4.5, R_{mf}=2.25 a.u.

Ferromagnetic			Antiferromagnetic		
$\Delta\rho_c$(a.u.)	$\Delta\rho_s$(a.u.)	E_{total}(-10164Ry-)	$\Delta\rho_c$(a.u.)	$\Delta\rho_s$(a.u.)	E_{total}(-10164Ry-)
2.41	1.40	.3674619	3.13	2.71	.3247652
2.18	1.35	.3679038	2.87	2.40	.3253374
1.99	1.30	.3682131	2.65	2.13	.3257198
1.83	1.24	.3684346	2.46	1.90	.3259790

Table II. (c) nkpt=30, k_{max}=4.5, R_{mf}=2.25 a.u.

Ferromagnetic			Antiferromagnetic		
$\Delta\rho_c$(a.u.)	$\Delta\rho_s$(a.u.)	E_{total}(-10164Ry-)	$\Delta\rho_c$(a.u.)	$\Delta\rho_s$(a.u.)	E_{total}(-10164Ry-)
4.64	7.53	.3534	4.18	6.03	.3109
4.11	.655	.3547	3.65	3.96	.3121
3.70	.158	.3552	3.22	2.70	.3126
3.30	.139	.3555	2.85	1.89	.3130

Table II. (d) nkpt=60, k_{max}=4.5, R_{mf}=2.25 a.u.

Ferromagnetic			Antiferromagnetic		
$\Delta\rho_c$(a.u.)	$\Delta\rho_s$(a.u.)	E_{total}(-10164Ry-)	$\Delta\rho_c$(a.u.)	$\Delta\rho_s$(a.u.)	E_{total}(-10164Ry-)
1.63	3.08	.3747265	3.06	1.52	.3263396
1.52	2.86	.3749126	2.86	1.35	.3265578
1.42	2.65	.3750528	2.68	1.20	.3267063
1.34	2.46	.3751681	2.52	1.08	.3268098

A.1.3 The First Tetragonal Structure

Table III. (a) nkpt=10, k_{max}=4.5, R_{mf}=2.25 a.u.

Ferromagnetic			Antiferromagnetic		
$\Delta\rho_c$(a.u.)	$\Delta\rho_s$(a.u.)	E_{total}(-10164Ry-)	$\Delta\rho_c$(a.u.)	$\Delta\rho_s$(a.u.)	E_{total}(-10164Ry-)
2.25	1.70	.3258993	2.17	2.47	.2926473
2.36	1.70	.3249331	2.05	2.23	.2926677
3.41	3.43	.3157452	1.93	2.03	.2926922
3.66	2.09	.3136979	1.81	1.84	.2927107
3.66	3.51	.3130029			

Table III. (b) nkpt=20, k_{max}=4.5, R_{mf}=2.25 a.u.

Ferromagnetic			Antiferromagnetic		
$\Delta\rho_c$(a.u.)	$\Delta\rho_s$(a.u.)	E_{total}(-10164Ry-)	$\Delta\rho_c$(a.u.)	$\Delta\rho_s$(a.u.)	E_{total}(-10164Ry-)
1.94	2.83	.3507690	2.76	1.78	.3058080
1.81	2.63	.3511086	2.54	1.69	.3060384
1.70	2.46	.3512584	2.44	1.52	.3060770
1.41	2.37	.3513525	2.15	1.70	.3061595

Table III. (c) nkpt=30, k_{max}=4.5, R_{mf}=2.25 a.u.

Ferromagnetic			Antiferromagnetic		
$\Delta\rho_c$(a.u.)	$\Delta\rho_s$(a.u.)	E_{total}(-10164Ry-)	$\Delta\rho_c$(a.u.)	$\Delta\rho_s$(a.u.)	E_{total}(-10164Ry-)
2.72	2.81	.3682	2.48	4.65	.31718
2.46	2.51	.3693	2.34	4.56	.31722
2.31	2.45	.36940	2.19	4.42	.31724
2.18	2.35	.36945	2.03	4.35	.31728
2.06	2.26	.36950	1.91	4.26	.31731
			1.80	4.14	.31732

Table III. (d) nkpt=60, k_{max}=4.5, R_{mf}=2.25 a.u.

Ferromagnetic			Antiferromagnetic		
$\Delta\rho_c$(a.u.)	$\Delta\rho_s$(a.u.)	E_{total}(-10164Ry-)	$\Delta\rho_c$(a.u.)	$\Delta\rho_s$(a.u.)	E_{total}(-10164Ry-)
1.60	3.20	.3720812	2.09	2.07	.3189196
1.50	2.94	.3722388	1.87	1.89	.3193354
1.39	2.73	.3723551	1.76	1.87	.3194160
1.32	2.54	.3724695			

A.1.4 The Second Tetragonal Structure

Table IV. (a) nkpt=10, k_{max}=4.5, R_{mf}=2.25 a.u.

Ferromagnetic			Antiferromagnetic		
$\Delta\rho_c$(a.u.)	$\Delta\rho_s$(a.u.)	E_{total}(-5082Ry-)	$\Delta\rho_c$(a.u.)	$\Delta\rho_s$(a.u.)	E_{total}(-5082Ry-)
3.84	2.49	.1291442	3.34	4.66	.0806015
3.68	2.34	.1292547	3.14	4.12	.0805428
3.53	2.27	.1293615	2.96	3.65	.0804988
3.38	2.13	.1294639	2.80	3.24	.0804709

Table IV. (b) nkpt=20, k_{max}=4.5, R_{mf}=2.25 a.u.

Ferromagnetic			Antiferromagnetic		
$\Delta\rho_c$(a.u.)	$\Delta\rho_s$(a.u.)	E_{total}(-5082Ry-)	$\Delta\rho_c$(a.u.)	$\Delta\rho_s$(a.u.)	E_{total}(-5082Ry-)
2.86	2.79	.1651943	4.38	7.35	.1321472
2.69	2.50	.1652026	3.87	6.32	.1335135
2.51	2.23	.1653829	3.48	5.47	.1344693
2.38	2.00	.1654795	3.17	4.75	.1351601

Table IV. (c) nkpt=30, k_{max}=4.5, R_{mf}=2.25 a.u.

Ferromagnetic			Antiferromagnetic		
$\Delta\rho_c$(a.u.)	$\Delta\rho_s$(a.u.)	E_{total}(-5082Ry-)	$\Delta\rho_c$(a.u.)	$\Delta\rho_s$(a.u.)	E_{total}(-5082Ry-)
5.08	10.3	.17140	3.67	5.35	.1531470
4.88	9.83	.17143	3.41	4.55	.1536290
4.67	4.83	.17168	3.20	3.88	.1540231
			3.02	3.32	.1543652
			2.81	2.85	.1548113

Table IV. (d) nkpt=60, k_{max}=4.5, R_{mf}=2.25 a.u.

Ferromagnetic			Antiferromagnetic		
$\Delta\rho_c$(a.u.)	$\Delta\rho_s$(a.u.)	E_{total}(-5082Ry-)	$\Delta\rho_c$(a.u.)	$\Delta\rho_s$(a.u.)	E_{total}(-5082Ry-)
3.18	2.29	.178905	5.20	3.50	.154812
3.07	2.17	.178940	5.00	3.36	.155256
2.97	2.11	.178970	4.82	3.23	.155699
2.87	2.00	.178998	4.64	3.11	.156135
			4.48	2.99	.156569

A.1.5 The Third Tetragonal Structure

Table V. (a) nkpt=10, k_{max}=4.5, R_{mf}=2.25 a.u.

Ferromagnetic			Antiferromagnetic		
$\Delta\rho_c$(a.u.)	$\Delta\rho_s$(a.u.)	E_{total}(-10164Ry-)	$\Delta\rho_c$(a.u.)	$\Delta\rho_s$(a.u.)	E_{total}(-5082Ry-)
3.13	5.05	.327656	2.64	3.92	.295070
2.99	4.83	.327681	2.54	3.81	.295117
2.86	4.63	.327704	2.45	3.71	.295155
2.73	4.42	.327726	2.37	3.61	.295184
2.61	4.24	.327745	2.29	3.51	.295190
2.50	4.05	.327768	2.21	3.42	.295207
2.39	3.89	.327787			

Table V. (b) nkpt=20, k_{max}=4.5, R_{mf}=2.25 a.u.

Ferromagnetic			Antiferromagnetic		
$\Delta\rho_c$(a.u.)	$\Delta\rho_s$(a.u.)	E_{total}(-10164Ry-)	$\Delta\rho_c$(a.u.)	$\Delta\rho_s$(a.u.)	E_{total}(-5082Ry-)
.928	2.06	.351951	1.63	2.89	.308344
.910	1.92	.351945	1.53	2.77	.3083563
.894	1.79	.351941	1.44	2.65	.3083560
.878	1.67	.351934	1.35	2.55	.308347
.863	1.55	.351927			

Table V. (c) nkpt=30, k_{max}=4.5, R_{mf}=2.25 a.u.

Ferromagnetic			Antiferromagnetic		
$\Delta\rho_c$(a.u.)	$\Delta\rho_s$(a.u.)	E_{total}(-10164Ry-)	$\Delta\rho_c$(a.u.)	$\Delta\rho_s$(a.u.)	E_{total}(-5082Ry-)
3.99	12.0	.36814	3.48	4.67	.320836
3.79	11.4	.36843	3.30	4.47	.320856
3.60	10.9	.36858	3.12	4.29	.320864
3.32	10.5	.36894	2.95	4.11	.320867
3.18	9.13	.36912	2.80	3.95	.320865
3.05	7.91	.36925	2.65	3.79	.320858
2.90	6.88	.36933			

Table V. (d) nkpt=60, k_{max}=4.5, R_{mf}=2.25 a.u.

Ferromagnetic			Antiferromagnetic		
$\Delta\rho_c$(a.u.)	$\Delta\rho_s$(a.u.)	E_{total}(-10164Ry-)	$\Delta\rho_c$(a.u.)	$\Delta\rho_s$(a.u.)	E_{total}(-5082Ry-)
2.75	5.79	.373090	2.96	4.48	.3235942
2.61	5.52	.373126	2.81	4.30	.3235935

A.2 Overall Results for FCT Structures (Updated)

Table VI. Total energy results (in mRy/atom) for ferromagnetic, anti-ferromagnetic, and nonmagnetic iron as a function of a and c. The values of the magnetic moments (in μ_B) are integrated within a muffin radius R_{mt}=2.10 a.u. around the atoms.

	a(Å)	c(Å)	E_{FM}(mRy)	E_{AF}(mRy)	E_{NM}(mRy)	$M_{FM}(\mu_B)$	$M_{AF}(\mu_B)$
Q	3.80	4.40	51.4	63.2		2.77	2.64
J	4.00	4.20	67.1	79.8		2.84	2.73
P	3.40	4.60	19.8	30.6		2.44	2.33
B	3.81	3.89	29.5	38.4		2.70	2.39
A	4.01	3.54	29.1	47.7		2.68	2.40
AA	4.40	3.00	28.4	58.4		2.64	2.51
X	3.10	4.80		38.6			1.96
W	3.20	4.40	6.6	15.0		2.22	1.98
C	3.44	3.89	-3.0	-5.8	4.7	2.31	1.80

(Table VI continued.)

O	3.61	3.54	0.0	-2.8	0.8	2.13	1.82
F	3.81	3.19	-6.6	11.8		2.26	1.59
L	4.01	2.88	-10.3	22.0		2.27	1.60
LB	4.21	2.60	-5.9	13.1		2.26	1.55
LC	4.40	2.38	3.7	12.6		2.15	1.68
LC†	4.40	2.38	-0.2	8.6		2.16	1.72
LD	4.60	2.18	17.9	29.2		2.11	1.85
GA	3.10	4.20	7.3	9.0		2.06	1.61
E	3.61	3.19	-4.1	-7.2	-7.2	2.00	0.97
HA	3.95	2.60	-11.7	4.6		2.01	0.83
Y	3.30	3.37	-16.4	-16.4		0.10	0.28
V	3.41	3.19	-14.6	-15.6	-14.6	0.58	0.46
S	3.56	2.92	0.1	-2.8	-2.2	0.21	0.40
TA	3.80	2.50	3.8	10.9		1.74	0.52

A.3 Total Energy Calculations for FCT Structures

A.3.1 Ferromagnetic Calculations

Table VII. (a) Total Energy (Ry) vs nkpt (k_{max}=4.5, R_{mf}=2.25)

nkpt	30		60		90		110		150
O	-2541.0		-2541.0		-2541.0		-2541.0		-2541.0
	675	14.8	823	2.9	794	1.4	808	1.1	819
O'(LF)	664		14.1		805		2.5		830
Δ (=O'- O)	1.1		2.2		-1.1		0.0		-1.1
B	424	13.2	556	2.5	531	1.2	543	1.1	554
A	437		10.1		538		2.0		558
N	637		11.1		748		2.3		771
R	667		10.8		775		1.8		793
C	707		11.7		824		2.5		849
F	751	13.3	884	1.5	869	0.9	878	0.7	885

(Table VII(a) continued.)

L	774		13.4		908		1.4	922
D	/				933		3.1	964
E	724		14.5		869		2.1	890
B-O	25.1	1.6	26.7	0.4	26.3	0.2	26.5	0.0	26.5
A-O	23.8		1.8		25.6		0.5	26.1
N-O	3.8		0.8		4.6		0.2	4.8
R-O	0.8		0.9		1.9		0.7	2.6
C-O	-3.2		0.2		-3.0		0.0	-3.0
F-O	-7.6	1.5	-6.1	1.4	-7.5	0.5	-7.0	0.4	-6.6
L-O	-9.9		1.5		-11.4		1.1	-10.3
D-O					-13.9		0.6	-14.5
E-O	-4.9		-2.6		-7.5		0.4	-7.1

Note: Small characters indicates differences between nearest nkpt's.

Table VII. (b) Total Energy (Ry) vs nkpt (k_{max}=4.5, R_{mf}=2.10)

nkpt	30		90		150
O	-2541.0701	11.9	-2541.0820	2.4	-2541.0844
O'(LF)	667	14.3	810	2.7	837
Δ (=O'-O)	3.4	2.4	1.0	0.3	0.7
Q	208	9.9	307	2.3	330
J	054	10.2	156	2.2	178
P	516	10.2	618	2.8	646
AA	447	10.5	552	1.3	565
I	609	10.8	717	2.4	741
IA	636	10.9	745	1.3	758
M	682	11.4	796	2.7	823
K	720	12.3	843	1.2	855
W	646	10.4	750	2.8	778
LA	791	13.9	930	1.4	944
LB	748	4.0	888	1.5	903
H1	825	15.0	975	1.6	991
HL	818	15.4	972	1.5	987
H2	819	15.9	978	1.6	994

(Table VII(b) continued.)

G	679	11.3	792	2.6	818
G'(HF)	709	12.1	830	2.8	858
Δ (=o'-o)	-3.0	0.8	-3.8	0.2	-4.0
U3	810	15.1	961	3.1	992
DA	812	16.2	974	3.0	1004
DA'(HF)	/		960	2.9	989
Δ (=o'-o)	/		1.4	0.1	1.5
H5	827	14.1	968	1.4	982
H	805	16.7	972	1.6	988
H3	798	16.9	967	1.6	983
HA	777	17.3	950	1.6	966
HB	700	19.0	890	1.8	908
U2	787	18.2	969	2.1	990
UA	812	16.2	974	3.9	1013
UB	826	16.6	992	3.3	1025
UC	825	17.2	997	3.3	1030
H4	780	17.1	951	1.6	967
U1	693	17.9	872	3.0	902
U	745	17.3	918	3.5	953
Y	787	18.1	968	3.5	1003
V	764	19.5	959	3.6	995
S	656	17.3	829	1.9	848
S'(LF)	682	16.9	851	2.0	871
Δ (=o'-o)	-2.6	0.4	-2.2	0.1	-2.3
T	634	18.9	823	1.9	842
TA	594	19.9	793	1.8	811
Z	527	21.1	738	4.1	779
Q-O	49.3	2.0	51.3	0.1	51.4
J-O	64.7	1.7	66.4	0.2	66.6
P-O	18.5	1.7	20.2	0.4	19.8
AA-O	25.4	1.4	26.8	1.1	27.9
I-O	9.2	1.1	10.3	0.0	10.3

(Table VII(b) continued.)

IA-O	6.5	1.0	7.5	1.1	8.6
M-O	1.9	0.5	2.4	0.3	2.1
K-O	-1.9	0.4	-2.3	1.2	-1.1
W-O	5.5	1.5	7.0	0.4	6.6
LA-O	-9.0	2.0	-11.0	1.0	-10.0
LB-O	-4.7	2.1	-6.8	0.9	-5.9
H1-O	-12.4	3.1	-15.5	0.8	-14.7
HL-O	-11.7	3.5	-15.2	0.9	-14.3
H2-O	-11.8	4.0	-15.8	0.8	-15.0
G-O	2.2	0.6	2.8	0.2	2.6
U3-O	-10.9	3.2	-14.1	0.7	-14.8
DA-O	-11.1	4.3	-15.4	0.6	-16.0
H5-O	-12.6	2.2	-14.8	1.0	-13.8
H-O	-10.4	4.8	-15.2	0.8	-14.4
H3-O	-9.7	5.0	-14.7	0.8	-13.9
HA-O	-7.6	5.4	-13.0	0.8	-12.2
HB-O	0.1	7.1	-7.0	0.6	-6.4
U2-O	-8.6	6.3	-14.9	0.3	-14.6
UA-O	-11.1	4.3	-15.4	1.5	-16.9
UB-O	-12.5	4.7	-17.2	0.9	-18.1
UC-O	-12.4	5.3	-17.7	0.9	-18.6
H4-O	-7.9	5.2	-13.1	0.8	-12.3
U1-O	0.8	6.0	-5.2	0.6	-5.8
U-O	-4.4	5.4	-9.8	1.1	-10.9
Y-O	-8.6	6.2	-14.8	1.1	-15.9
V-O	-6.3	7.6	-13.9	1.2	-15.1
S-O	4.5	5.4	-0.9	0.5	-0.4
T-O	6.7	7.0	-0.3	0.5	0.2
TA-O	10.7	8.0	2.7	0.6	3.3
Z-O	17.4	9.2	8.2	1.7	6.5

Table VII. (c) Total Energy (Ry) vs nkpt (k_{max}=4.5, R_{mf}=2.00)

nkpt	30		90		150
O	-2541.0730	11.8	-2541.0848	2.6	-2541.0874

(Table VII(c) continued.)

Z1	471	19.6	667	3.0	697
Z2	305	22.2	527	3.2	495*
Z2'(HS)	312	21.4	526	2.0	546
Δ (=O'-O)	-0.7	0.8	0.1	5.2	-5.1
Z3	0.9936	23.7	173	4.3	216
Z4	0.9750	19.1	0.9941	2.4	0.9965
Z1-O	25.9	7.8	18.1	0.4	17.7
Z2-O	42.5	10.4	32.1	5.8	37.9*
Z3-O	79.4	11.9	67.5	1.7	65.8
Z4-O	98.0	7.3	90.7	0.2	90.9

*: not well converged

A.3.2 Nonmagnetic Calculations

Table VIII. Total Energy (Ry) vs nkpt (kmax=4.5, NM)

O: R_{mf}=2.25; Z1-Z4: R_{mf}=2.00; Other: R_{mf}=2.10

nkpt	30		60		90		110		150
O	-2541.0		-2541.0		-2541.0		-2541.0		-2541.0
	675	14.8	823	2.9	794	1.4	808	1.1	819
O*	640		14.4		784		2.7		811
Δ (≡NM-FM)	3.5		2.5		1.0		0.2		0.8
X(F)	476		4.4		554		2.6		580
X*	282		5.4		336		2.0		356
Δ	19.4		2.4		21.8		0.6		22.4
W	646		10.4		750		2.8		778
W*	465		8.0		545		1.9		564
Δ	18.1		2.4		20.5		0.9		21.4
C	707		11.7		824		2.5		849
C*	614		13.2		746		2.6		772
Δ	9.3		1.5		7.8		0.1		7.7

(Table VIII continued.)

F	751	11.8	869	1.6	885
F*	570	12.8	698	1.8	716
Δ	18.1	1.0	17.1	0.2	16.9
L	774	13.4	908	1.4	922
L*	461	12.6	587	1.2	599
Δ	11.3	0.8	12.1	0.2	12.3
LA	791	13.9	930	1.4	944
LA*	493	13.9	632	1.3	645
Δ	29.8	0.0	29.8	0.1	29.9
LB	748	14.0	888	1.5	903
LB*	509	14.0	649	1.3	662
Δ	23.9	0.0	23.9	0.2	24.1
LC(FM)	1517	12.2	1639	2.1	1660
(LC(F)/2-δ)	664	11.6	780	3.2	812
LC*	468	12.4	592	1.8	610
Δ	19.6	0.8	18.8	0.4	20.2
LD(FM)†	1207	14.8	1355	2.1	1376
(LD(F)/2-δ)	510	14.4	654	1.6	670
LD*	354	5.5	409	2.3	432
Δ	15.6	8.9	24.5	0.7	23.8
G	679	11.3	792	2.6	818
G*	671	12.2	793	2.7	820
Δ	0.8	0.9	-0.1	0.1	-0.2
U3	810	15.1	961	3.1	992
U3*	812	15.2	964	3.0	994
Δ	-0.2	0.1	-0.3	0.1	-0.2
D	/		933	3.1	964
D*	791	15.6	947	3.1	978
Δ	/		-1.4	0.0	-1.4
DA	812	16.2	974	3.0	1004
DA*	812	16.2	974	3.0	1004
Δ	0.0	0.0	0.0	0.0	0.0

(Table VIII continued.)

E	724	14.5	869	2.1	890
E*	732	16.4	896	2.5	921
Δ	-0.8	3.5	-2.7	0.4	-3.1
Y2	787	18.2	969	2.1	990
Y2*	790	16.4	954	3.1	985
Δ	–0.3	1.8	1.5	1.0	0.5
UA	812	16.2	974	3.9	1013
UA*	819	16.4	983	3.2	1015
Δ	-0.7	0.2	-0.9	0.7	-0.2
UB	826	16.6	992	3.3	1025
UB*	829	16.8	997	3.3	1030
Δ	-0.3	0.2	-0.5	0.0	-0.5
UC	825	17.2	997	3.3	1030
UC*	826	17.2	998	3.3	1031
Δ	-0.1	0.0	-0.1	0.0	-0.1
U1	693	17.9	872	3.0	902
U1*	697	17.0	867	3.3	900
Δ	-0.4	0.9	0.5	0.3	0.2
U	745	17.3	918	3.5	953
U*	753	17.5	928	3.2	960
Δ	-0.8	0.2	-1.0	0.3	-0.7
Y	787	18.1	968	3.5	1003
Y*	791	18.1	972	3.4	1006
Δ	-0.4	0.0	-0.4	0.1	-0.3
V	764	19.5	959	3.6	995
V*	770	19.2	962	3.3	995
Δ	-0.6	0.3	-0.3	0.3	0.0
S	656	17.3	829	1.9	848
S*	682	16.9	851	2.1	872
Δ	-2.6	0.4	-2.2	0.1	-2.3

(Table VIII continued.)

T	634	18.9	823	1.9	842
T*	539	16.8	707	1.8	725
Δ	9.5	2.1	11.6	0.1	11.7
Z	527	21.1	738	4.1	779
Z*	532	21.4	746	4.0	786
Δ	-0.5	0.3	-0.8	0.1	-0.7
Z1	471	19.6	667	3.0	697
Z1*	475	0.0	475	1.8	697
Δ	-0.5	19.7	19.2	19.2	0.0
Z2	305	22.2	527	3.2	495†
Z2*	292	18.7	479	2.0	499
Δ	1.3	3.5	4.8	5.2	-0.4†
Z3	0.9936	23.7	173	4.3	216
Z3*	0.9940	24.2	182	4.1	223
Δ	-0.4	0.5	-0.9	0.2	-0.7
Z4	0.9750	19.1	0.9941	2.4	0.9965
Z4*	0.9760	19.1	0.9951	2.1	0.9972
Δ	-1.0	0.0	-1.0	0.2	-0.7

*: The configuration is non-magnetic under the choice of "non -polarized".
†: The result cannot be well converged.

A.3.3 Antiferromagnetic Calculations

Table IX. Total Energy (Ry) vs nkpt (k_{max}=4.5, R_{mf}=2.10)

nkpt	30		90		150
δ(=FM-F)	-9.4		-2.4		-1.8
O(FM)	-5082.1602	9.8	-5082.1700	3.4	-5082.1734
O'(AF)	1655	11.3	1768	2.3	1791
Δ ≡ (o'-o)/atom	-2.6	1.2	-3.4	0.6	-2.8
Q(F)	208	9.9	307	2.3	330
(Q(F)+δ)*2	0604	5.8	0662	3.4	0696

(Table IX continued.)

Q'(AF)	0412	4.2	0454	1.6	0470
Δ	9.6	0.8	10.4	0.9	11.3
J(F)	0054	10.2	0156	2.2	0178
(J(F)+δ)*2	0296	6.4	0360	3.2	0392
J'(AF)	0083	3.9	0122	1.5	0137
Δ	10.6	1.3	11.9	0.9	12.8
P(F)	516	10.2	618	2.8	646
(P(F)+δ)*2	1220	6.4	1284	4.4	1328
P'(AF)	1052	5.2	1104	1.9	1123
Δ	8.4	0.6	9.0	1.2	10.2
B	424	10.7	531	2.3	554
(B(F)+δ)*2	1036	7.4	1110	3.4	1144
B'(AF)	0880	6.6	0946	2.0	0966
Δ	7.8	0.5	8.2	0.7	8.9
A	437	10.1	538	2.0	558
(A(F)+δ)*2	1062	6.2	1124	2.8	1152
A'(AF)	0683	7.9	0762	1.8	0780
Δ	19.0	0.9	18.1	0.5	18.6
AA	447	10.5	552	1.3	565
(AA(F)+δ)*2	1082	7.0	1152	1.4	1166
AA'(AF)	0465	9.5	0560	0.6	0566
Δ	30.8	1.2	29.6	0.4	30.0
X(F)	0476	4.4	0554	2.6	0580
(X(F)+δ)*2	1140	1.6	1156	3.0	1196
X'(AF)	0891	4.4	0935	2.6	0961
Δ	12.4	1.4	11.0	0.8	11.8
W(FM)	1410	11.1	1521	4.6	1567
W'(AF)	1334	7.0	1404	3.0	1434
Δ	3.8	2.0	5.8	0.8	6.6
W(F)	-2541.0646	10.4	0750	2.8	0778
W(F)†	-2541.0693	10.2	0795	2.7	0822
Δ =(O'-O)	-4.7	0.2	-4.5	0.1	-4.4

(Table IX continued.)

C(FM)	1653	8.3	1736	4.2	1778
C'(AF)	1714	10.1	1815	3.0	1849
Δ=(o'-o)/atom	-3.0	1.0	-4.0	0.4	-3.6
F	751	11.8	869	1.6	885
(F(F)+δ)*2	1690	9.6	1786	2.0	1806
F'(AF)	1360	11.8	1478	2.0	1498
Δ	16.5	1.1	15.4	0.0	15.4
L	774	13.4	908	1.4	922
(L(F)+δ)*2	1736	12.8	1864	1.6	1880
L'(AF)	1165	11.8	1283	1.2	1295
Δ	28.6	0.4	29.0	0.2	29.2
LB	748	14.0	888	1.5	903
(LB(F)+δ)*2	1684	14.0	1824	1.8	1842
LB'(AF)	1318	13.4	1452	2.0	1472
Δ	18.3	0.3	18.6	0.1	18.5
LC(FM)	1517	12.2	1639	2.1	1660
LC'(AF)	1338	12.6	1464	1.9	1483
Δ	9.0	0.2	8.8	0.0	8.8
LC(FM)†	1596	12.1	1717	2.1	1738
LC'(AF)†	1415	12.7	1542	2.0	1562
Δ†	9.0	0.2	8.8	0.0	8.8
LD(FM)†	1207	14.8	1355	2.1	1376
LD'(AF)†	1046	8.9	1135	1.4	1149
Δ†	8.0	3.0	11.0	0.4	11.4
GA (FM)	1428	11.5	1543	4.5	1588
GA'(AF)	1432	9.4	1526	2.7	1553
Δ	-0.2	1.0	0.8	1.0	1.8
E	724	14.5	869	2.1	890
E(FM)*2+δ	1636	15.0	1786	3.0	1816
E'(AF)	1672	16.5	1837	4.1	1878
Δ	-1.8	0.8	-2.6	0.5	-3.1

(Table IX continued.)

HA	777	17.3	950	1.6	966
HA(FM)*2+δ	1742	20.6	1948	2.0	1968
HA'(AF)	1463	16.2	1625	1.7	1642
Δ	14.0	2.2	16.2	0.1	16.3
Y(FM)	1821	19.2	2013	4.8	2061
Y'(AF)	1824	19.0	2014	4.7	2061
Δ	-0.2	1.2	0.0	0.0	0.0
V	764	19.5	959	3.6	995
V(FM)*2+δ	1716	25.0	1966	6.0	2026
V'(AF)	1795	20.1	1996	4.9	2045
Δ	-4.0	2.5	-1.5	0.5	-1.0
S	656	17.3	829	1.9	848
S(FM)*2+δ	1500	20.6	1706	2.6	1732
S'(AF)	1553	21.1	1764	2.7	1791
Δ	-2.6	0.5	-3.1	0.1	-3.0
TA	594	19.9	793	1.8	811
TA(FM)*2+δ	1376	25.8	1634	2.4	1658
TA'(AF)	1318	18.2	1500	1.6	1516
Δ	2.9	3.8	6.7	0.4	7.1

†: R_{mt} = 1.978; nrd = 359. Normally, R_{mt} = 2.100; nrd = 361.

A.4 Magnetic Moment Calculations

A.4.1 Ferromagnetic Calculations

Table X. (a) Magnetic Moment vs nkpt (k_{max}=4.5, R_{mf}=2.25)

nkpt	30	60	90	110	150
O	2.181 -17	2.164 -46	2.118 -3	2.115 6	2.121
O'(LS)	1.298	6	1.292	10	1.282
B	2.582 39	2.621 37	2.658 2	2.660 14	2.674
A	2.589	42	2.631	15	2.646

(Table X(a) continued.)

N	2.433	32		2.465	13		2.478	
R	2.440	-8		2.432	8		2.440	
C	2.334	-33		2.301	2		2.303	
F	2.304	-44	2.260 -30	2.230	2	2.232 3	2.235	
L	2.360	-85		2.275	-27		2.248	
D	/			1.245	-96		1.149	
E	2.121	-88		2.033	- 33		2.000	

Note: Small characters indicates differences between nearest kpt's.

Table X. (b) Magnetic Moment vs nkpt (k_{max}=4.5, R_{mf}=2.10)

nkpt	30		90		150
O	2.171	48	2.123	18	2.141
O'(LS)	0.240	31	0.271	22	0.293
Q	2.722	28	2.750	21	2.771
J	2.716	82	2.798	30	2.828
P	2.396	29	2.425	18	2.443
AA	2.586	10	2.596	14	2.610
I	2.532	23	2.555	1	2.556
IA	2.462	7	2.455	26	2.481
M	2.346	7	2.353	2	2.355
K	2.412	73	2.339	9	2.348
W	2.145	69	2.214	13	2.227
LA	2.312	100	2.212	5	2.207
LB	2.372	111	2.261	10	2.251
H1	2.204	78	2.126	0	2.126
HL	2.248	102	2.146	7	2.139
H2	2.172	81	2.091	2	2.089
G	0.702	30	0.672	4	0.676
G'(HS)	2.049	35	2.084	19	2.103
U3	0.366	31	0.335	18	0.317
DA	0.195	11	0.184	4	0.180
DA'(HS)	/		1.230	87	1.143
H5	2.189	56	2.133	1	2.134

(Table X(b) continued.)

H	2.088	64	2.024	3	2.021
H3	2.102	69	2.033	8	2.025
HA	2.067	59	2.008	8	2.000
HB	2.090	137	1.953	45	1.908
U2	0.291	48	0.243	27	0.216
UA	0.445	53	0.402	34	0.368
UB	0.325	43	0.282	23	0.259
UC	0.238	28	0.210	14	0.196
H4	2.020	53	1.967	11	1.956
U1	0.213	68	0.145	26	0.119
U	0.690	98	0.592	62	0.530
Y	0.126	13	0.113	9	0.104
V	0.758	110	0.648	69	0.579
S	1.699	53	1.646	44	1.602
S'(LS)	0.273	51	0.222	14	0.208
T	1.829	6	1.823	16	1.807
TA	1.830	63	1.767	22	1.745
Z	0.324	84	0.240	48	0.192

Table X. (c) Magnetic Moment vs nkpt (k_{max}=4.5, R_{mf}=2.00)

nkpt	30		90		150
O	2.269	40	2.229	2	2.231
Z1	0.582	145	0.437	76	0.361
Z2	0.519	110	0.629	5	0.634
Z2(HS)	1.466	32	1.434	4	1.438
Z3	0.183	99	0.084	32	0.052
Z4	0.282	2	0.280	23	0.303

A.5 Elastic Constants and Bulk Modulus

For a orthorhombic structure, one would use the following quadratic function to fit a minimum in the total energy calculations:

$$u = \frac{U}{V} = c_1(a-a_0)^2 + c_2(b-b_0)^2 + c_3(c-c_0)^2 + c_4(a-a_0)(b-b_0) + c_5(b-b_0)(c-c_0) + c_6(c-c_0)(a-a_0)$$

where u is the total energy per volume; a, b, c are lattice constants (0 denotes the lattice constants at the minimum); $c_{1\text{-}6}$ indicate the fitting parameters.

From the definition of elastic constants { C_{ij} }, we can calculate C_{11}, C_{12}, and C_{33} as follows, where e_{ij} are fractional strain components:

$$C_{11} = \frac{\partial^2 E}{\partial e_{xx}^2} = a_0^2 \frac{\partial^2 E}{\partial a^2} = 2c_1 a_0^2;$$

$$C_{12} = \frac{\partial^2 E}{\partial e_{xx} \partial e_{yy}} = a_0 b_0 \frac{\partial^2 E}{\partial a \partial b} = a_0 b_0 \frac{\partial}{\partial a}(2c_2(b-b_0)+c_4(a-a_0)+c_5(c-c_0)) = c_4 a_0 b_0;$$

$$C_{13} = \frac{\partial^2 E}{\partial e_{xx} \partial e_{zz}} = a_0 c_0 \frac{\partial^2 E}{\partial a \partial c} = a_0 c_0 \frac{\partial}{\partial a}(2c_3(c-c_0)+c_5(b-b_0)+c_6(a-a_0)) = c_6 a_0 c_0;$$

$$C_{33} = \frac{\partial^2 E}{\partial e_{zz}^2} = c_0^2 \frac{\partial^2 E}{\partial c^2} = 2c_3 c_0^2;$$

In our calculations, we use the following formula to fit the minimum for a face-centered-tetragonal structure (therefore a=b and $a_0=b_0$) :

$$u = \alpha(a-a_0)^2 + \beta(a-a_0)(c-c_0) + \gamma(c-c_0)^2$$

Compare the above formula with that of orthorhombic structure, we have:

$\alpha = c_1 + c_2 + c_4 = 2c_1 + c_4$; (because $c_1=c_2$, by symmetry)

$\beta = c_5 + c_6 = 2c_6$; (because $c_5=c_6$, by symmetry)

$\gamma = c_3$;

Using the C_{ij} results for orthorhombic structure, C_{ij} for FCT can be written as:

$$C_{11} + C_{12} = \alpha\, a_0^2;\ C_{13} = \frac{1}{2}\beta\, a_0 c_0;\ C_{33} = 2\,\gamma\, c_0^2.$$

Similarly, we can calculate bulk modulus for FCT structure.

In cubic case, by symmetry, $C_{11} = C_{33}$, $C_{12} = C_{13}$, and

$$U = V\bullet\,(\alpha(a-a_0)^2 + \beta(a-a_0)(c-c_0) + \gamma(c-c_0)^2\,) = V\bullet(\alpha+\beta+\gamma)\,(a-a_0)^2,$$

where $V=a^3$. Then after some simple algebra, the formula of bulk modulus for cubic structure is:

$$B \equiv V\frac{\partial^2 E}{\partial V^2} = V\frac{da}{dV}\frac{d}{da}\left[\frac{da}{dV}\frac{dE}{da}\right]\Big|_{cubic} = \frac{2}{9}\,(\alpha+\beta+\gamma)\,a_0^2$$

$$= \frac{2}{9}\,(\,C_{11}+C_{12}+2C_{13}+\frac{1}{2}C_{33}\,) = \frac{1}{3}\,C_{11}+\frac{2}{3}C_{12}$$